ENGINEERING THE FRACTAL-LIKE POROUS ARCHITECTURE OF FIBROUS MATERIALS

XIAO BOQI

Ph.D

The Hong Kong Polytechnic University

2015

The Hong Kong Polytechnic University

Institute of Textiles and Clothing

Engineering the Fractal-Like Porous Architecture of Fibrous Materials

Boqi Xiao

A thesis submitted in partial fulfillment of the requirements for the degree of Doctor of Philosophy

July 2014

CERTIFICATE OF ORIGINALITY

I hereby declare that this thesis is my own work and that, to the best of my knowledge and belief, it reproduces no material previously published or written, nor material that has been accepted for the award of any other degree or diploma, except where due acknowledgement has been made in the text.

_____ (Signed)

Boqi Xiao (Name of student)

To My Parents, Wife and Son

For Their Loves,
Patience and Support

Abstract

Porous fibrous materials have wide applications in many different fields including textile fabric, fiber reinforced composite, fuel cells, filtration, thermal insulation, paper products, and tissue scaffold. In most of these applications, it is essential to optimize the transport properties. For example, permeability, diffusivity and thermal conductivity are the key parameters to affect the optimization of fibrous materials such as minimum permeability for wind proof and minimum effective thermal conductivity for clothing insulation.

The transport phenomena in fibrous porous media are complex processes. The understanding and modeling of these processes can lead to the optimization and innovation of fibrous materials. However, the geometric structure of fibrous materials is very complex and difficult to determine. The transport properties of fibrous materials have been studied for many years, but the effects of the geometric parameters of the fibrous materials on the heat and mass transfer are still to be fully elucidated. Therefore, the current studies are aimed at elucidating the relationship between the transport properties (viz. permeability, diffusivity and thermal conductivity) and the geometric parameters of fibrous materials, obtaining the optimization of the fractal like architecture of porous fibrous materials related to total effective thermal conductivity, effective diffusivity, and effective permeability based on the established theoretical models, and predicting the optimized structure of porous

fibrous materials for different applications.

The first part of this work was aimed at studying the relative permeability with the effect of capillary pressure based on fractal geometry and the Monte Carlo simulations in the unsaturated porous material. The relative permeability was expressed as a function of porosity, the fractal dimension of tortuous capillaries, the area fractal dimension of pore, saturation and capillary pressure. It was found that the capillary pressure increased with decreasing saturation, and the capillary pressure increased sharply with decreasing saturation at small saturation. In addition, it was shown that the fractal dimensions of wetting phase and non-wetting strongly depended on the porosity of the unsaturated porous material. The predicted relative permeability obtained by the present Monte Carlo simulation was shown to have a good agreement with the available experimental result. Thus the proposed model improved the understanding of physical mechanisms of the liquid transport through the unsaturated porous material.

The second part obtained a novel analytical model for the permeabilities of the fibrous gas diffusion layer in proton exchange membrane fuel cells. In this model, the geometry structure of fibrous gas diffusion layer was characterized in the light of the water and gas fractal dimensions, the porosity, the tortuosity fractal dimension, and the pore area fractal dimension. It was shown that the water and gas relative permeabilities have no relationship with the porosity and were a function of the water saturation of fibrous gas diffusion layer only. Besides, it was found that the dimensionless permeability decreased markedly with increasing tortuosity fractal

dimension. However, there was only a small decrease in the water and gas relative permeabilities when tortuosity fractal dimension increased. The model calculations were compared with the available experimental results and past models results, and good agreement was found. One advantage of the proposed analytical model was that it contained no empirical constant, which was normally required in past models.

In the third part, the optimization of the fractal like architecture of porous fibrous materials related to permeability, diffusivity, and thermal conductivity was analyzed by applying the established theoretical models. In this analysis, the geometrical structure of porous fibrous materials was characterized in the light of the fractal dimension of pore area, the porosity, and the tortuosity fractal dimension. It was observed that the ratio of dimensionless permeability over dimensionless effective diffusivity ($Y_3 = (K / D_f^2) / (D_e / D_b)$) of the fractal like architecture of porous fibrous materials decreased with the decrease of porosity and tortuosity fractal dimension, respectively, which implied that lower porosity and tortuosity fractal dimension were beneficial to wind/water resistant fabric, as it reduced the ratio of dimensionless permeability over dimensionless effective diffusivity ($Y_3 = (K / D_f^2) / (D_e / D_b)$), resulting in lower permeability and higher diffusivity. Besides, it was shown that the ratio of dimensionless total effective thermal conductivity over dimensionless effective diffusivity ($Y_5 = (k_{eff} / k_g) / (D_e / D_b)$) of the fractal like architecture of porous fibrous materials decreased with the increase of porosity when porosity was lower than 0.92. On the other hand, it was found that the ratio of dimensionless total effective thermal conductivity over dimensionless

effective diffusivity ($Y_5 = (k_{eff} / k_g) / (D_e / D_b)$) increased with porosity when porosity was greater than 0.92. In addition, it was found that the ratio of the dimensionless total effective thermal conductivity over dimensionless effective diffusivity ($Y_5 = (k_{eff} / k_g) / (D_e / D_b)$) increased with tortuosity fractal dimension, which implied lower tortuosity fractal dimension was beneficial to clothing insulation, as it reduced the ratio of dimensionless total effective thermal conductivity over dimensionless effective diffusivity ($Y_5 = (k_{eff} / k_g) / (D_e / D_b)$). The optimization results indicated that fabrics with more aligned fibers were preferred for protective clothing, as the low tortuosity fractal dimension implied fibers in the fibrous materials should be more aligned.

Based on above findings and models, further investigations may be directed towards modifying and improving the established theoretical models for the optimization of the fractal like architecture of porous fibrous materials wherever necessary, fabricating electronspun nano- and micro fibrous membranes for the validation of established theoretical models, and fabricating prototypes of the optimized heterogeneous fibrous materials for clothing, and filters.

List of Publications from the Study

International journals:

1. Boqi Xiao, Jintu Fan, Feng Ding. A fractal analytical model for the permeabilities of fibrous gas diffusion layer in proton exchange membrane fuel cells, *Electrochimica Acta*, 2014, 134: 222-231.

2. Boqi Xiao, Jintu Fan, Feng Ding. Prediction of relative permeability of unsaturated porous media based on fractal theory and monte carlo simulation, *Energy & Fuels*, 2012, 26(11): 6971-6978.

3. Boqi Xiao, Guoping Jiang, Jintu Fan, Lingxia Chen. Study on heat transfer mechanism of subcooled pool boiling under high pressure, *Chinese Journal of High Pressure Physics*, 2014, 28(2): 209-214.

4. Boqi Xiao, Jintu Fan, Feng Ding. Optimization of the fractal like architecture of porous fibrous materials related to permeability, diffusivity and thermal conductivity, submitted.

International conference:

1. Boqi Xiao, Jintu Fan, Feng Ding. Prediction of hydraulic permeability in porous fibrous materials with a fractal approach, *Book of Abstracts of The Fiber Society 2013 Fall Conference*, Clemson, South Carolina, USA, October 23-25, 2013.

Acknowledgements

I am very grateful to my chief supervisor, Dr. Feng Ding, for his kind help in my life and studying, and for his technical advice and useful discussions that contributed to this thesis. I was always inspired by his enthusiasm in scientific pursuit and rigorous attitude towards research work.

I would like to convey my deep and sincere gratitude to my co-supervisor, Prof. Jintu Fan, for giving me an opportunity to work on this interesting and rewarding project. I was fortunate to have been a student of Prof. Fan. Although now Prof. Fan works at Cornell University, he has always been a patient guide and his continuous encouragement has cultivated in me to conduct scientific research. His enthusiasm in scientific pursuit and indefatigable dedication to research study always inspired me. Also, I greatly appreciate him giving me great confidence in the past three years, which will benefit and accompany me during my whole life.

I wish to send my sincere gratitude to Prof. Xiaoming Tao, for her detailed and constructive comments on the confirmation of registration for my PhD study which are very helpful in improving this thesis.

My thanks also give to my colleagues who gave suggestions to my project or helped me in various aspects throughout my completion of this thesis. They include but not limited to Dr. Qing Chen, Dr. Dahua Shou, Dr. Maofei Mei, Dr. John Wu, Dr.

Zheng zhao, Dr. Gang Li, Ms. Chao Sun, Ms. Maggie Tong, Ms. Shengyan Li, Mr. Zhengyue Wang, Mr. Xing Tu, Mr. Huawen Hu, Mr. Jia Yang, and Mr. Yi Yang in The Hong Kong Polytechnic University.

I would like to acknowledge the funding support of Research Grant Council of Hong Kong SAR through a GRF project (PolyU 5158/10E) and Departmental Earnings Account of Institute of Textiles and Clothing of The Hong Kong Polytechnic University.

Finally, I wish to thank my parents and my wife for their never-ending love and support. Without their support and encouragement, I could not finish my PhD study successfully. Also, I am thankful for my son who brings me happiness and enjoyment every day.

Table of Contents

List of Figures

Nomenclature

A	Empirical constant (A=5.55)
A_{ca}	Contact area, m^2
A_{cs}	Cross-section area, m^2
A_p	Total pore area, m^2
B	Empirical constant (B=10.1)
C	Concentration, kgm^{-3}
c_1	Proportionality constant
C_e	Empirical constant
C_2	Geometric factor
C_3	A constant determined by fiber orientation (C_3=5.4)
d_f	Area fractal dimension of pores
$d_{f,w}$	Fractal dimension for the wetting phase
$d_{f,g}$	Fractal dimension for non-wetting phase
D	Hydraulic diameter of the pipe, m
D_b	Bulk diffusivity coefficient, m^2s^{-1}
D_e	Effective diffusion coefficient, m^2s^{-1}
D_f	Average fiber diameter, m
D_T	Tortuosity fractal dimension
e	Surface emissivity of the fibre

F	Shape factor depending on geometry of a medium and on flow direction
h	Convection heat transfer coefficient, $Wm^{-2}\ K^{-1}$
J	Diffusive mass flux, $kgm^{-2}s^{-1}$
K	Intrinsic or absolute permeability, m^2
K_w	Permeability for wetting phase in unsaturated porous media, m^2
K_g	Permeability for the non-wetting phase in unsaturated porous media, m^2
k_{rw}	Relative permeability for the wetting phase in unsaturated porous media
k_{rg}	Relative permeability for non-wetting phase in unsaturated porous media
k	Thermal conductivity, $Wm^{-1}K^{-1}$
k_c	Kozeny-Carman constant
$k_{c,eff}$	Effective thermal conductivity to heat conduction, $Wm^{-1}K^{-1}$
$k_{tot,eff}$	Total effective thermal conductivity to heat conduction and radiation, $Wm^{-1}K^{-1}$
k_g	Thermal conductivity of gas phase, $Wm^{-1}K^{-1}$
k_{rh}	Radiative heat conductivity, $Wm^{-1}K^{-1}$
k_s	Thermal conductivity of solid phase, $Wm^{-1}K^{-1}$
l_0	Straight length or thickness of a sample, m
l_t	Actual length of streamlines, m
n'	Exponent
P	Pressure, Pa

ΔP	Pressure difference, Pa
P_g	Gravitational pressure, Pa
P_m	Mechanical pressure or injection pressure, Pa
P_c	Capillary pressure, Pa
P_0	Empirical/fitting parameter by fitting the experimental data
Pr	Prandtl number
Q	Total flow rate in saturated porous media, m^3s^{-1}
q	Flow rate through a single tortuous capillary, m^3s^{-1}
q_h	Heat flux, Wm^{-2}
Q_h	Rate of heat flow, W
Q_w	Total flow rate for wetting phase in unsaturated porous media, m^3s^{-1}
Q_g	Total flow rate for non-wetting phase in unsaturated porous media, m^3s^{-1}
Re	Reynolds number
R_h	Thermal resistance, m^2KW^{-1}
r_f	Average fiber radius, m
r_h	Average hydraulic radius of pore, m
S	Saturation of the wetting phase
T	Temperature, K
T_w	Object temperature, K

T_∞ Fluid free-stream temperature, K

T_{st} Surface tension of fluids, Nm^{-1}

t Time, s

$\overline{U}$ Average fluid velocity, ms^{-1}

u Bulk velocity of fluid, ms^{-1}

V_p Total pore space volume, m^3

V_t Total porous body materials volume, m^3

Greek symbols

α Empirical constant

α_f Thermal diffusivity of fluid, $m^{-2}s$

β Forchheimer coefficient

δ Half distance between two adjacent cylinders, m

σ Boltzmann constant, ($\sigma = 5.672 \times 10^{-8}\, Wm^{-2}K^{-4}$)

μ Viscosity of the fluid, Nsm^{-2}

μ_g Viscosity of the gas, Nsm^{-2}

μ_w Viscosity of the liquid, Nsm^{-2}

ν Kinematic viscosity of fluid, $m^{-2}s$

ρ_f Fluid density, gm^{-3}

ϕ Porosity

ϕ_c Critical value of porosity

ϕ_g Volume fractions for gas phase

ϕ_m Micro porosity in the cluster

ϕ_p Empirical constant

ϕ_w Volume fractions for water phase

θ Contact angle between liquid and solid

τ Tortuosity

τ_{av} Average tortuosity

λ Pore/capillary diameter, *m*

λ_{av} Average pore/capillary diameter, *m*

$\lambda_{\max}$ Maximum diameter of pore, *m*

$\lambda_{\min}$ Minimum diameter of pore, *m*

λ_g Equivalent diameter for non-wetting phase, *m*

$\lambda_{\max,g}$ Maximum equivalent diameter for non-wetting phase, *m*

$\lambda_{\min,g}$ Minimum equivalent diameter for non-wetting phase, *m*

λ_w Equivalent diameter for the wetting phase, *m*

$\lambda_{\max,w}$ Maximum equivalent diameter for the wetting phase, *m*

$\lambda_{\min,w}$ Minimum equivalent diameter for the wetting phase, *m*

Chapter 1 Introduction

1.1 Background

Porous fibrous materials have a variety of applications in many different fields including fiber reinforced composite, textile fabric, filtration, thermal insulation, paper products, apparel products, fuel cells, medical science, tissue engineering. In most of these applications, fibrous materials serve as porous media, through which fluids, heat, particles, photons or electrons pass through. It is therefore essential to understand the transport phenomena within fibrous porous media so as to optimize the transport properties of fibrous materials for specific applications.

The importance of the study of transport phenomena in porous fibrous materials such as heat transfer (Fan et al., 2000; Feng et al., 2004), permeation (Shou et al., 2011; Xiao et al., 2012; Xiao et al., 2014), diffusion (Zheng et al., 2012; Shou et al., 2013), and sorption (Fan et al., 2003; Cai et al., 2012) has long been recognized and considerable literature is available. The understanding and modeling of these processes can lead to the optimization and innovation of new fibrous materials.

Past investigations have shown that the transport processes in fibrous porous media are very complex and depend on the complicacy of fibrous microstructure of fibrous materials (Yu and Lee, 2000; Yazdchi et al., 2011; Bal et al., 2011; Xiao et al., 2014). Many parameters such as porosity, pore size, fiber diameter, fiber orientation, tortuosity of capillaries and capillary pressure are very important for design and manufacture of fibrous materials for different applications, as these parameters are

closely related to the heat and mass transfer of fibrous porous media including permeability, diffusivity and thermal conductivity.

The transport properties of fibrous porous media are essential to the optimization of fibrous materials such as minimum permeability for wind proof and/or water resistant fabric and minimum effective thermal conductivity for clothing insulation. But the geometric microstructure of fibrous porous media is very involute and difficult to analyze. And it may be more complicated to describe the transport phenomena of heat and mass transfer within fibrous systems, especially when different transport mechanisms take part simultaneously. Modeling the transport properties of fibrous materials therefore presents a great challenge.

The term “fractal” was first introduced by mathematician Mandelbrot (1982) to describe self-similar patterns, which widely exists in nature’s creation, for example, trees, river basins and animal’s cardiovascular systems, bronchi systems and neural networks. In nature, the porous fibrous materials have been proven to be fractal substances (Yu et al., 2002; Shi et al., 2008; Shou et al., 2010; Wu et al., 2011; Xiao et al., 2014). These mean that the classical fractal geometry approach can be used to study transport property of porous fibrous materials.

The proposed project is to apply fractal theory to predict the optimized structure of fibrous materials for different applications by applying the established theoretical models of transport properties. Once we have established the formulae relating the heat and mass transfer of porous fibrous materials to the fractal geometric

parameters, we can then conduct numerical simulation to find the optimum geometric parameters to enhance the properties and performance for different applications. For example, maximum permeability and minimum effective thermal conductivity are desirable for cold protective clothing. This work will significantly improve the understanding of physical principles for heat and mass transport through porous fibrous materials.

1.2 The objectives of the project

In view of the above, this project set out to study the transport properties of porous fibrous materials by using a fractal approach. Besides, the effects of geometrical parameters of porous fibrous materials on heat and mass transfer were discussed. Furthermore, we predicted the optimized structure of porous fibrous materials for several applications by applying the established theoretical models. So the goals of this project are listed below.

(1) To develop theoretical models of heat and mass transport through porous fibrous materials based on fractal theory.

(2) To analyze the effects of geometrical parameters of fibrous materials on the transport properties by applying the established theoretical models.

(3) To analyze the optimization of the fractal like architecture of porous fibrous materials related to effective permeability, effective diffusivity, and effective thermal conductivity.

(4) To conduct numerical simulations so as to identify optimum geometric parameters of fibrous materials for different applications.

(5) To explore the optimization of porous fibrous materials based on different application requirements.

(6) To improve the understanding and lay the foundation of engineering design of fibrous materials for improved performance.

1.3 Project significance

In the present project, we obtained the analytical formulas for the transport properties of porous fibrous materials based on fractal geometry and the Monte Carlo simulations. Besides, we analyzed the optimization of the fractal like architecture of porous fibrous materials related to permeability, diffusivity, and thermal conductivity by applying the established theoretical models. Our models will contribute towards the knowledge archives of transport mechanisms in porous fibrous materials, which is important to many branches of sciences and technology, for example, fuel cells, soil physics, oil recovery, wood drying, tissue engineering, chemical engineering, etc. We have had a better comprehensive understanding of physical phenomena for heat and mass transport through porous fibrous materials from this project. The improved understanding based on the new models will then be applied to engineer the porous architecture of fibrous materials for enhanced transport and barrier properties for different applications. For example, for fibrous battings used for thermal insulation in

cold protective clothing, it is required to have maximum permeability and minimum overall effective thermal conductivity. For materials used for surgical gown, maximum permeability is required under the constraint of barrier performance, which is directly connected with the size distribution of pores and surface properties of outer layer. For fibrous materials used for tissue scaffold, maximum permeability is required under the constraint of mechanical strength (a minimum porosity may be used in numerical simulation to safeguard the mechanical strength). For sportswear and summer wear, permeability and capillary pressure should be optimized to facilitate the transmission of moisture vapour and wicking of liquid sweat. This proposed work will significantly improve the understanding and lay the foundation of engineering design of fibrous porous media for improved performance.

1.4 Methodology

In this project, transport properties of fibrous porous media were investigated by fractal techniques and Monte Carlo simulation. Moreover, we proposed to apply fractal based models for optimizing the material parameters. These methods revealed the physical principles of the heat and mass transfer through the fibrous porous media.

(1) The fractal techniques are advantageous in the optimization analysis, since analytical solutions can be derived. Besides, fractal based models require much less computational cost for optimization solutions as key transport properties of the fibrous materials can be expressed analytically. In general, the microstructure of

porous fibrous materials is disordered, which cannot be described by Euclidean geometry (Yu and Cheng, 2002). Models of heat and mass transport through fibrous materials based on classical Euclidean geometry, although well established in the literature, are less appropriate for optimizing the transport properties of porous fibrous materials. Fortunately, in nature the porous fibrous materials have been proven to be fractal substances (Yu et al., 2002; Shi et al., 2008; Shou et al., 2010; Wu et al., 2011; Xiao et al., 2014). Thus, considering the effects of fibrous structure including the porosity and tortuosity fractal dimension on transport properties of porous fibrous materials, heat and mass transfer of porous fibrous materials were investigated by fractal techniques. Moreover, we predict the optimized structure of fibrous materials for different applications by applying the established fractal theoretical models.

(2) The porous fibrous materials are made up of clusters of fibers which are bunched together by the small fibers. Since the fibers of fibrous porous media are randomly distributed, and the macro-pores and micro-pores are randomly distributed. Thus, based on stochastic sampling of fibers, transport properties of porous fibrous materials were investigated by Monte Carlo simulation.

1.5 Outlines of this thesis

This thesis can be divided into six chapters:

Chapter 1 Introduction (viz. current chapter). This chapter introduces the background, objectives, significance and methodology of this work. Besides, the outline of this thesis is also given.

Chapter 2 Literature Review. The second chapter presents a comprehensive and systematic review of published work on the transport properties of porous fibrous materials including permeability, diffusion and heat transfer. Besides, the research methods, the summary and conclusions of published work are also given in Chapter 2. In addition, Chapter 2 introduces the fractal theory and some structural parameters of porous fibrous materials including porosity and tortuosity.

Chapter 3 presents an investigation on the relative permeability with the effect of capillary pressure based on fractal geometry and the Monte Carlo simulations in unsaturated porous media.

Chapter 4 obtains the fractal analytical models of dimensionless permeability, and water and gas relative permeabilities of fibrous gas diffusion layer in proton exchange membrane fuel cells.

Chapter 5 analyzes the optimization of the fractal like architecture of porous fibrous materials related to permeability, diffusivity, and thermal conductivity by applying the established theoretical models.

Chapter 6 summarizes this thesis and presents suggestions for the future work.

Chapter 2 Literature review

2.1 Introduction

From Chapter 1, although the transport properties of fibrous porous media have been studied for many years, the effects of the geometric parameters of the fibrous materials on the transport properties are still to be fully elucidated. Further studies in this area are essential to the optimization of fibrous porous media for various practical applications.

In this chapter, a comprehensive and systematic review of representative publications on the heat and mass transfer through fibrous porous media including fluid permeation, diffusion and heat transfer are provided. Besides, the fractal theory and some structural parameters of porous fibrous materials are also presented in this chapter. For the above purpose, the first part is devoted to introducing the permeability and Kozeny-Carman relationship in porous media. The second section introduces experimental measurements, a variety of correlations and models for diffusion coefficient in porous fibrous materials. The third section discusses the mechanisms of heat transfer including heat conduction, convection and radiation in porous media. The fourth part is devoted to introducing the fractal geometry and some structural parameters of porous fibrous materials including porosity and tortuosity. The summary and conclusions of literature review are given in the fifth section.

2.2 Permeability and Kozeny-Carman relationship

Permeability is an important transport property, which is connected with the geometric structure of fibrous porous media. Besides, it represents the porous media in relation to resistance to the flow of fluids at a given pressure. Thus, it can greatly affect the comfortability of apparel fabric. The estimation of permeability is important in the design and fabrication of textile materials. And it is the most significant physical parameter which can influence the flow of fluids through fibrous porous media. In addition, permeability states the velocity of the flow of fluids to pressure gradient in porous medium. Thus, the permeability is the estimation of the easiness of the flow of fluids in porous media.

Figure 2-1 is a good example of the fields of flow inside a calendared porous nonwoven medium (Zobel et al., 2007). It can be seen from Figure 2-1 the porous nonwoven medium are inhomogeneous geometry structures which lead to the change of the fields of flow inside the porous filter. There are some directional characteristics in the anisotropic preforms, and the permeability (K) can be expressed in three directions by K_{xx}, K_{yy} and K_{zz}. The condition for isotropic preforms is $K=K_{xx=}K_{yy}=K_{zz}$. Figure 2-2 displays the directional character of K_{xx}, K_{yy} and K_{zz} (Hu, 2008). In general, there are two different geometry methods to measure of the permeability including the channel flow experiment of 1-D and the radial flow experiment of 2-D. So a researcher can observe the circular flow front for isotropic porous materials in 2-D radial flow experiment for isotropic materials. However, the above circular flow front can become the elliptic for anisotropic materials. In order to measure the transverse

permeability of porous fibrous materials, Figure 2-3 (A) and (B) show an experiment bed using gravity-driven (Tamayol and Bahrami, 2011). The testing apparatus are made up of an entry part, a sample holder part, a high reservoir, and an exit part with a ball port. Figure 2-4 is a radial flow test equipment which is equipped to test some samples of gas diffusion layer for the plane permeability at different levels of the compressive strain (Feser et al., 2006). In order to measure the out-of-plane permeability, the experimental mold as shown in Figure 2-5 was designed and used (Song et al., 2009). The mold consisted of a pair of porous circular walls.

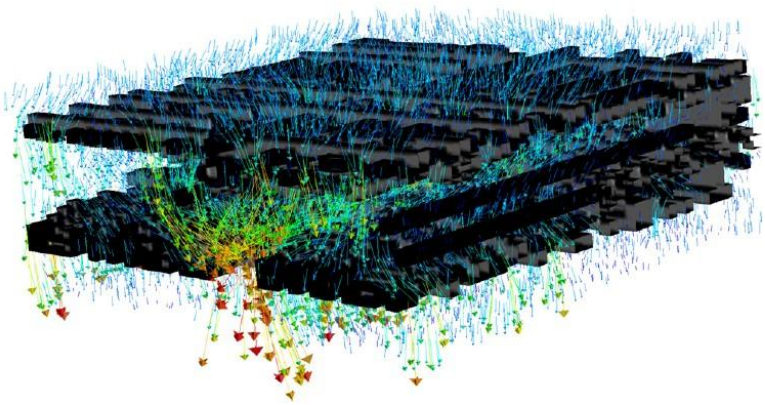

Figure 2-1 Velocity flow field inside a calendered nonwoven structure (Zobel et al., 2007)

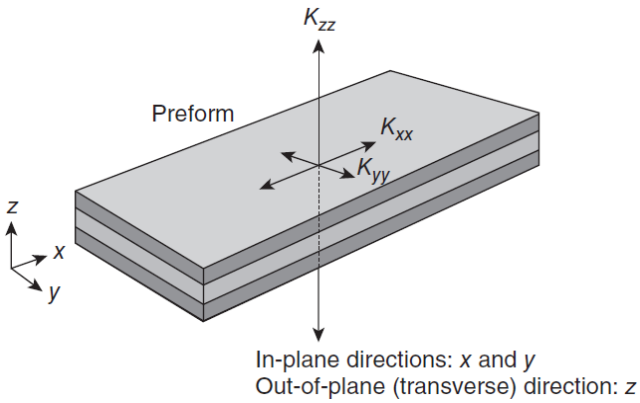

Figure 2-2 Directional characteristics of K_{xx}, K_{yy}, K_{zz} (Hu, 2008)

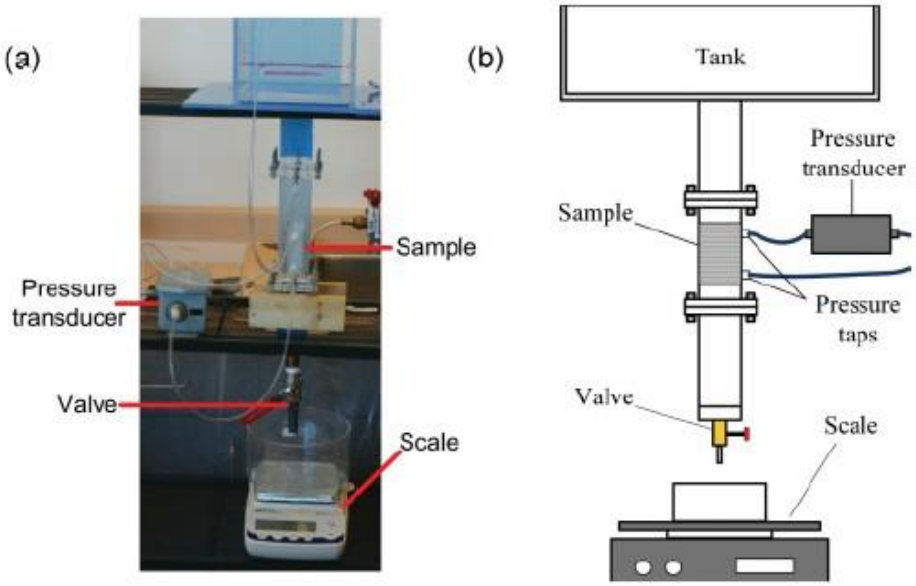

Figure 2-3 The experiment bed using gravity-driven and experimental samples: (a) experimental apparatus, (b) schematic of experimental equipment (Tamayol and Bahrami, 2011)

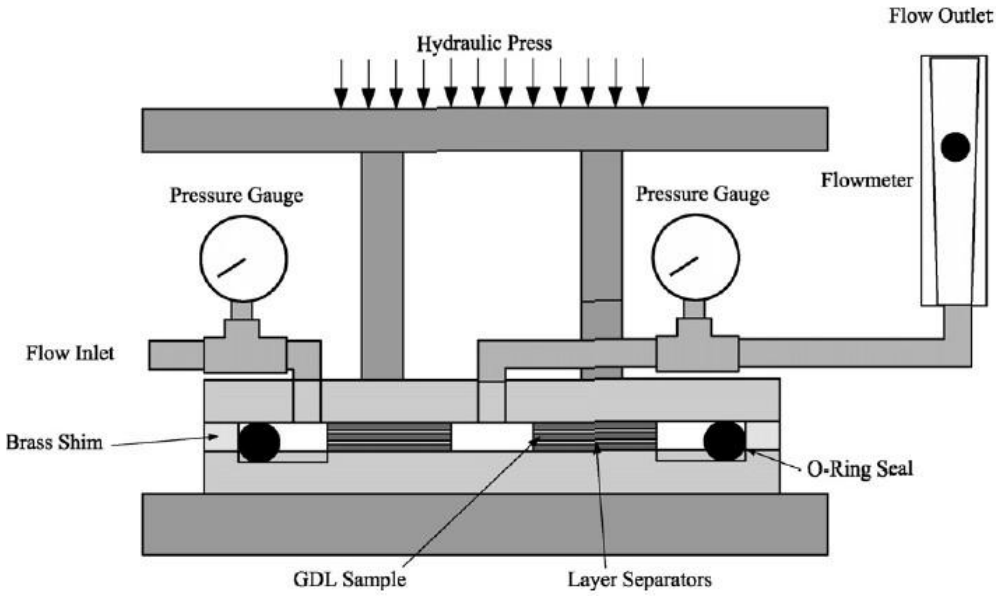

Figure 2-4 Radial flow permeability testing apparatus (Feser et al., 2006)

Figure 2-5 Experimental mold for measurement of out-of-plane permeability (Song et al., 2009)

Since the late 1990s, a number of authors have investigated the permeability of fibrous materials to fluid flow through theoretical, numerical and experimental studies. A modification of Kozeny's permeability equation was developed considering the effect of effective porosity (Koponen et al., 1997). The permeability was simulated by a cellular automaton using lattice-gas (Koponen et al., 1997). Considering the effect of compressibility of woven and non-woven fabrics, the permeability of GDL was studied by employing a radial flow technique (Feser et al., 2006). In addition, permeability measurements were conducted on some samples of carbon woven and non-woven gas diffusion layer at different levels of compression (Feser et al., 2006). The dimensionless permeability of the fibrous materials was calculated based on CFD tools and experimental results (Zobel et al., 2007). Besides, the effect of the orientation of fiber on the permeability of the fabric was analyzed (Zobel et al., 2007).

It was shown that the dimensionless permeability decreased with increasing directionality of the fibers (Zobel et al., 2007). Taking into account the influence of the aspect ratio of unit cell and the diameter of fiber, an analytical model for the permeability with ordered fibrous porous media to the normal and parallel flow was obtained (Tamayol and Bahrami, 2009). The transverse permeability of different fibrous porous body was investigated both experimentally and theoretically in porous fibrous materials (Tamayol and Bahrami, 2011). In the approach, the transverse permeability was determined by employing a scale analysis technique. It was found the permeability was a function of the diameter of fiber, porosity and tortuosity of porous fibrous materials (Tamayol and Bahrami, 2011). Considering the effects of microstructure of fibrous materials, an analytical–numerical approach was developed for computing the permeability (Yazdchi et al., 2011). The double scale case of the flow of fluid through 3-D multifilament woven fabrics was studied by the lattice Boltzmann method again (Nabovati et al., 2010). The through-thickness permeabilities of 3-D woven fabrics were computed by using direct simulations of the flow of fluid (Nabovati et al., 2010). In addition, the permeabilities of three different porous materials (soft, synthetic and fibrous) were investigated by using an experimental setup called “permeameter” (Crawford et al., 2011). And the microstructures of porous materials were observed using a scanning electron microscope and a stereomicroscope (Crawford et al., 2011).

Although permeability of porous fibrous materials has been studied for many years, a widely accepted formula relating to geometric parameters of the fibrous

materials is still lacking, especially for lowly permeable porous media. Until now the permeability was one of the most controversial subjects for the estimation of the flow of fluid in porous fibrous materials. So, a comprehensive and unified theory on permeability is highly desirable.

2.2.1 Existing models of permeability of porous fibrous materials

Generally, the permeability is investigated by applying the theoretical models presented for flow of fluid through fibrous porous media. At low Reynolds number, for creeping flow through porous fibrous materials, the permeability of porous fibrous materials is expressed by Darcy's Law (Darcy, 1856):

$$-\nabla p = \frac{\mu}{K}\overline{U} \tag{2-1}$$

Or

$$Q = \frac{KA_{cs}\Delta P}{\mu l_0} \tag{2-2}$$

where μ is the viscosity of the fluid, ∇P is the pressure gradient, ΔP is pressure difference, $\overline{U}$ is the average fluid velocity, A_{cs} is cross-section area, l_0 is straight length, Q is the total flow rate, and K is the intrinsic or absolute permeability of fibrous porous media.

Prediction of the flow characteristics of fibrous porous media, including the permeability and Kozeny–Carman constant, has drawn the attention of many investigators. The known Kozeny–Carman (KC) equation is a relation between the

permeability and porosity, which is applied in various fields such as textile engineering, reservoir engineering, medical science, biochemical and thermal insulation, etc. So far, the most widely known model of intrinsic permeability of porous materials is the Kozeny–Carman equation (Kozeny, 1927; Carman, 1956; Henderson et al., 2010):

$$K = \frac{\phi^{n'+1}}{C_e(1-\phi)^{n'}} \tag{2-3}$$

where, ϕ is the porosity of fibrous porous media, n' and C_e are the exponent and empirical constant, respectively. However, the KC formula is a semi-empirical equation, which has its limitations since its inception. The n' and C_e may vary with different porous materials, and it is only valid for a given empirical constant. For the above purpose of predicting the intrinsic permeability of porous carbon paper, n'=2 (Tomadakis and Robertson, 2005), n'=2.04~3.57, and C_e=0.0045~0.024 were proposed for different fibrous mats (Shih and Lee, 1998). Feser et al. (2006) validated the Kozeny–Carman equation using experimentally measured intrinsic permeability of GDL made of woven and non-woven carbon fibers. Two computed empirical constants ($C_e^{-1}=1.267\times10^{-11}$, n' =2) for TGP-60-H were introduced into Kozeny–Carman equation.

Apart from the Kozeny–Carman equation, the KC constant can also be used to predict the permeability (Kozeny, 1927; Carman, 1956; Tomadakis and Robertson, 2005):

$$K = \frac{r_h^2}{4k_c}\phi \tag{2-4}$$

where r_h is the average hydraulic radius of pore, and k_c is the famous KC constant.

For fiber structures, a relationship between the average hydraulic radius for systems of cylinders and average fiber diameter (D_f) is given by (Tomadakis and Robertson, 2005)

$$r_h = \frac{D_f}{2\ln\phi} \tag{2-5}$$

By inserting Eq. (2-5) into Eq. (2-4), we can derive the dimensionless permeability of fibrous porous media:

$$\frac{K}{D_f^2} = \frac{\phi}{16k_c \ln^2 \phi} \tag{2-6}$$

Eq. (2-6) is a modified Kozeny-Carman relation, and is only dependent on fiber diameter and porosity.

Kozeny-Carman relationship is widely applied in porous fibrous materials (Choi et al., 1998; Ngo and Tamma, 2001; Bechtold and Ye, 2003; Chen and Papathanasiou, 2006; Wang and Hwang, 2008; Wang and Tarabara, 2009). For example, Choi et al. (1998) predicted the dimensionless permeability of fibrous porous media by using Kozeny-Carman relationship. In the model (Choi et al., 1998), the flow of fluid through the fibre mat involved the macro-flow that the distributed fluid surrounded a fixed fibre bundle and the micro-flow that penetrated in the fixed fibre bundle (see Figure 2-6). Figure 2-6 shows the clear information on the

microscopic flow case of fluid in the level of some separate fibres and the macroscopic flow surrounded the bundles. Considering a porous fibrous material with aligned geometry structure of the long fibres, Wang and Hwang (2008) calculated the dimensionless permeability based on Kozeny-Carman relationship. Figure 2-7 shows a good example cross-section geometry structure of the unidirectional porous fibrous materials (Wang and Hwang, 2008). In Figure 2-7, the fluid flow can be directed perpendicular to fixed fibre axis. Besides, Wang and Tarabara (2009) derived a model for calculating the permeability of mixed particle–fiber porous media (see Figure 2-8) based on Kozeny-Carman relationship. However, in Kozeny-Carman relationship, KC constant may be not a constant and is connected with the porosity because KC relation may be a semi-empirical relationship and KC constant may be an empirical constant.

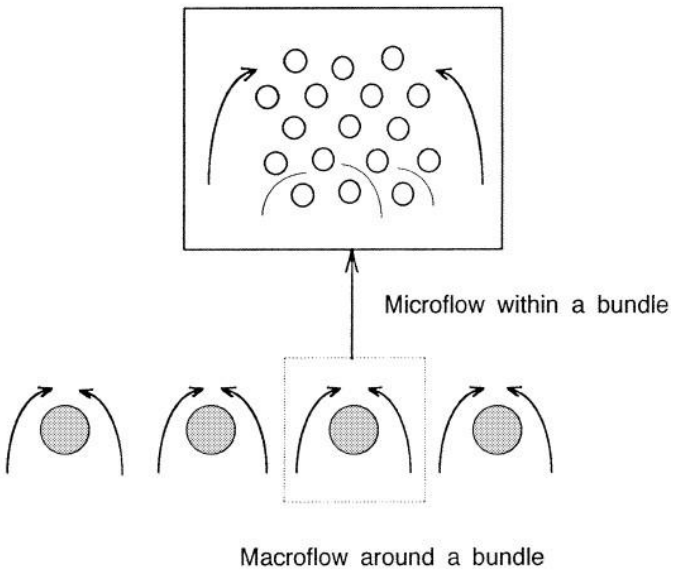

Figure 2-6 Schematic of the micro-flow within a fixed fibre bundle and the micro-flow surrounded a fixed fibre bundle (Choi et al., 1998)

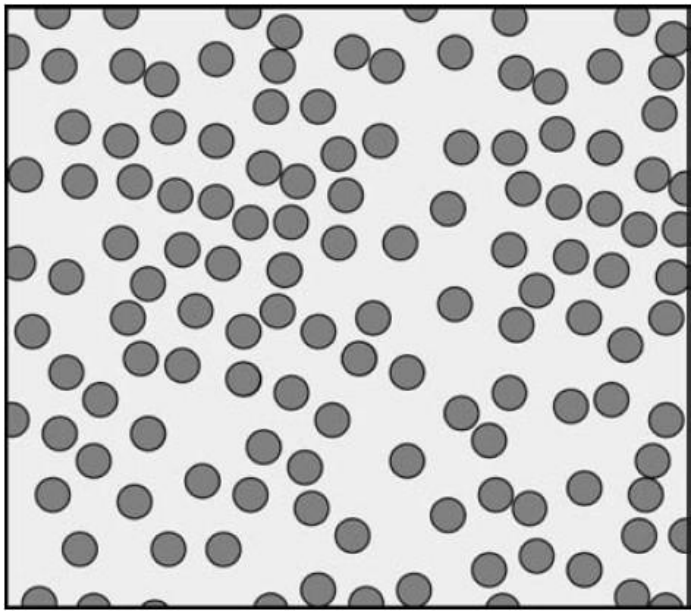

Figure 2-7 An example intersecting surface geometry structure of the unidirectional porous fibrous materials (Wang and Hwang, 2008)

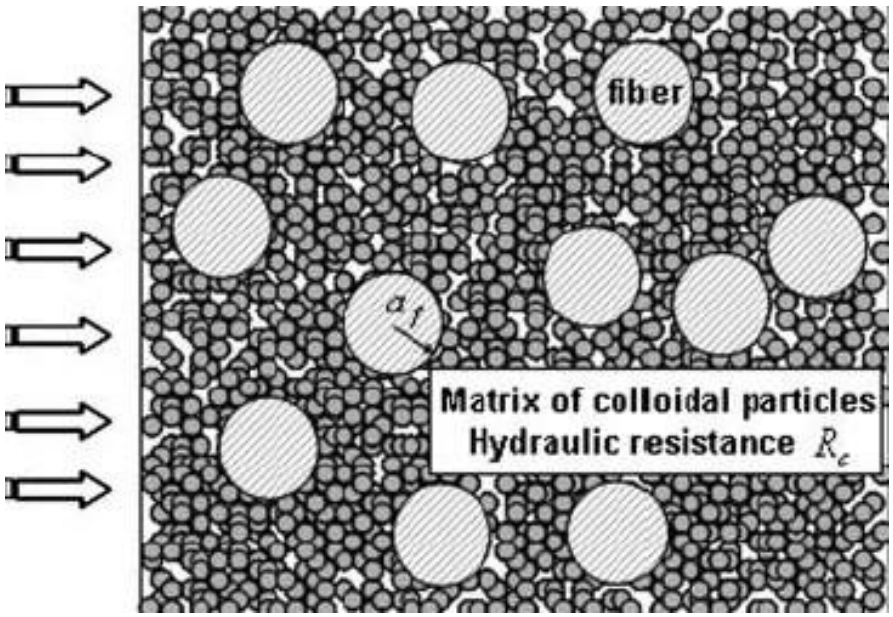

Figure 2-8 Schematic of a cross-sectional view of colloid-fiber porous matrix (Wang and Tarabara, 2009)

Apart from the Kozeny-Carman relationship, there are other models of permeability, which are reviewed below.

At low Reynolds number, in order to obtain a scaling estimate for permeability in term of cylinders arrays with the fixed axes perpendicular to the direction of flow (see Figure 2-9), Clague et al. (2000) presented a very simple calculation for the known Stokes flow formulas.

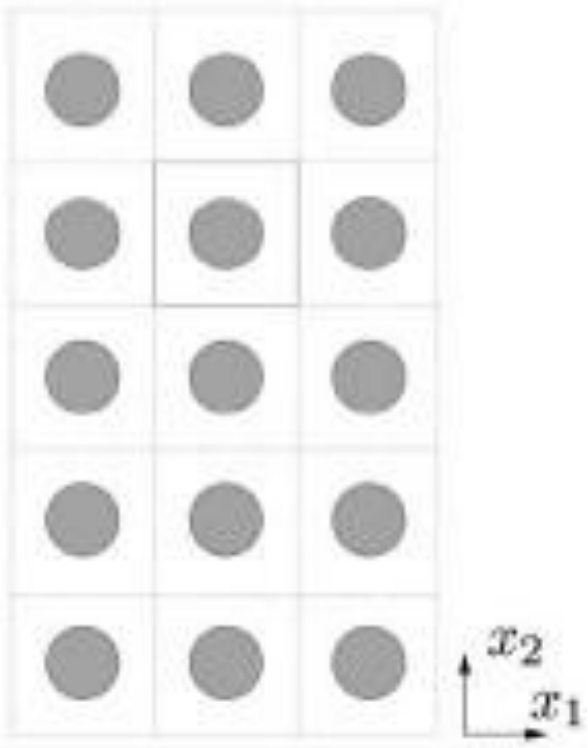

Figure 2-9 The regular array of fiber cylinders with the fixed axes perpendicular to the direction of flow (Clague et al., 2000)

Based on the continuity equation, the simple scaling analysis can be expressed as (Clague et al., 2000)

$$\nabla \cdot U = 0 \qquad (2\text{-}7)$$

Stokes flow equations:

$$\mu\nabla^2 U - \nabla p = 0 \tag{2-8}$$

Making a half distance (δ) between the two adjacent fiber cylinders as the feature length with geometry scale over which quick variations of the physical velocity appear in both the x_1 and x_2 geometry directions, and making $\overline{U}$ as the feature velocity, they obtained following characteristic scaling equation for the Stokes flow in fibrous porous media:

$$\nabla p \sim \mu \frac{\overline{U}}{\delta^2} \tag{2-9}$$

By inserting Eq. (2-1) (Darcy's Law) into Eq. (2-9), a relationship between the permeability and the half distance between the fiber cylinders can be found:

$$K = c_1 \delta^2 \tag{2-10}$$

where, c_1 is the proportionality constant. Although Eq. (2-10) provides a simple physical description of the geometric dependences of permeability, it is not a rigorous relationship.

Based on Eq. (2-10), to obtain the dimensionless permeability for the regular cyclical square array in porous fibrous media, the diagram representation of a calculative unit cell for a cyclical square array is presented in Figure 2-10 (Sobera & Kleijn, 2006).

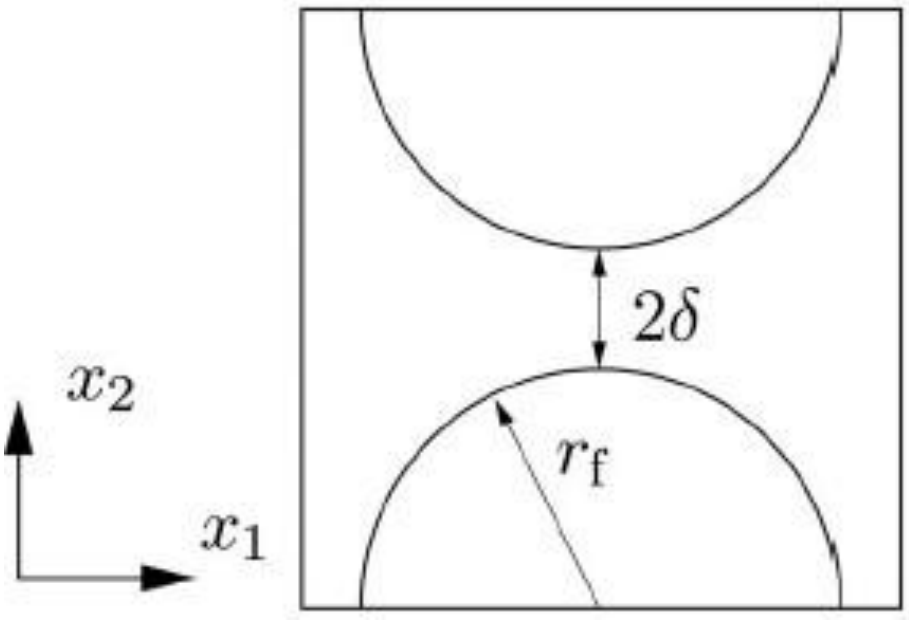

Figure 2-10 Schematic of a calculative unit cell for a regular cyclical square array of unanimously distributed fiber cylinders. The flow direction is in the x_1 geometry direction (Sobera & Kleijn, 2006)

In Figure 2-10, r_f is the average fiber radius ($r_f = D_f / 2$), so the porosity can be expressed as

$$1-\phi = \frac{\pi(D_f/2)^2}{(D_f+2\delta)^2} \tag{2-11}$$

The fixed half distance between the two fiber cylinders in the regular cyclical array can be obtained with the aid of Eq. (2-11)

$$\delta = \frac{D_f}{2}\left(\frac{1}{2}\sqrt{\frac{\pi}{1-\phi}}-1\right) \tag{2-12}$$

By inserting Eq. (2-12) into Eq. (2-10), so the dimensionless permeability for the regular cyclical array in porous fibrous media can be written as:

$$\frac{K}{D_f^2} = \frac{c_1}{4}\left(\frac{1}{2}\sqrt{\frac{\pi}{1-\phi}} - 1\right)^2 \qquad (2\text{-}13)$$

Although Eq. (2-13) shows a good estimation for permeability in the dilute (high ϕ) area, it gives very poor prediction in the dense (low ϕ) area. The superficial fluid velocity ($\overline{U}$) is chosen as velocity scale, leading to the above consequence.

Besides, Drummond and Tahir (1984) predicted the permeability of real disordered layered fibrous structures using Stokes equations, viz.

$$\frac{K}{D_f^2} = \frac{\{-\ln(1-\phi) - 1.476 + 2(1-\phi) - 1.774(1-\phi)^2 + O[(1-\phi)^2]\}}{32(1-\phi)} \qquad (2\text{-}14)$$

Using lattice Boltzmann method (LBM), Jackson and James (1986) calculated the permeability of porous fibrous materials based on cubic lattice method, viz.

$$\frac{K}{D_f^2} = \frac{3[-\ln(1-\phi) - 0.931]}{80(1-\phi)} \qquad (2\text{-}15)$$

The cubic lattice method by Jackson and James (1986) may be only valid in the specific dilute limit area ($\phi \geq 0.75$).

Based on Eq. (2-15), Stylianopoulos et al. (2008) studied the hydraulic permeabilities of fiber networks (see Figure 2-11). Figure 2-12 displays the streamlines for the fluid flow through the isotropic fiber network (Stylianopoulos et al., 2008). In Figure 2-12, the flow paths of fluid are tortuous when the fluid goes through the fibres.

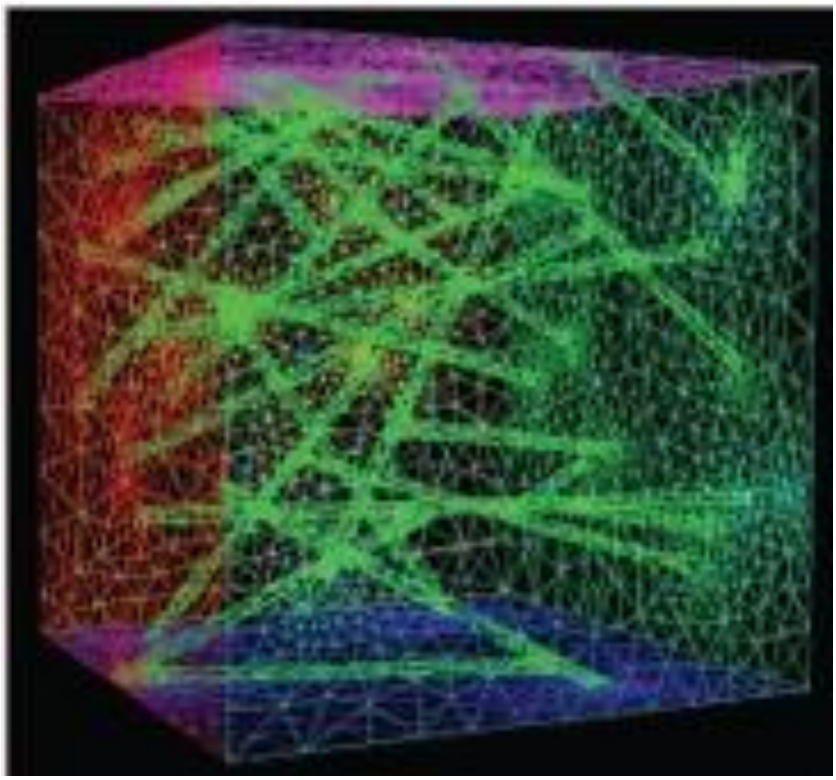

Figure 2-11 A schematic of fiber networks (Stylianopoulos et al., 2008)

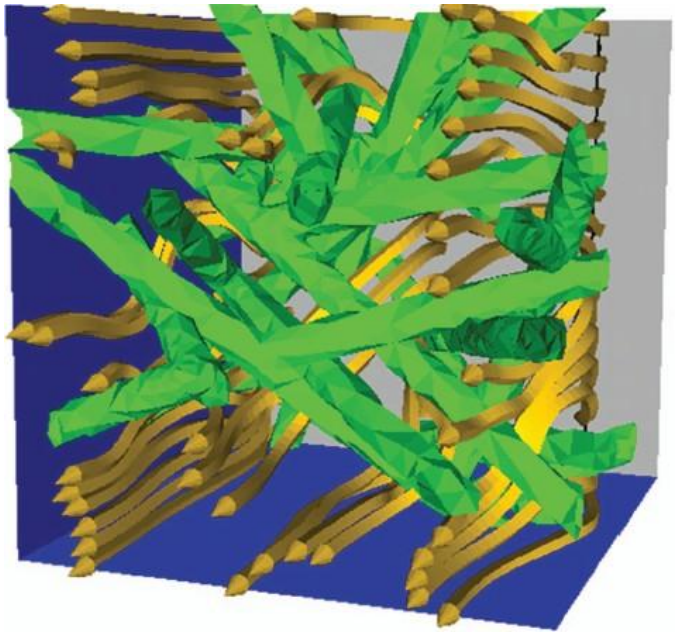

Figure 2-12 The geometry streamlines for the fluid flow via the specific isotropic fibre network (Stylianopoulos et al., 2008)

Gebart (1992) presented a combined experimental, numerical and theoretical study for the permeability of regular fiber arrays:

$$\frac{K}{D_f^2} = C_2(\sqrt{\frac{1-\phi_c}{1-\phi}} - 1)^{2.5} \tag{2-16}$$

where ϕ_c is the critical data of the porosity under which there is no permeating or diffusing flow and C_2 is the geometric structure factor (for a square array, $C_2 = 64/9\sqrt{2}\pi$ and $\phi_c = 1-\pi/4$; for a hexagonal array, $C_2 = 64/9\sqrt{6}\pi$ and $\phi_c = 1-\pi/2\sqrt{3}$).

However, Eqs. (2-14)-(2-16) contain several empirical constants which are only valid under given assumptions.

Based on lattice Boltzmann method, a model of the dimensionless permeability of 3D random fiber webs was derived (Koponen et al., 1998):

$$\frac{K}{D_f^2} = \frac{A}{4[e^{B(1-\phi)} - 1]} \tag{2-17}$$

In Figure 2-13, a sample was created by the lattice Boltzmann algorithm (Koponen et al., 1998). The result showed that the permeability depended exponentially on the porosity over a wide scope of porosity (Koponen et al., 1998). The calculated permeability of the fiber web could be found to be in good agreement with the available experimental results, when two empirical constants *A*=5.55 and *B*=10.1 were given (Koponen et al., 1998). The authors acknowledged that they had no theoretical arguments to support their above model (Koponen et al., 1998).

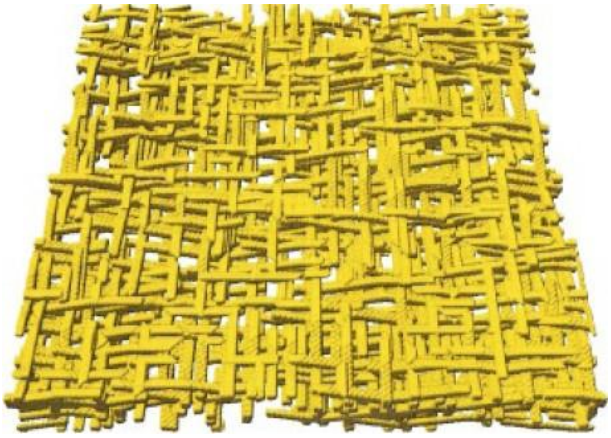

Figure 2-13 The sample of fiber web structured with the specific deposition geometry model (Koponen et al., 1998)

According to electrical conduction principles, the permeability for the specific viscous flow through mixed and disorderly fibre frameworks used as the fibre preforms in mixed manufacture procedures was studied (Tomadakis and Robertson, 2005). The more comprehensive equation to calculate dimensionless permeability in specific in-plane and through-plane geometry directions for optionally overlapping fibre constructions based on random-walk simulation was derived (Tomadakis and Robertson, 2005)

$$\frac{K}{D_f^2} = \frac{\phi(\phi-\phi_p)^{\alpha+2}}{32(\ln\phi)^2(1-\phi)^{\alpha}[(\alpha+1)\phi-\phi_p]^2} \tag{2-18}$$

where ϕ_p and α are two empirical constants. In Eq. (2-18), ϕ_p is the fixed percolation threshold of fibrous materials and α depends on the fluid flow direction and the geometry structure of fibrous materials. Tomadakis and Robertson (2005) obtained that $\phi_p = 0.11$ regardless of fluid flow direction, and $\alpha = 0.521$ and

$\alpha = 0.785$ for the specific in-plane and through-plane geometry directions, respectively.

Shou et al. (2010) applied a mathematics approach including difference and fractal to study the permeability of porous fibrous materials, and they established the following relationship:

$$\frac{K}{D_f^2} = \frac{\pi}{6.376}\frac{\phi(\phi-0.11)^{0.785}}{1-\phi}(1+\frac{\pi}{2\ln\phi})^2\frac{2-d_f}{4-d_f}(\frac{d_f-1}{d_f})^2 \qquad (2\text{-}19)$$

where d_f is the area fractal dimension of pores, and D_T is the tortuosity fractal dimension. The validity of proposed model (Shou et al., 2010) was verified by experimental data. However, the model did not consider the effects of tortuosity fractal dimension (D_T) on permeability. Actually, most flow paths are tortuous, which implies the importance of tortuosity fractal dimension on mass transport through porous fibrous media. Besides, Shou et al. (2010) used several empirical constants (viz. 6.376 and 0.785) in Eq. (2-19).

Furthermore, using Darcy's Law, Tamayol and Bahrami (2010) proposed an approach for calculating the specific parallel permeability of square fiber arrangements:

$$\frac{K}{D_f^2} = \frac{[-1.479-\ln(1-\phi)+2(1-\phi)-0.5(1-\phi)^2-0.0186(1-\phi)^4]}{16(1-\phi)} \qquad (2\text{-}20)$$

Although Eq. (2-20) was in good agreement with several collected experimental data, the proposed model (Tamayol and Bahrami, 2010) held only to square fiber arrangements. Besides, Eq. (2-20) contains several empirical constants.

2.3 Diffusion

Diffusion of gas through porous fibrous materials is of importance in many practical applications such as apparel, face masks, and gas diffusion layers of fuel cells. Diffusion can be modeled by Fick's Law, which can be described as follows:

$$J = -D_e \nabla C \tag{2-21}$$

where, D_e is the effective diffusion coefficient, J is the diffusive mass flux, ∇C is the concentration gradient, and C is concentration.

Combing Eq. (2-21) with the mass balance equation yields

$$\frac{\partial C}{\partial t} + \nabla J = 0 \tag{2-22}$$

where t(s) is time. If the diffusion coefficient is constant, Eq. (2-22) can be reduced to

$$\frac{\partial C}{\partial t} = D_e \nabla^2 C \tag{2-23}$$

2.3.1 Experimental measurements

A lot of experiments have been used to predict the diffusivity of fibrous porous media. Figure 2-14 shows the experimental apparatus used to measure oxygen diffusivity (Utaka et al., 2009). A specific underprop for controlling the fibrous porous specimen to be tested is installed to a fixed oxygen sensor of galvanic cell, making up of a common metal anode, an expensive metal cathode, a special electrolyte and a fixed gas diffusing membrane. The test results showed that the diffusivity in fibrous microporous media couldn't be estimated on the basis of the

porosity of fibrous porous media alone, but that it might be affected by several factor including the tortuosity (Utaka et al., 2009).

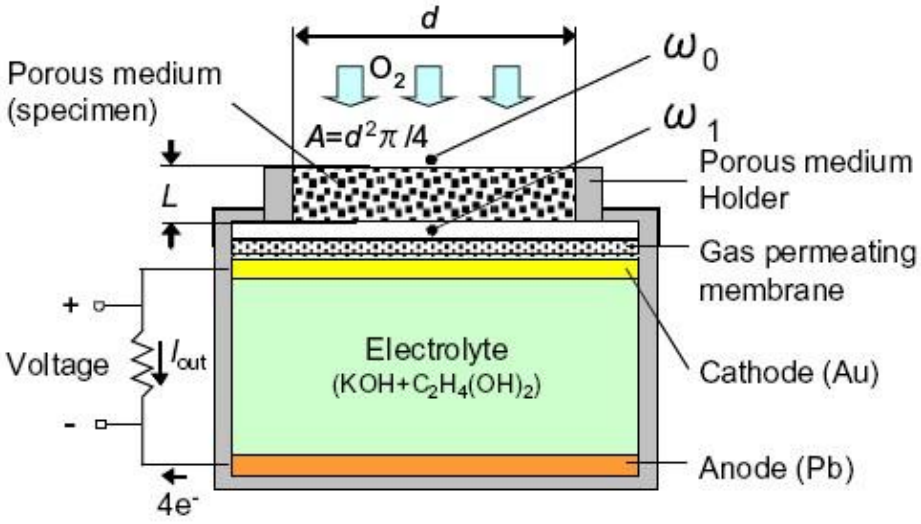

Figure 2-14 A schematic of experimental apparatus for measuring oxygen diffusivity (Utaka et al., 2009)

In Figure 2-15 and 2-16, a special cell apparatus was used to test the effective diffusion coefficient of porous carbon paper in gas diffusion layer (Zamel et al., 2010). Ant the effects of porosity and the operating temperature on effective diffusion coefficient were studied in the special experiment (Zamel et al., 2010). Figure 2-15 is an experimental apparatus of diffusion cell which consisted of two chambers (Zamel et al., 2010). After deriving the effective diffusion coefficient, the gas resistance net works presented in Figure 2-16 can be used to obtain the equivalent diffusion coefficient in the special samples of porous TORAY carbon paper (Zamel et al., 2010). Figure 2-17 represents the vapor diffusion case, where the gas phase can be transported through a special domain which is a porous substrate (Li et al., 2011). The gas transport as shown in Figure 2-17 is the 1-D transport with the concentration

constant of vapor over the crosssection (Li et al., 2011). So the vapor concentration can be determined at the wall of the domain undisturbed by porous substrate particles (Li et al., 2011). From testing mass flux gravimetrically and the known concentration gradient of gas, the gas effective diffusion coefficient through the special wet and dry sand was estimated in the above experiment (Li et al., 2011).

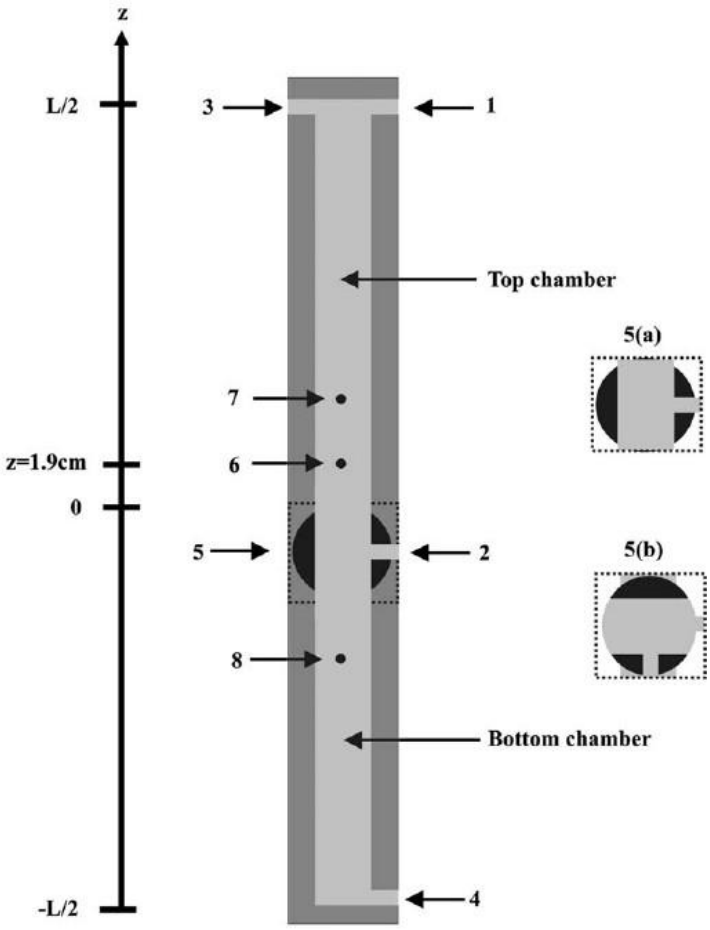

Figure 2-15 A schematic of the special diffusion cell-1: the inlet of gas 1; 2: the in let of gas 2; 3 and 4: the outlets of gas; 5: the special ball valve; 5(a): the fixed open position of valve; 5(b): the fixed closed position of valve; 6: the special oxygen sensor; 7 and 8: humiditysensors (Zamel et al., 2010)

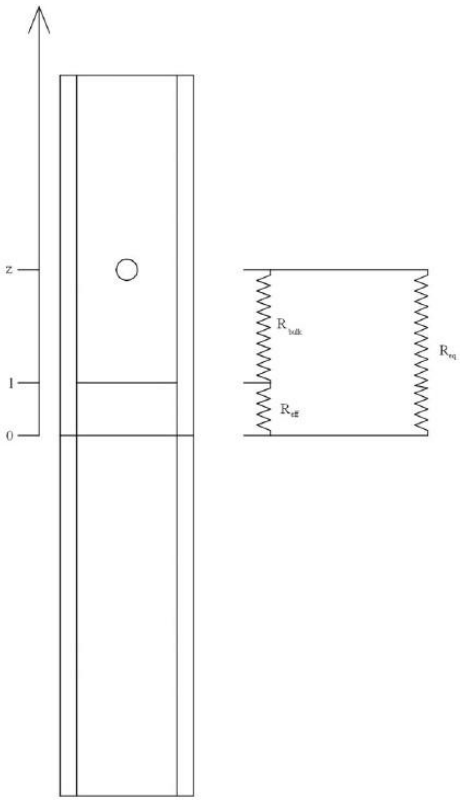

Figure 2-16 The gas resistance net because of diffusion and the special samples of porous TORAY carbon paper (Zamel et al., 2010)

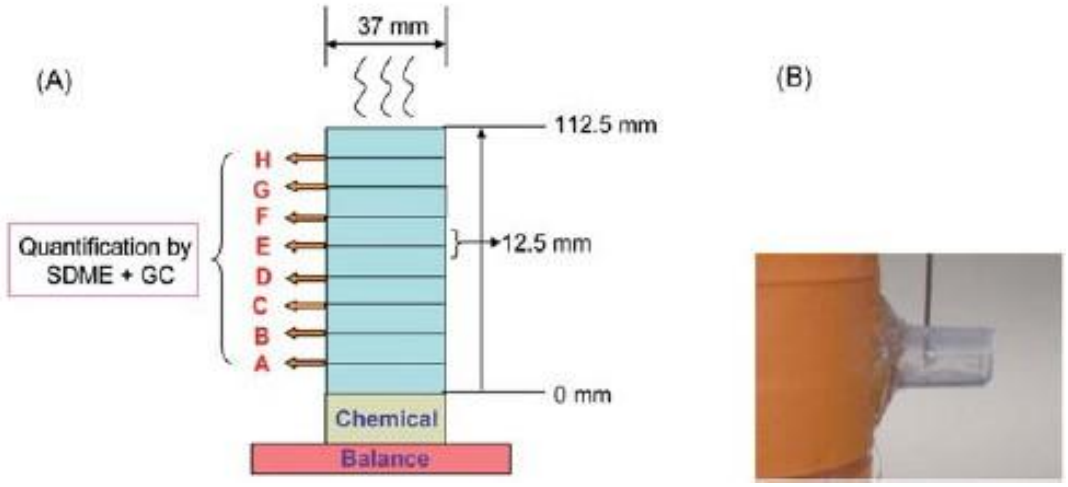

Figure 2-17 (A) A test setup for the diffusion of vapor, (B) The special sample (Li et al., 2011)

Besides, Bartelt-Hunt and Smith (2002) measured effective diffusion coefficients for trichloroethene in undisturbed soil samples. Furthermore, an experimental investigation of diffusivity in the polymer electrolyte fuel cells was developed (Flückiger et al., 2008). It was found that the fibrous gas diffusion layer plays a significant role for the special electrochemical losses because of the fixed limitations of gas transport at large present densities (Flückiger et al., 2008).

2.3.2 Numerical simulations and theoretical models

Many theoretical models and numerical methods have also been developed to investigate the physical mechanism of diffusion in porous media.

Monte Carlo methods are quite useful for simulating the transport properties of porous media. Effective diffusion coefficients were simulated by Monte Carlo techniques based on the average square distance of optional walkers going in the inside of fibrous porous media (Tomadakis and Sotirchos, 1993a). It was found that the effective diffusivity depended on the Knudsen number, the porosity of fibrous porous media, and the orientational distribution of the capillaries (Tomadakis and Sotirchos, 1993a). The results of extensive Monte Carlo numerical simulation of gas diffusion in disordered media with long-range correlations were also presented (Saadatfar and Sahimi 2002). Besides, taking into account the influence of the physical roughness of pore surface on the Knudsen diffusion, Knudsen self-diffusion in the micro nanoporous media was studied by using mathematical analytical

computes and Monte Carlo methods (Malek and Coppens, 2003). In addition, for Knudsen numbers of 10^{-3}-10^{10}, the effective diffusivities were computed by using Monte Carlo numerical simulation (Zalc et al., 2004). The results showed that tortuosity of capillaries were independent of diffusion mechanism for all pores fractions when the equivalent Knudsen diffusivity was accurately defined (Zalc et al., 2004). Apart from Monte Carlo simulations, the diffusion mechanisms of moisture into the hygroscopic porous fabrics during the humidity transients were investigated by a mathematical simulation (Li and Luo, 2000).

The fractal techniques are also quite useful for estimating the transport properties of fibrous porous media. Diffusion coefficients in microporous solids were calculated from structural parameters based on fractal geometry (Schieferstein and Heinrich, 1997). It was shown that the calculation of diffusion coefficients in microporous solids from structural data was possible in literature (Schieferstein and Heinrich, 1997). Taking into account the effect of the Knudsen, the oxygen effective diffusivity of fibrous GDL in PEMFC for both the wet and dry environments was determined by fractal techniques (Wu et al., 2011). The results showed that the Knudsen had a significant influence on the oxygen transport through the fibrous GDL (Wu et al., 2011). And taking into account the specific phase changes and the water vapor diffusion, according to the fractal distribution of pores an effectual mathematical model for the coupled heat and mass transfer was obtained in porous fibrous materials (Zhu et al., 2011). Besides, the influences of the porosity on the heat and mass transfer were also investigated in fibrous porous media (Zhu et al., 2011).

Furthermore, considering the effect of rarefied gas in porous media, a fractal model for gas diffusivity was obtained (Zheng et al., 2012). Apart from the Monte Carlo methods and fractal techniques, the network models can also be used to determine the effective diffusivity of the fibrous porous media. Using the network model for the several species diffusion, the effective diffusivity was predicted as a function of the porosity and water saturation in fibrous porous media (Nam and Kaviany, 2003). Taking into account the influence of the pore size distribution and connectivity on effective diffusion coefficient of the optional porous media, a classical model of 3-D bond pore network was developed (Mu et al., 2008). It was found that the effective diffusion coefficient of the fibrous porous media strongly depended on the pore size when average pore size was less than $1\mu m$ (Mu et al., 2008). Additionally, a three-dimensional network which was made up of the special spherical pores and the fixed cylindrical throats was developed and used to study the effect of geometry structural parameters of GDL on the oxygen effective diffusivity using Fick's law (Wu et al., 2010).

Apart from the classical fractal models and network models, there are other models of diffusion in porous media, which are reviewed below. Considering the sorption mechanisms of water vapor in wool fiber, an improved mathematical model was derived for gas diffusion (Li and Luo, 1999). The formula of calculating diffusion coefficient was used to depict and estimate coupled the moisture and heat transport through wool fabrics (Li and Luo, 1999). In order to elucidate the properties of the special drying-rate curve of the fibrous porous media, a microscopic geometry model

for the special drying was derived considering random-walk diffusion (Mehrafarin and Faghihi, 2001). The constant drying-rate time could be considered as a common diffusion procedure (Mehrafarin and Faghihi, 2001). Besides, the water saturation distribution was calculated by applying a 1-D description of the special condensation kinetics of the water vapor, the special species mass diffusion, and the capillary movement of the fixed condensate in the special hydrophobic porous fibrous materials (Nam and Kaviany, 2003). In addition, a comprehensive review of the available equations for the measured diffusion coefficient with the tortuosity of porous fibrous materials, the fixed sensitivity tests with the analytical methods was presented (Shen and Chen, 2007). The double diffusion around a special horizontal cylinder of the elliptic intersecting surface with well-proportioned wall fluxes of heat and mass was also investigated in the common porous medium (Cheng, 2011). Furthermore, a quick and reliable method was obtained, which was used to predict the vapor concentration in the fibrous porous substrate (Li et al., 2011). For the dry medium grain sand, the effective diffusion coefficient of n-pentane was measured by the mentioned technique (Li et al., 2011). Recently, Shou et al. (2013) presented a mathematical model to calculate the effective diffusivities in porous fibrous materials including 1D, 2D and 3D fibre assembles. Besides, the effects of the special orientation of fibre, the porosity, and fiber distribution were also analysed (Shou et al., 2013).

2.3.3 Existing models of gas diffusion through fibrous porous media

Various diffusion models through fibrous materials have been proposed by past researchers. Considering the effect of porosity (ϕ) and tortuosity (τ), the effective diffusivity (D_e) is directly connected with the free diffusivity (D_b), given by a normalized form (Tomadakis and Sotirchos, 1993b), viz:

$$\frac{D_e}{D_b} = \frac{\phi}{\tau} \tag{2-24}$$

For diffusion around cylindrical fibers, an equation to calculate the effective diffusivity in fibrous porous media was derived (Nilsson and Stenstrom, 1995):

$$\frac{D_e}{D_b} = \frac{\phi}{2-\phi} \tag{2-25}$$

However, Eq. (2-25) is only valid in the dilute fibrous porous media (Falla et al., 1996).

For gas transport through one-dimension compact cylinders with the special square packing structure in porous fibrous materials, Shen and Springer (1981) estimated the effective diffusivity:

$$\frac{D_e}{D_b} = 1 - 2\sqrt{\frac{1-\phi}{\pi}} \tag{2-26}$$

Now Eq. (2-26) was commonly used to estimate the effect of the diffusion of water vapor on the physical mechanical properties of the common composites.

Using effective medium approximation, gas transport through the fibrous GDL in PEMFCs was investigated based on the Bruggeman model (Pharoah et al., 2006):

$$\frac{D_e}{D_b} = \phi^{1.5} \tag{2-27}$$

But the common Bruggeman relation was obtained for the well-distributed spherical particles rather than abnormal cylindrical fibers. The validity of Bruggeman relation applied to porous fibrous materials was questionable.

Using Monte Carlo simulations, Tomadakis and Sotirchos (1993b) predicted the effective diffusivity of the special chemical species in the packing of superposition fibers randomly distributed in the fixed plane:

$$\frac{D_e}{D_b} = \phi\left(\frac{\phi-\phi_p}{1-\phi_p}\right)^{\alpha} \tag{2-28}$$

where ϕ_p and α are the special constants determined by the geometrical rank of porous fibrous materials, which are given by Eq. (2-18).

Although a variety of correlations and models for gas diffusion through porous fibrous materials has been proposed, there is still much controversy in determining the diffusion coefficient of porous fibrous materials. So, comprehensive and unified models are still desirable for diffusion in fibrous porous media.

2.4 Heat transfer

In thermodynamics, heat can be defined as the transfer of heat energy through the well-defined boundary round the special thermodynamic system. Besides, the heat is always accompanied by the entropy transfer. The well known second law of thermodynamics indicates that the heat always flows through the boundary of a system in the special direction of the fixed falling temperature. Heat transfer in fibrous porous media is the reflection of the details of fibrous porous structure. Furthermore, heat transfer is estimated by the physical mechanisms of the basic transport procedures within the distrinct phases of fibrous porous media and thermal exchange in a interface. Heat transfer can be classified into different mechanisms including the heat conduction, the convective heat transfer and the radiative heat transfer. Heat transfer by convection occurs because of motion of fluid within the common pores in porous fibrous materials. Convective heat transfer can be neglected for small sizes of pore ($<100\mu m$) at lower temperatures (<373 K) in fibrous porous media because of lack of intensive fluid-circulation within the pores under weak wind (Olives and Mauran, 2001). Thermal radiation occurs because of the scattering of radiation and the absorption emission by the pores wall in porous fibrous materials. At low temperature, radiative heat transfer is very low and can be neglected in the special refractory fiber materials of alumina-silicate (Xia et al., 2010). However, radiative heat transfer plays an important role and should be considered at high temperature (Xia et al., 2010; Xie et al., 2013).

Heat transfer is important in wide fields of engineering and sciences. For example, clothing has protective functions, which can provide warmth when the human body interacts with external environment. Figure 2-18 shows a clothing system containing a single layer of porous textile material (Xu et al., 2011).

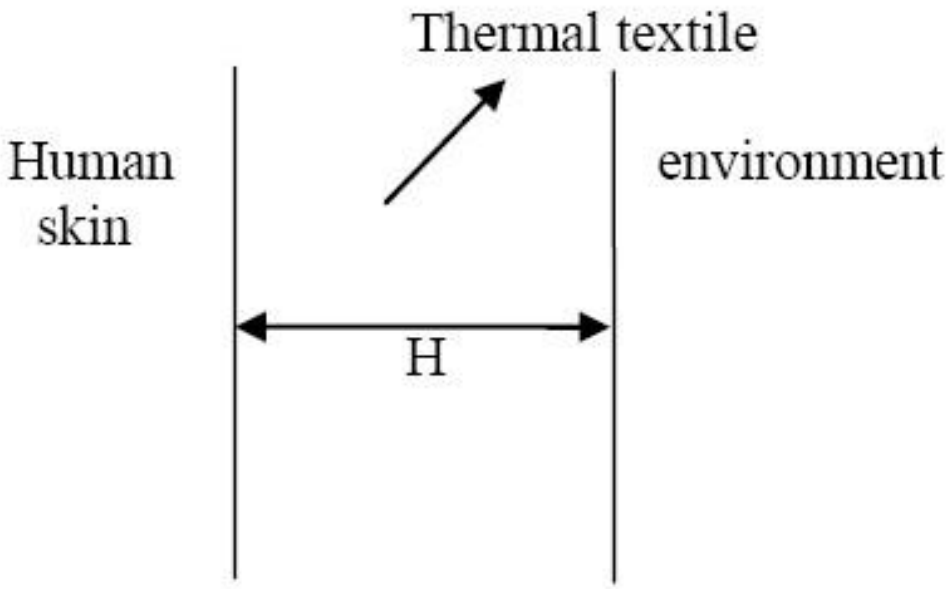

Figure 2-18 A clothing system containing a single layer of porous textile material (Xu et al., 2011)

2.4.1 Heat conduction and effective thermal conductivity

Heat conduction is the transfer of energy between near molecules in an object as a result of temperature gradient. Regions with more kinetic energy of molecules can pass the heat energy to areas with the less kinetic energy of molecules via direct molecules impact, the procedure known as the heat conduction. The above process is similar to the physics mechanism of diffusion. Note heat conduction can occur in

solids, fluids and gases. In metals, an important part of the transported heat energy can be taken by the free electrons. However, the heat conduction is the only process of energy transfer in solids in which heat cannot transmit through convection and radiation. In fluids and gases, heat conduction is superimposed on convection and radiation in the energy transport.

The rate at which thermal energy is transmitted through an object is proportional to the contact area common to the flow of heat and to the temperature gradient through the path of the flow of heat. Its most general form for multidimensional conduction can be given by the well known Fourier's law

$$q_h = -k \cdot \nabla T \tag{2-29}$$

where k is the thermal conductivity, q_h is the heat flux, ∇T is the temperature gradient and T is the temperature. Eq. (2-29) is analogous to the well known Darcy's law in gas flow and Fick's law in the gas diffusion.

Another inherent thermal property of a material is the thermal resistance (R_h) which is defined by

$$R_h = A_{ca} \frac{\Delta T}{Q_h} \tag{2-30}$$

where Q_h is rate of heat flow, A_{ca} is contact area, and ΔT is temperature difference.

Heat conduction in porous fibrous materials is extremely complicated. Generally speaking, the effective thermal conductivity of porous fibrous materials depends on several factors including the thermal properties of every phase,

distribution of pores, the volume fraction of fibre, the fiber size and the specific orientation of fibre .

2.4.1.1 Experimental measurements of the effective thermal conductivity

Many experiments are used to test the effective thermal conductivity of the fibrous porous media. Figure 2-19 displays the picture of the steady state test setup (Daryabeigi, 1999). The effective thermal conductivity of the fixed Q-fibre test sample with a large temperature difference maintained across the sample thickness was measured by the thermal steady state test (Daryabeigi, 1999). The main framework of the testing apparatus is made up of an Inconel septum plate, test specimen, a quartz lamp radiant heater array, a water cooled plate, and refractory ceramic board insulation. The heat flux and temperature were measured by the water-cooled plate which was equipped with nine thin film heat flux gages. The septum plate was equipped with 23 metal-sheathed Type K thermocouples, and was heated by the radiant heater array. Actually, most porous fibrous materials may be a two-phase system with solid and gas composition. For fibrous porous media such as fabrics, where the multiphase renders the heat equalizing process unstable and slow, the above steady state test methods may be noneffective and even wrong. Among thermal unsteady test methods, transient test method may be the most preferred in which a thermal disturbance is imposed at a designated place of the measured porous

fibrous material (Lei et al., 2010). Besides, the thermal response to the perturbation can be recorded in another given place. Thus, the corresponding parameters of thermal properties can be obtained by using the established theoretical law. Figure 2-20 shows the working principle for the stepwise transient method (Lei et al., 2010). The test apparatus are also shown in Figure 2-21 (Lei et al., 2010). The testing apparatus are made up of two plates with guard-bars. The temperature response of sample can be measured and recorded by a computer data acquisition module through the temperature sensor placed inside the sample in the test apparatus. The heat conduction in fibrous porous media consisted of highly conductive fibres and put in a poorly conductive matrix was also measured above the percolation threshold (Vassal et al., 2008). The porous fibrous materials of isotropic conductivity are shown in Figure 2-22 (Vassal et al., 2008). In addition, Mangal et al. (2003) tested the effective thermal conductivity of the pineapple leaf fibre with special reinforced phenolformaldehyde composites using the transient flat surface source method. The influence of fibre surface case on thermal conductivity of the natural fibre composite was investigated experimentally (Kim et al., 2006). Furthermore, Behzad and Sain (2007) measured the in-plane and the transverse thermal conductivities of the hemp fibre reinforced composites using a simple method. The experimental results (Behzad and Sain, 2007) showed that fiber direction had a significant effect on the thermal conductivity of the special fibre reinforced composites. Besides, Li et al. (2008) measured thermal conductivity of natural fiber-plastic composites based on the

line-source technique. However, the influence of the fibre orientation on the thermal conductivity was not analyzed in the experiment (Li et al., 2008).

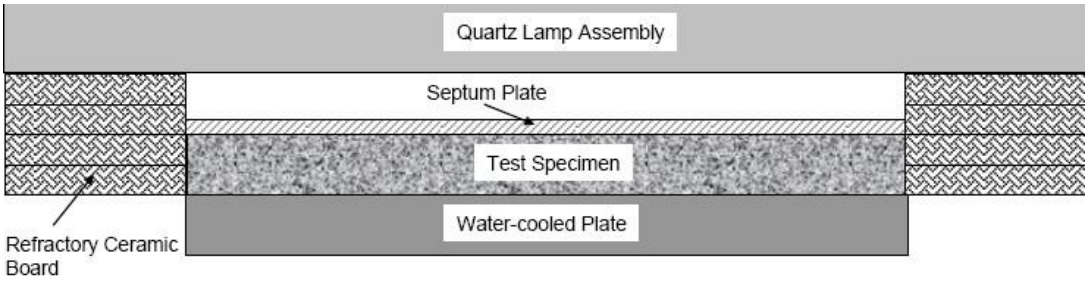

Figure 2-19 Schematic of thermal steady state test setup (Daryabeigi, 1999)

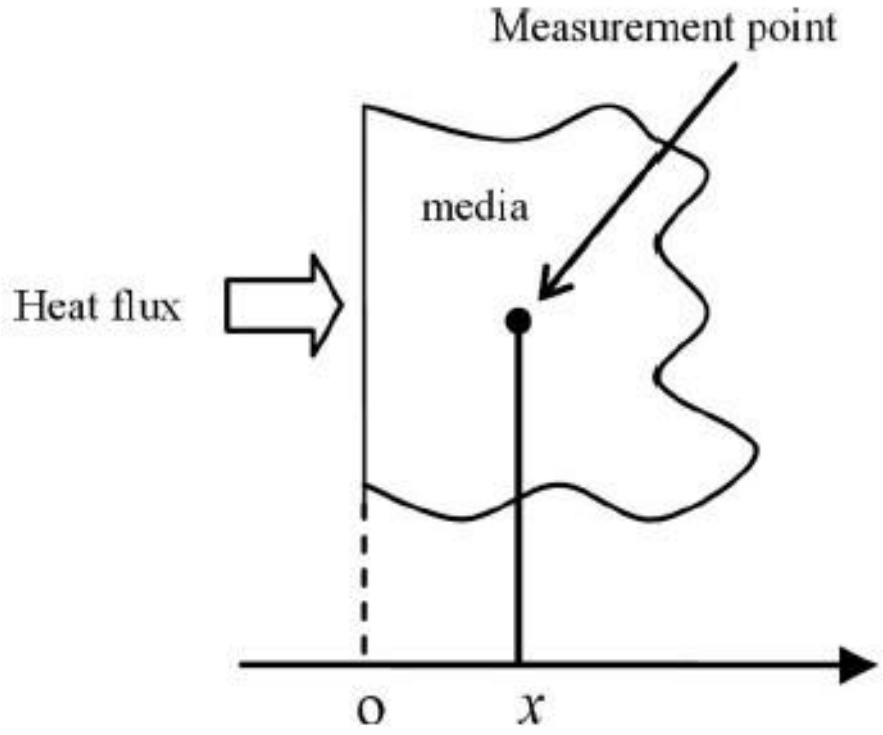

Figure 2-20 Working principle of stepwise transient method (Lei et al., 2010)

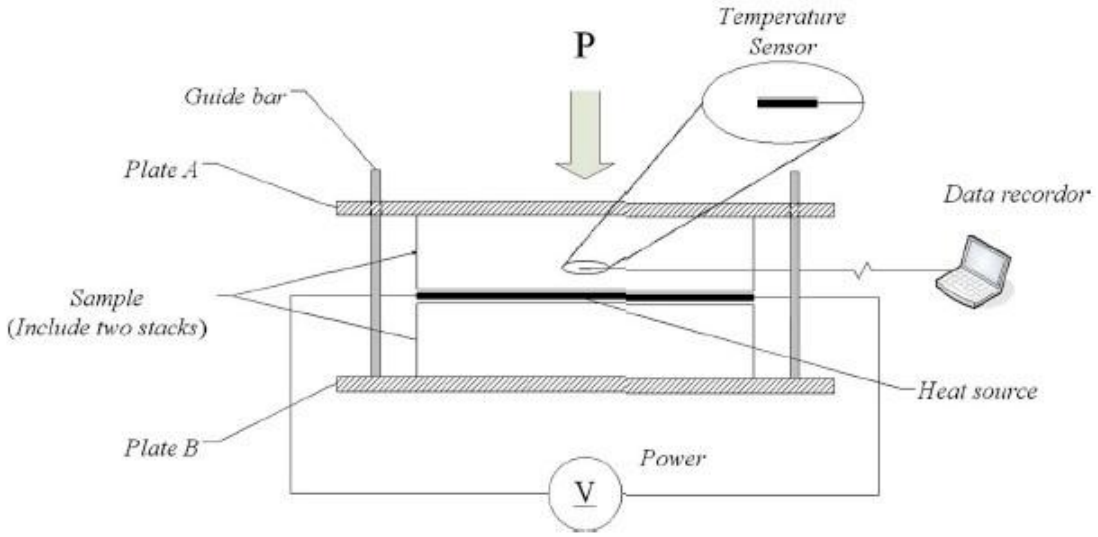

Figure 2-21 Schematic of stepwise transient test apparatus (Lei et al., 2010)

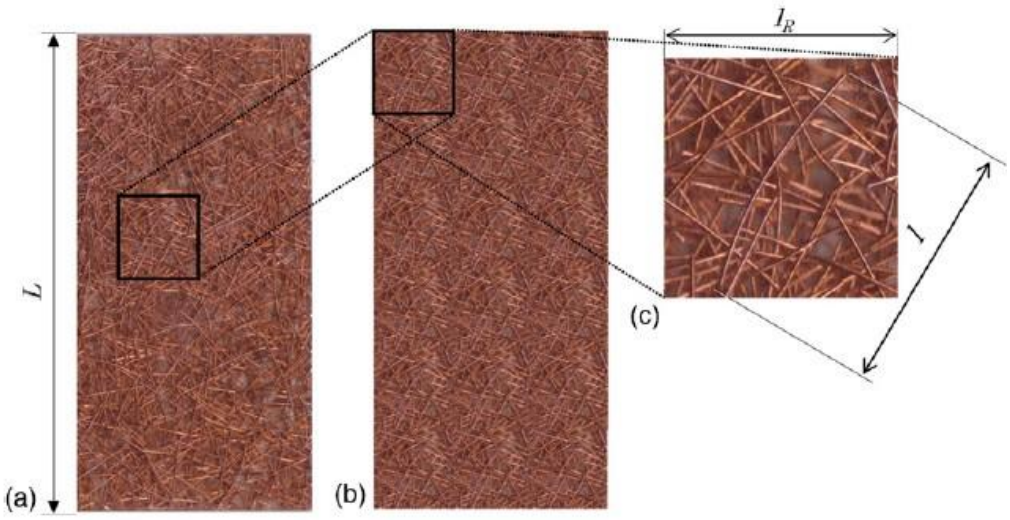

Figure 2-22 The composite material is consisted of conductive copper fibres put into a PMMA matrix (Vassal et al., 2008)

The heat transfer through fibrous GDL is a very key procedure for the special design and optimization of PEMFCs. The effective thermal conductivity of the fibrous GDL used in the PEMFCs is also a very key parameter for quantitative analysis of the heat transfer in the membrane electrodes assembly. The effective thermal conductivity of the fibrous GDL in the PEMFCs was measured (Ramousse et al., 2008). The

samples were placed in between two fixed copper plates. The test apparatus (Ramousse et al., 2008) are shown in Figure 2-23. The experimental investigation was performed to test the in-plane effective thermal conductivity of fibrous GDL based on parallel thermal conductance method (Teertstra et al., 2011). Figure 2-24 shows the experimental equipment for the in-plane thermal conductivity measurements (Teertstra et al., 2011). In addition, Sadeghi et al. (2011) tested in-plane effective thermal conductivity of GDL for the different polytetrafluoroethylene contents using a new thermal measurement technique. Toray-120 carbon papers with polytetrafluoroethylene content of 5-30% were used in the experiments. Figure 2-25 shows the test equipment for the measurement of in-plane thermal conductivity (Sadeghi et al. 2011). The test chamber is made up of a special metal bed and a fixed bell jar enclosing the experimental column.

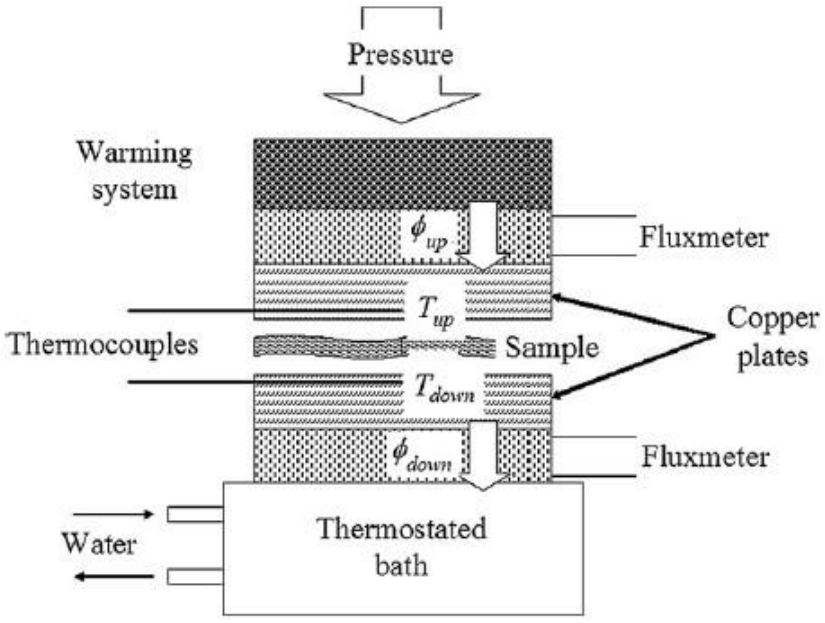

Figure 2-23 A schematic of experimental apparatus (Ramousse et al., 2008)

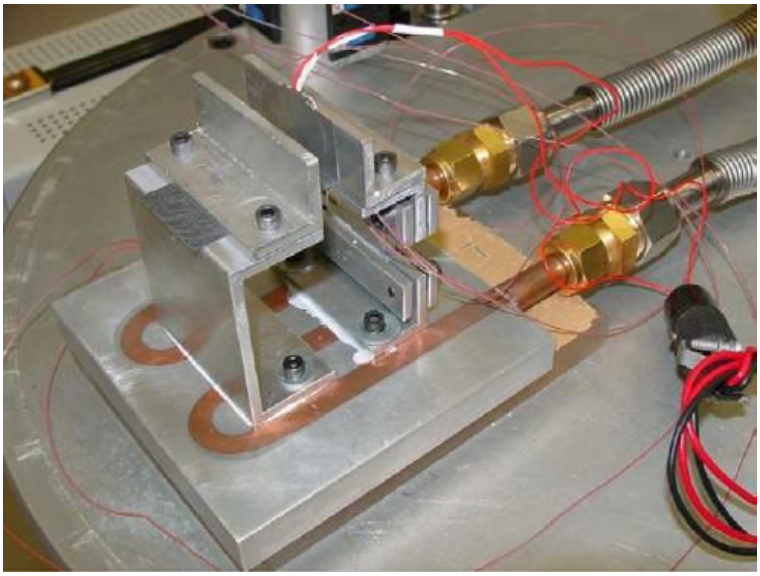

(A)

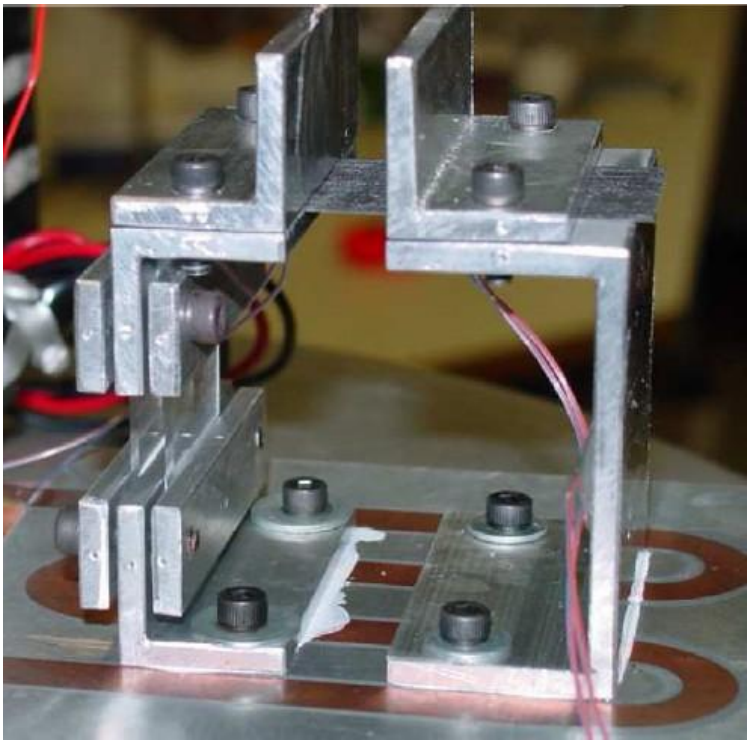

(B)

Figure 2-24 Experimental test apparatus for the in-plane thermal conductivity measurements based on parallel thermal conductance method (Teertstra et al., 2011)

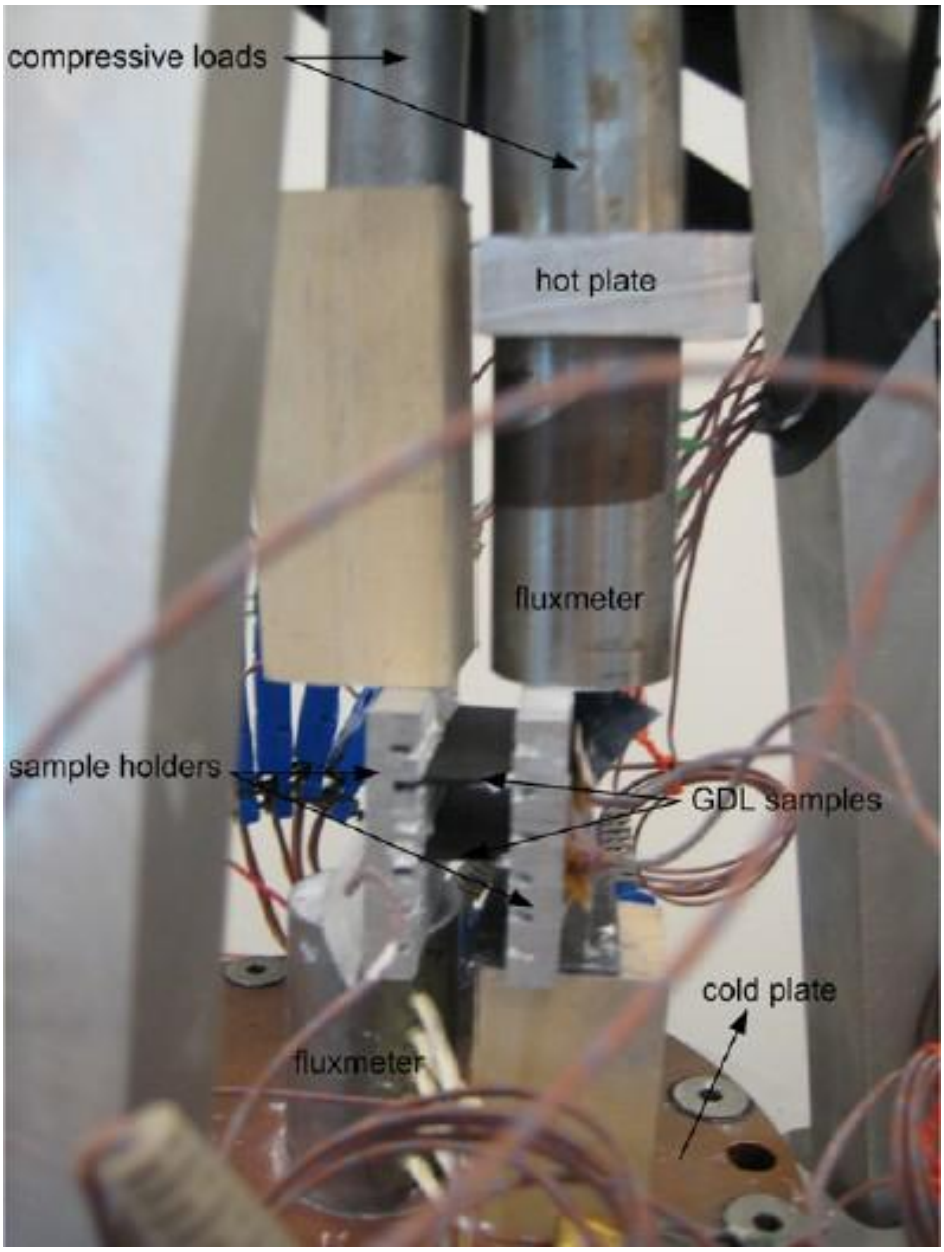

Figure 2-25 Experimental test apparatus for measuring the special in-plane thermal conductivity (Sadeghi et al. 2011)

2.4.1.2 Theoretical investigations of effective thermal conductivity

Generally speaking, the special parallel model and series model are used to calculate the thermal conductivity of the fibrous porous media for a two-phase system.

Using parallel model, the effective thermal conductivity (k_{eff}) of fibrous porous media can be expressed as

$$k_{eff} = k_g\phi + k_s(1-\phi) \tag{2-31}$$

where k_{eff} is effective thermal conductivity of the fibrous porous media, k_g and k_s are the thermal conductivities of solid (viz. fiber) and gas (in most cases, it is still air) phases phases, respectively.

The series model for effective thermal conductivity (k_{eff}) of the fibrous materials can be obtained as

$$\frac{1}{k_{eff}} = \frac{\phi}{k_g} + \frac{1-\phi}{k_s} \tag{2-32}$$

Many theoretical models were used to investigate the effective thermal conductivity of the fibrous porous media. For example, Zou et al. (2002) derived a mathematical model for the transverse thermal conductivities of the special unidirectional fibrous composites using the electrical analogy technique. Figure 2-26 shows the transversal surface view of the fiber-reinforced unidirectional composite in the model (Zou et al., 2002). Figure 2-27 displays a representative cell of fixed cylindrical filament and the square rank model for the special transverse heat conduction (Zou et al., 2002). Liu et al. (2012) presented a square arrayed pipe filament model for estimating the transverse effective thermal conductivity of the special unidirectional natural fibre composites using heat-electrical similar method. In this model (Liu et al., 2012), the fibre bundle containing a lot of lumens, which was

simulated as the unit cell of square arrayed polyporous filament as shown in Figure 2-28.

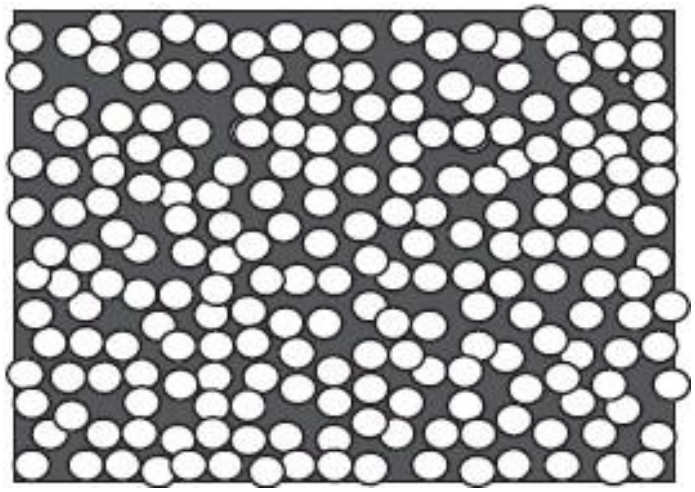

Figure 2-26 The transversal surface view of the fiber-reinforced composite with the special unidirectional fibers (Zou et al., 2002)

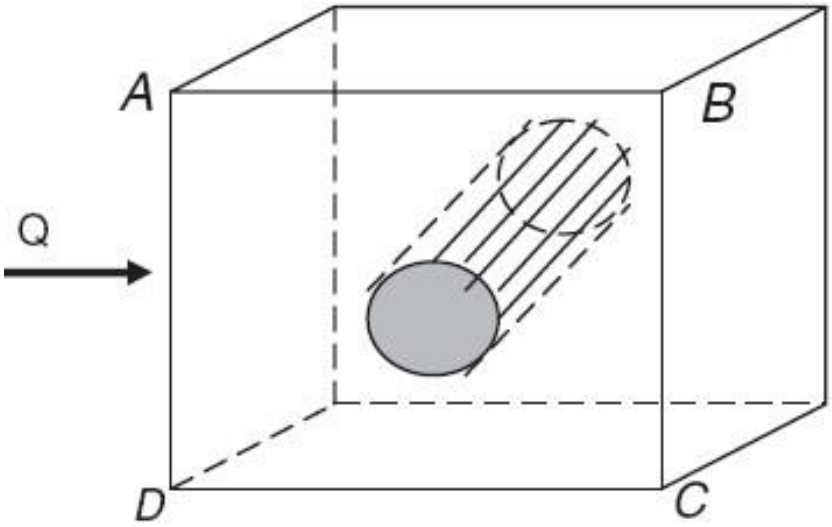

Figure 2-27 The special unit cell of fixed cylindrical filament and the square rank model for the special transverse heat conduction (Zou et al., 2002)

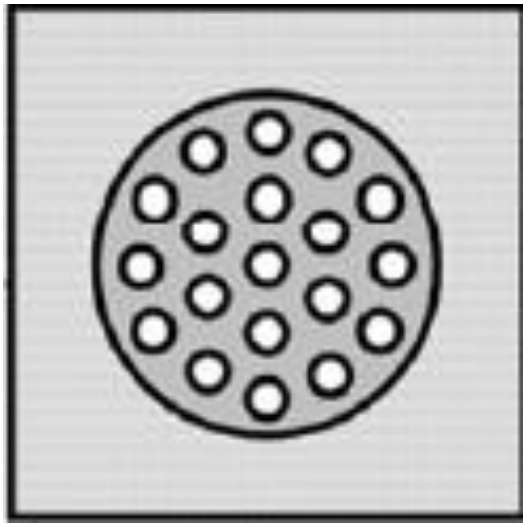

Figure 2-28 The unit cell of square arrayed polyporous filament (Liu et al., 2012)

There are other theories and approaches for calculating the effective thermal conductivity of the porous fibrous materials such as fractal theory, volume averaging theory, self-consistent field theory and lattice Boltzmann method. Based on fractal theory, Pitchumani and Yao (1991) developed a theoretical model for the special transverse thermal conductivities of the common unidirectional fiber composites with the ideal contact between the fixed fiber matrix and filament. The influents of dispersion and tortuosity on effective thermal conductivity of the common porous media were studied analytically based on volume averaging theory (Yang and Nakayama, 2010). Akbari et al. (2013) studied effective thermal conductivity of the anisotropic fibrous porous media using the well known self-consistent field theory. But it is difficult to derive the analytical models of the effective thermal conductivity because each fibre has at least one contact with another in fibrous porous media. Wang et al. (2007) obtained a simple mathematical model for calculating effective thermal conductivity of natural fibrous materials using lattice Boltzmann algorithm. It

was shown that a smaller angle of fiber orientation led to the much stronger anisotropy of the effective thermal conductivity (Wang et al., 2007). Furthermore, solving the temperature distribution by matrix around a special single coated fiber, Lu et al. (1995) investigated the effective thermal conductivity of the common fiber-reinforced composites comprising N fibers in a fixed circle. However, the study did not give the comparison with the available experimental data (Lu et al., 1995).

Many geometric parameters of porous fibrous materials such as the volume fraction of fiber, the fiber orientation, the length of fiber and porosity are closely related to the effective thermal conductivity. Fu and Mai (2003) investigated the influences of the length of fiber, the orientation of fiber, and the volume fraction of fiber on the thermal conductivity of short-fiber-reinforced polymer composites. It was shown that the thermal conductivity of short-fiber-reinforced polymer composites increased with the average length of fiber but decreased with the average orientation angle of fiber related to the measured direction (Fu and Mai, 2003). Zamel et al. (2012) discussed the effects of the microporous layer structure and porosity on the effective thermal conductivity in the common PEMFCs. It was observed that the thermal conductivity of the microporous layer increased with the volume of small pores (Zamel et al., 2012).

To the best of our knowledge, no general theoretical models of the effective thermal conductivity of the porous fibrous materials have been reported in published literature.

2.4.2 Convective heat transfer

Convective heat transfer is the heat transfer by mass movement of fluids including the air and the water when the heating fluids are caused to go away from the general heat source, taking heat energy with it. Thus, the heat convection is heat transfer from one location to another by the movement of fluids, a physical process that is essentially transfer of heat by means of mass transfer. Besides, the energy is transported not only via the heat conduction but by the macroscopic motion of fluids in flowing fluids. In the fluids natural convection may take place when the fluids movement is caused by buoyancy forces that lead to density difference due to temperature gradient. Forced convection is a type of transport when the heated fluid is forced to flow on the heating surface by the some external sources (like suction device, fan, pump, stirrer, etc.). Forced convection is accompanied by natural convection in some cases. In general, convective heating or cooling can be expressed by Newton's equation of cooling. Newton’s law can be used when the rate of heat loss from convection is a linear function of the temperature difference, which can be derived from heat transfer. However, in some cases heat convection may be nonlinear, namely heat convention is not linearly dependent on temperature gradients. In these cases,

Newton's equation does not apply. According to the description of the well known Newton's law-the percent of the heat energy loss of an object is proportional to the temperature difference between an object and the surrounding environments, the heat convection can be expressed by Newton's equation of cooling

$$Q_h = hA_{ca}(T_w - T_\infty) = hA_{ca}\Delta T \tag{2-33}$$

The general constant of proportionality h is termed the convection heat transfer coefficient, T_w and T_∞ are the object temperature and the fluid free-stream temperature, respectively.

In convective heat transfer, there are two important parameters: Reynolds number (Re) and Prandtl number (Pr).

In fluid mechanics, the Reynolds number is a dimensionless number named after Osborne Reynolds. And the Reynolds number can be used to predict the dynamic similitude between the diverse experimental conditions. When the special dimensional analysis of the fluid dynamics cases is performed, Reynolds numbers are frequently used. The Reynolds number can be defined by

$$\mathrm{Re} = \frac{uD}{\nu} = \frac{\rho_f uD}{\mu} \tag{2-34}$$

where u is the bulk velocity of fluid, D is the hydraulic diameter of the pipe, ν is kinematic viscosity of fluid, μ is dynamic viscosity, and ρ_f is density of fluid.

Prandtl number is named after German physicist Ludwig Prandtl. In heat convection Prandtl number of fluid is also a dimensionless number, which is defined as

$$\mathrm{Pr} = \frac{\nu}{\alpha_f} = \frac{\mu}{\rho_f \alpha_f} \tag{2-35}$$

where α_f is thermal diffusivity of fluid.

Prandtl discovered boundary layer in 1904. The boundary layer of fluids is close to the wall and has a significant influence on the heat transfer. And the velocity component parallel to the wall varies in the boundary layer, from zero at the wall to a maximum velocity presenting over a very small length in the core fluid. Figure 2-29 is a schematic of heat convection.

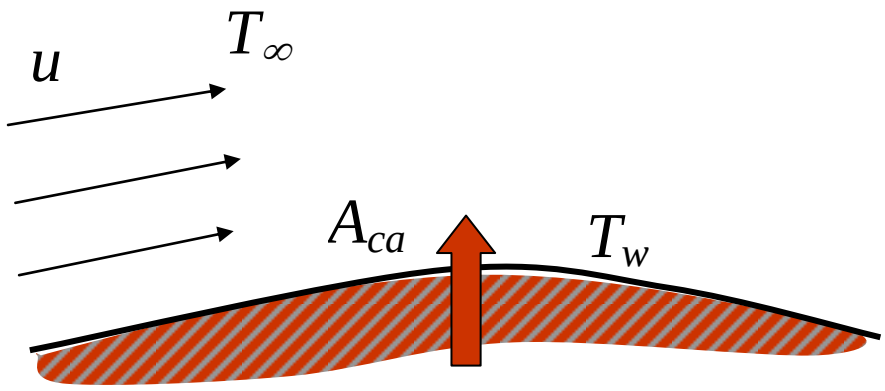

Figure 2-29 A schematic of heat convection

Convective heat transfer widely takes place in porous fibrous materials, such as fiber glass, rockwool, rigid metallic fibrous materials, etc. These porous fibrous materials are ordinarily installed in attics to reduce heat losses to the attic space in our life. For example, fibrous insulation is made up of fibers and air. The fibers can eliminate convection, absorb and scatter thermal radiation, resulting in reducing heat losses through the insulated region. If excellently designed, all fibrous attic insulation products may effectively reduce heat loss. Heat convection in porous fibrous materials involves the composing of complex fluid flow and the temperature fields round the individual fibres. Beavers and Sparrow (1969) pointed out that flow abruption might happen round the general fibres at higher velocities in fibrous porous media.

Considering forced convection through fibrous porous media of different thermal conductivities, it was found that porous materials enhanced heat transfer from the heated surface as compared to the estimated results for the slug or for the common laminar flow in the channel (Hunt and Tien, 1988). In the channel filled with the fibrous porous media of very high porosity, high Reynolds number forced convection was investigated by Angirasa (2002). Figure 2-30 shows 2-D forced flow via the common channel filled with the fibrous porous media (Angirasa, 2002). The results (Angirasa, 2002) revealed the thickness of fiber had important influence on thermal dispersion. Besides, Jeng and Tzeng (2007) investigated experimentally the heat convection and the physical pressure drop in the metal porous bulk with the restrictive slot air jet.

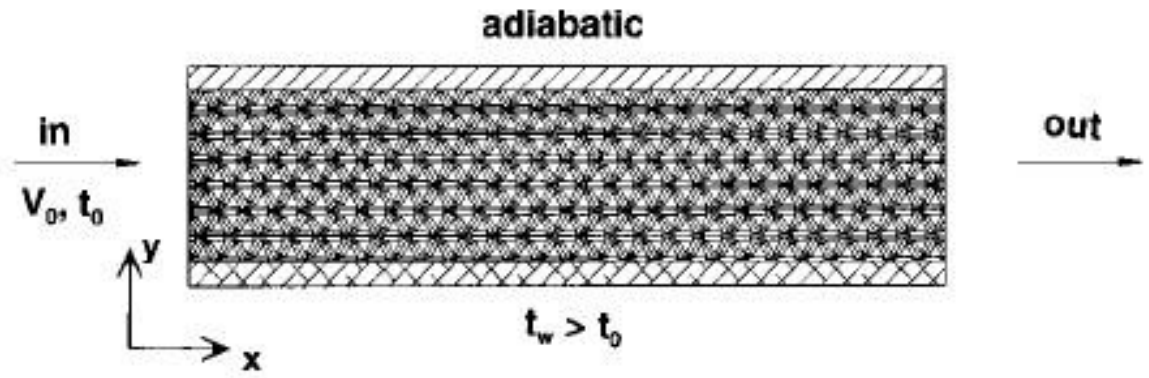

Figure 2-30 Physical configuration of 2-D forced fluid flow via the channel filled with the fibrous porous media (Angirasa, 2002)

In general, many investigations of convective heat transfer in the fibrous porous media are based on the Darcy flow model. However, these investigations do not take into account convective inertia, form drag and viscous shearing effects. The

above factors are significant, especially at high Reynolds number flows. Actually, it is difficult to describe the flows in full detail because of complexity of tortuous path in porous fibrous materials.

2.4.3 Radiative heat transfer

When the temperature of a body is greater than absolute zero, thermal radiation can occur. The electromagnetic waves from all objects can emit thermal radiation which shows a transfer of thermal energy into electromagnetic energy. Note thermal radiation is fundamentally different from heat conduction and heat convection. The electromagnetic waves from object can transfer energy in the vacuum. This means that radiative heat transfer does not need the appearance of substance. Thermal radiation depends on the properties and temperature of material.

With regard to radiative heat transfer of the fibrous porous media, the radiative heat conductivity can be estimated by (Strong et al., 1960; Wan et al., 2009; Song and Yu, 2012)

$$k_{rh} = C_3 \sigma T^3 \frac{r_f}{e(1-\phi)} \tag{2-36}$$

where σ is Boltzmann constant ($\sigma = 5.672 \times 10^{-8}\, Wm^{-2}K^{-4}$), T is the temperature, e is the surface emissivity of the fibre, r_f is the mean radius of the fibres, and C_3=5.4 (Wan et al., 2009) is a constant determined by fiber orientation.

Reduction of radiation heat transfer is possible in porous fibrous materials for thermal protection systems and insulation systems. Due to economization in both room and heft, the low density fibrous insulation media are being applied rapidly in practical application such as functional clothing, automobiles, house, industrial equipment, and aircraft, etc. A great deal of void room is possessed by the lightweight insulations; generally gas can occupy more than 95% of their volume (Larkin and Churchill, 1959). The common fibrous media being used in those insulations can be general wood fibers, glass fibers, polyurethane and polystyrene.

Several studies have been reported on thermal radiation in the porous fibrous materials. Radiant heat transfer via the common foamed and fibrous insulating media was studied both experimentally and theoretically (Larkin and Churchill, 1959). The results were exciting, which provided detailed design data and described the contributions of the several physical mechanisms of heat transfer (Larkin and Churchill, 1959). Figure 2-31 (A) and (B) illustrate the two-flux model for radiative heat transfer and experimental apparatus from the literature (Larkin and Churchill, 1959), respectively. Tong and Tien (1980) obtained a mathematical model for calculating radiative heat transfer in the porous fibrous materials using common conductive method. Lee (1989) proposed a radiation model for evaluating the influence of the orientation of fibre on the thermal radiation via the porous fibrous materials between the parallel plane diffuse borders. The results showed that the polar orientation of fibres intensely affected both radiative heat transfer and the backscatter factor (Lee, 1989). Boulet et al. (1993) developed a mathematical matrix model for

the thermal radiation in fibrous porous media. Zeng et al. (1995) derived an approximate formula for coupled the heat conduction and radiative heat transfer via the porous materials with the random optical thickness. The effects of different parameters on radiative heat transfer were also analyzed using the spectral two-flux model (Langlais et al., 1995). Roux (2003) studied the radiative characters of large and small density fiberglass insulation materials in the special 4-38.5 μm wavelength area using the nonlinear least squares approach. Asllanaj et al. (2004) investigated the transient radiative and heat conduction in the porous fibrous materials with anisotropic optical properties. Assuming arbitrary distribution of the fibres in fibrous materials, the radiation heat transfer was simulated by Monte Carlo method (Nisipeanu and Jones, 2003). The results showed that the radiative heat flux was highly dependent on bias in the polar orientation angle (relative to the boundary planes) of the fibers. Du et al. (2007) obtained a modified model for heat transfer via the penguin feathers. Besides, Veiseh and Hakkaki-Fard (2009) investigated the thermal radiation using Monte Carlo Ray-Trace (MCRT) approach. And the model of radiative heat transfer was coupled with the nonlinear heat conduction formula. Furthermore, Arambakam et al. (2012) investigated steady-state thermal radiation via porous fibrous insulation media using MCRT simulation technique. And it was shown that the heat flux via the fibrous porous media decreased with the increase of the volume fraction of the solid of the fibres (Arambakam et al., 2012).

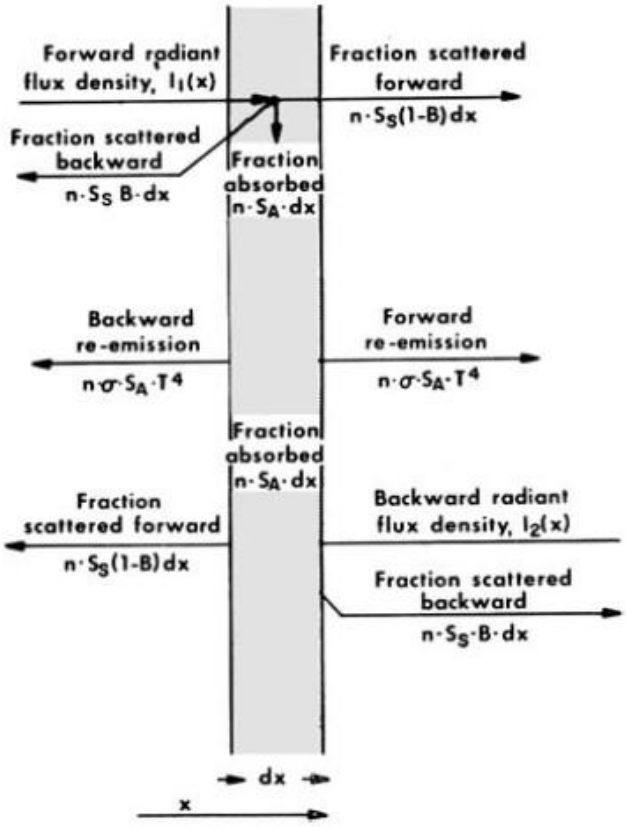

(A)

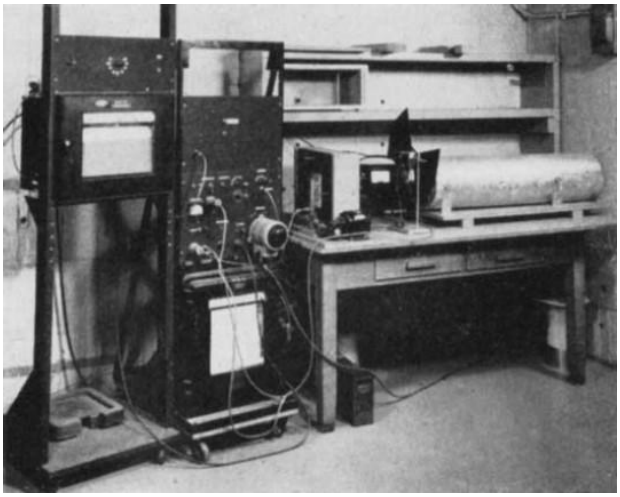

(B)

Figure 2-31 (A) The two-flux mathematical model for thermal radiation, (B) Experimental apparatus (Larkin and Churchill, 1959)

Although heat transfer has been studied for many years, the available and valid computational tools for the estimation of radiation heat transfer are desirable in fibrous porous media.

2.5 Fractal theory and some structural parameters of porous fibrous materials

2.5.1 Fractal theory

In general, the ordered curves, geometry cubes and common surfaces can be characterized by the well known Euclidean geometry. However, it is found that a number of objects such as the mountains, islands, surfaces of desert, coastlines, lakes and rivers, are random and anomalous in nature (Mandelbrot, 1982). And the above disordered objects can not be characterized by applying the Euclidean geometry due to the scale-dependent measurements of the special length, volume or area. So the disordered bodies can be named fractals. Besides, the dimensions of such bodies can be defined as the well known fractal dimensions which are non-integral. Thus, the fractal dimension (d_f) of these objects can be expressed by a scaling law (Mandelbrot, 1982):

$$M(L) \sim L^{d_f} \tag{2-37}$$

where $M(L)$ may be the mass of a body or the volume of a special cube or the length of a geometry line or the area of a special surface. Eq. (2-37) shows the characteristic of the self-similarity, which hints the fractal dimension from Eq. (2-37) is a physical

constant over a scope of the special length scales (L). For example, the geometry frameworks of the well known Sierpinski carpet and Koch curve are self-similar fractals (Mandelbrot, 1982). Two well-known examples on fractals (Mandelbrot, 1982) are shown in Figure 2-32. The Koch curve can be obtained by starting with a small unit segment in Figure 2-32. The fractal dimension of Koch curve can be calculated by $d_f = \ln 4 / \ln 3 = 1.262$. Sierpinski gasket is an accurately self-similar fractal, which can be used to analyze the fractal fibrous porous media. The Sierpinski gasket can be constructed from an equilateral triangle, subdividing it into four smaller triangles and taking out the central triangle. Thus, the fractal dimension of Sierpinski gasket can be computed by $d_f = \ln 3 / \ln 2 = 1.585$. Figure 2-32 represents the property of self-similarity. Because fibrous porous media consisting of many anomalous pores of distributed sizes over some orders of magnitude in the special length scales show fractal character, they can be described by self-similarity method (Shou et al., 2010; Xiao et al., 2012). Fractal theory has therefore been applied for modelling the heat and mass transport through the fibrous porous media (Xiao et al., 2012; Shou et al., 2010).

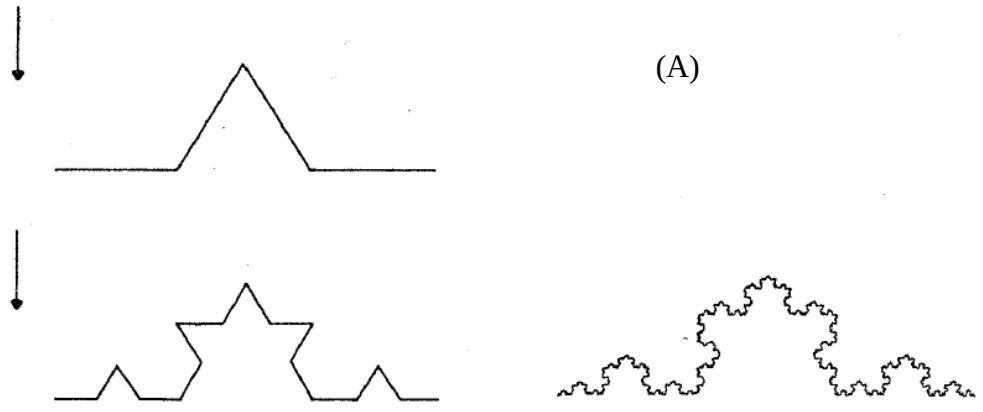

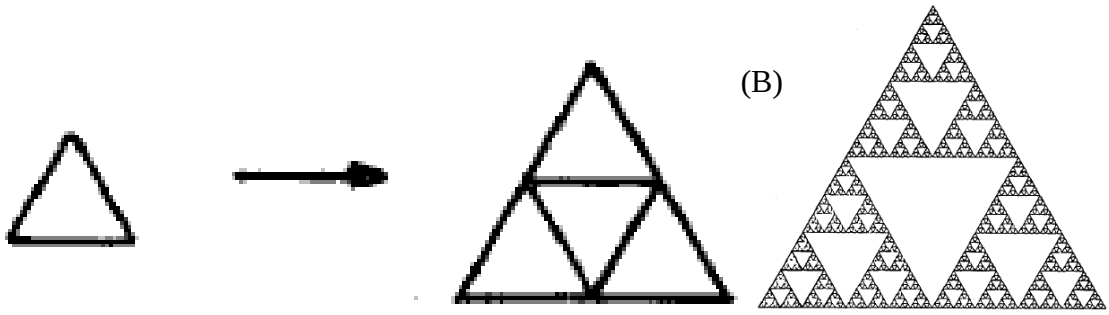

Figure 2-32 (A) Koch curve, (B) Sierpinski gasket

2.5.2 Some structural parameters of porous fibrous materials

2.5.2.1 Porosity

Porosity has an important influence on the heat and mass transfer of the fibrous materials. Porosity (ϕ) of the porous fibrous materials can be defined as the special ratio of the total pore space volume (V_p) to the total porous body materials volume (V_t):

$$\phi = \frac{V_p}{V_t} \tag{2-38}$$

Being briefly a percent part of total volume, ϕ can change from 0 to 1, commonly changing between 0.1 and 0.4 for underground sandstones, between 0.3 and 0.7 for soils. Besides, the maximal porosity of glass fiber can reach 0.83-0.93. The relation between porosity and tortuosity was investigated based on lattice Boltzmann model (LBM) (Matyka et al., 2008). Figure 2-33 (A) and (B) are two examples of porous media structured by arbitrarily put and randomly overlapping squares for two different porosities with $\phi = 0.5$ and $\phi = 0.8$. The dark regions

display fixed solid obstructions, while the special white section is taken up by the flow fluid of porous fibrous materials (Matyka et al., 2008). Figure 2-34 represents another example of the physical velocity field computed by LBM approach for a small porosity in the porous medium (Matyka et al., 2008). Figure 2-35 shows computer-generated fiber distributions at $\phi = 0.7$ with the diverse minimum inter-fibre lengths (Chen and Papathanasiou, 2006). The image consisted of 196 fibre intersecting surfaces and was produced by Monte Carlo technique, beginning from a 14×14 square arrangement.

In general, the porosity is a geometry structural parameter of porous fibrous materials, which is related to the heat and mass transfer of porous media including permeability, diffusivity and heat transfer. Porosity can be calculated through volumetric measurements of core samples.

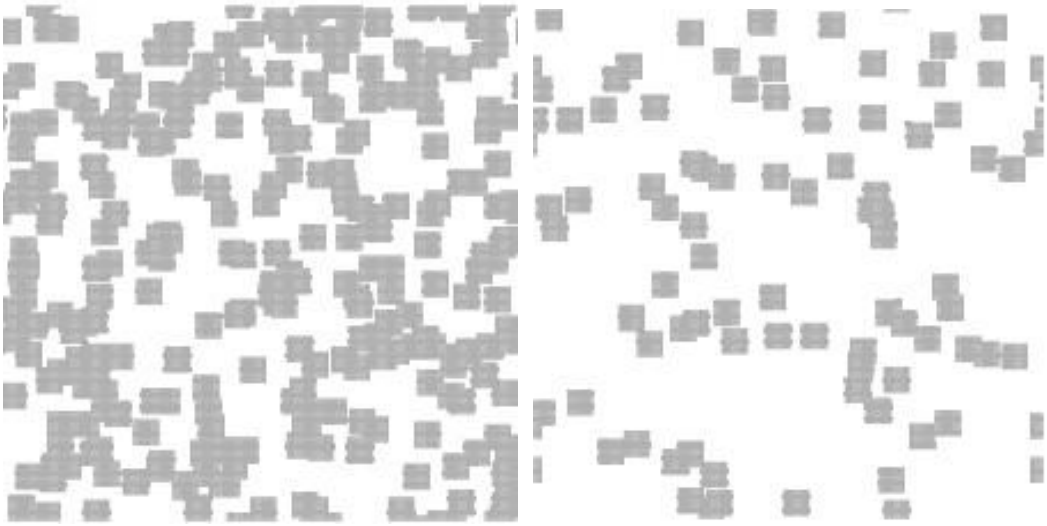

(A) $\phi = 0.5$ (B) $\phi = 0.8$

Figure 2-33 (A) (B) Two examples of porous systems for two different porosities with $\phi = 0.5$ and $\phi = 0.8$ (Matyka et al., 2008)

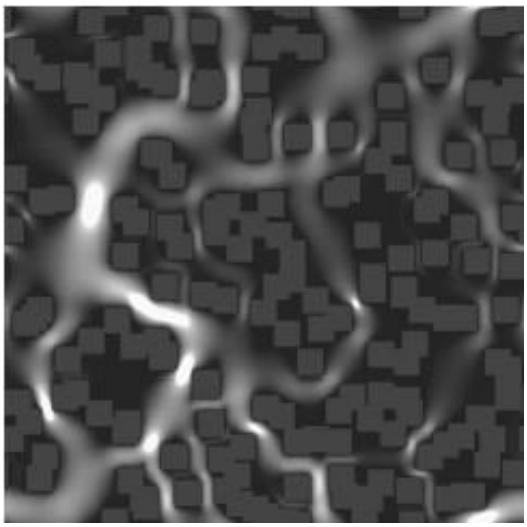

Figure 2-34 Velocity magnitudes squared computed on a 600×600 numerical grid at $\phi = 0.65$ (Matyka et al., 2008)

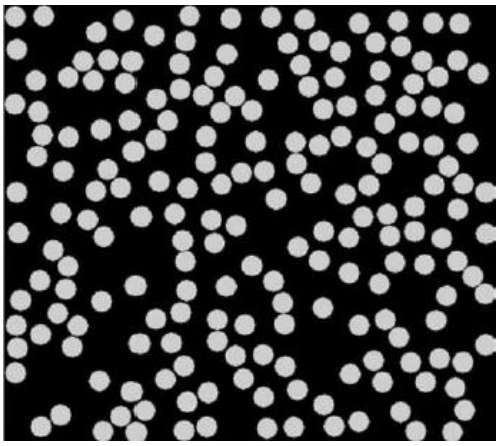

Figure 2-35 The computer-generated fiber distributions based on Monte Carlo method (Chen and Papathanasiou, 2006)

2.5.2.2 Tortuosity

The heat and mass transfer of the fibrous materials have captured much attentions due to the applications in science and engineering. These physical transport parameters such as the permeability, thermal conductivity and diffusion coefficient

are usually connected with the tortuosity of fluid flow path followed by the special transported media. And the tortuosity can be defined by (Bear, 1972; Dullien, 1979)

$$\tau = \frac{l_t}{l_0} \tag{2-39}$$

where l_t and l_0 are the actual effective distance of streamlines and the straight distance or thickness of a fixed sample/unit cell along the actual physical pressure gradient, respectively. Figure 2-36 is the schematic of tortuous flow via the porous material (Yu, 2005). Figure Figure 2-37 displays another schematic of fluid flow via the special bi-dispersed porous material and its tortuosity (Yu and Cheng, 2002). It is shown that tortuosity $\tau \geq 1$ in Figure 2-36 and Figure 2-37.

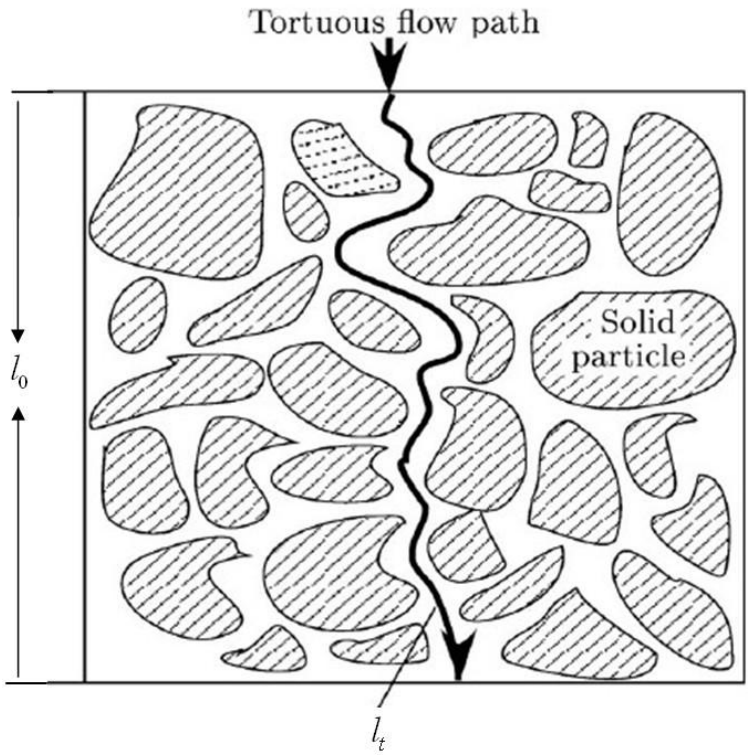

Figure 2-36 Schematic of tortuous streamtubes through a porous media (Yu, 2005)

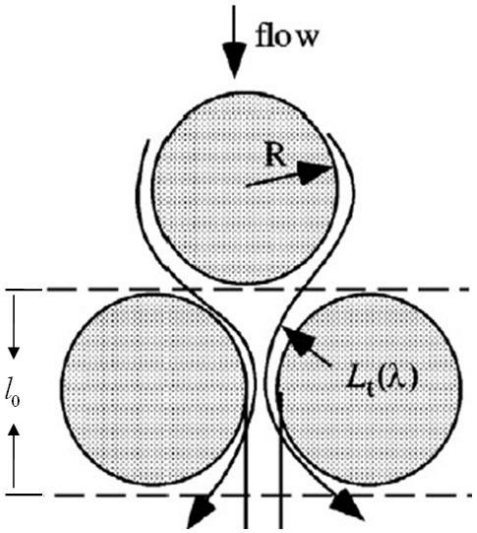

Figure 2-37 A schematic of tortuous flow via the special bi-dispersed porous material (Yu and Cheng, 2002)

Based on the lattice gas automata approach, Koponen et al. (1996) numerically analyzed a creeping fluid flow of the special Newtonian incompressible fluid in a common 2-D porous media structured by arbitrarily located rectangles of equivalent size and with freely overlap. There is a type of empirical relation such as the linear function. For example, a relationship between the tortuosity and porosity of the porous material is given by (Koponen et al., 1996)

$$\tau = 0.8(1-\phi)+1 \qquad (2\text{-}40)$$

where 0.8 is a mathematical fitting parameter from the special numerical simulation data.

Based on the ratio of the fluid volume enclosed by a unit cell to the minimum pore intersecting surface flow region in the fixed unit cell, Westhuizen and Pless (1994) obtained an analytical model for tortuosity:

$$\tau = 1 + \sqrt{1-\phi} \tag{2-41}$$

Another correlation of the form such as logarithmic function can be expressed by (Comiti and Renaud, 1989)

$$\tau = 1 + P_0 \ln(\frac{1}{\phi}) \tag{2-42}$$

where P_0 is a mathematical empirical/fitting parameter by fitting the available experimental results, $P_0 = 0.63$ for cubic particles and $P_0 = 0.41$ for spherical particles.

The condition $\tau = 1$ at $\phi = 1$ is satisfied for Eqs. (2-40), (2-41) and Eq. (2-42), which is consistent with the practical physical phenomena. But no literature was published for the tortuosity of geometry streamlines with cylindrical particles in fibrous porous media.

Wheatcraft and Tyler (1988) obtained a classical fractal scaling relation for the tortuosity in porous media. The relationship can be expressed as

$$l_t = \lambda_{\min}^{1-D_T} l_0^{D_T} \tag{2-43a}$$

$$\tau = \frac{l_t}{l_0} = (\frac{l_0}{\lambda_{\min}})^{D_T - 1} \tag{2-43b}$$

where $\lambda_{\min}$ is the minimum pore or capillary diameter in the fibrous porous media, D_T is the well known fractal dimension of the tortuosity capillary, with $1 < D_T < 2$ figuring the scope of the convolutedness capillary flow path via the porous fibrous materials.

Yu and Cheng (2002) modified above Eq. (2-43) as

$$\tau = \frac{l_t}{l_0} = (\frac{l_0}{\lambda})^{D_T - 1} \tag{2-44}$$

where λ is the diameter of a tortuous capillary. Eq. (2-44) shows that the smaller tortuous capillary diameter, the longer actual capillary length, and the larger tortuosity. And this is expected and connected with the practical physical condition.

According to Eq. (2-44), the average tortuosity can be expressed by

$$\tau_{av} = (\frac{l_0}{\lambda_{av}})^{D_T - 1} \tag{2-45}$$

where λ_{av} is the average size of pore/capillary.

Besides Eqs. (2-40)-(2-45), there are some other models for the tortuosity of the porous fibrous materials. Two common geometry models for the tortuosities of tortuous streamlines in the 2-D porous materials with the cubic (Yu and Li, 2004) and the spherical particles (Yun et al., 2005) were developed. Besides, a 3-D mathematical geometry model for the tortuosity of fluid flow in the porous materials with the spherical, the cubic and platelike grains was obtained (Yun et al., 2006). Furthermore, based on the self-similarity of the well known Sierpinski carpet, Li and Yu (2011) proposed a very simple mathematical recursive model for tortuosity of the fluid flow path in the mentioned Sierpinski carpet. However, these mentioned models are only valid for a given assumption such as cubic or spherical particles, which cannot show the universality for tortuosiy in porous media.

2.6 Summary and Conclusions

(1) From the literature review, although numerous studies have been carried on the heat and mass transfer of the fibrous porous media, the relation between the transport properties and the geometry parameters of the special fibrous porous media is still not fully understood.

(2) Although a large amount of experimental data may be available in the published literature, the reported results from diverse experimental approaches often differ obviously.

(3) There is a lack of understanding on the creep and inertial flow through periodic and disordered arrays as well as how the size of the system affects the permeability of random/disordered structures.

(4) The effective gas diffusivity coefficient in fibrous materials may be different for different gas, which may be related to the property of gas. Besides, the effective diffusivity may vary with fibrous structure under the wet condition.

(5) Although computational techniques for heat transfer have been studied for decades, the validity of these techniques is not fully examined.

Chapter 3 An investigation on the relative permeability with the effect of capillary pressure in unsaturated porous material by using fractal-Monte Carlo simulations

3.1 Introduction

The mass transport via the porous fibrous materials is a significant topic to the engineers and scientists in different areas such as textile engineering, fuel cells, soil science and oil engineering, etc. Besides, the relative permeability and capillary pressure are two very key parameters that affect liquid transport through porous media. Past investigations (Yu and Lee, 2000; Yu and Cheng, 2002; Feng et al., 2004; Shi et al., 2008; Wu et al., 2011; Zheng et al., 2012) have shown that the transport processes in porous media is very complex and dependent on the complicacy of the geometrical microstructure of the porous fibrous materials. Many parameters such as porosity, size of pore and tortuosity of capillaries are highly relevant to permeability of the porous materials. Besides, the frameworks of most porous materials are highly complex and difficult to depict. They are even more complex to analyse the transport behaviors within unsaturated porous systems, particularly when the diverse transfer mechanisms take part simultaneously. Modeling the permeability of unsaturated porous media therefore presents a great challenge. So far, a number of experimental techniques (Ayatollahi et al., 2005; Song et al., 2009; Lee, 2010; Lee et al., 2010; Tamayol and Bahrami, 2011; Hou et al., 2012) have been developed to measure permeability of the porous materials. Experiments are, however, generally expensive and time-consuming.

Experiments are usually complicated by the inter-dependence of permeability and capillary pressure, especially in cases where phase change takes place. It is, therefore, always desirable to develop theoretical models. Many of the reported theoretical works (Koponen et al., 1997; Koponen et al., 1998; Tomadakis and Robertson, 2005; Yu and Cheng, 2002; Shou et al., 2010; Wu et al., 2011) assumed simplified pore geometry structures, which allowed analytical solutions of the special microscopic flow types. In early studies, Ayatollahi et al. (2005) studied the influences of the temperature on the relative permeability of heavy oil during the tertiary gas oil gravity drainage mechanism. The results (Ayatollahi et al., 2005) showed that the elevated temperature was the leading factor behind the wettability variation and the relative permeability of heavy oil. Besides, it was experimentally proved that the rock permeability is dependent on the pores connectivity by Lee et al. (Lee, 2010; Lee et al., 2010). In their experiment with altering permeability (Lee, 2010), a decrease of the permeability caused a decrease in the gas production and an increase in the dissociation rate. Recently, Shou et al. (2010) applied a difference-fractal approach and unit cell approach (Shou et al., 2011) to model the hydraulic permeability of high porosity porous media. Additionally, Bal et al. (2011) analyzed spontaneous liquids flow via the layered heterogeneous porous fibrous materials using the fractal geometry. The models reported in Refs. (Shou et al., 2010; Shou et al., 2011; Bal et al., 2011) are, however, limited to saturated porous media. In addition, Hou et al. (2011; 2012) have experimentally and theoretically investigated the relative permeability of water-oil. And the results showed that the calculated water phase relative permeability

curve is larger and the calculated oil phase relative permeability curve is smaller than the measured relative permeability curve if the capillary pressure can be neglected (Hou et al., 2012). In practice, most porous media are unsaturated in nature. It is therefore essential to predict the relative permeability of unsaturated porous media.

In this chapter, we propose an overall mechanistic model to consider the coupled effects of the porosity of porous medium (ϕ), the tortuosity of capillaries (D_T), the saturation (S) and the capillary pressure (P_c), and the pore size (λ) in unsaturated porous media. In order to elucidate the effect of these parameters on relative permeability, Monte Carlo simulation was performed.

3.2 Model description

The porous media in nature can be and have been described as fractal bodies (Katz and Thompson, 1985; Yu and Cheng, 2002; Shou et al., 2010; Wu et al., 2011; Zheng et al., 2012). This means that the classical fractal theory can be used to estimate transport property of the porous materials. Besides, the distribution of pore size and tortuosity of capillaries have also been shown to follow the well known fractal scaling laws (Yu and Cheng, 2002; Wu et al., 2011; Zheng et al., 2012), i.e. the cumulative number (N) of pores in porous fibrous materials whose sizes are greater than or equal to λ can be expressed according to the fractal scaling law (Yu and Cheng, 2002)

$$N(L \geq \lambda) = (\lambda_{\max} / \lambda)^{d_f} \quad \text{with} \quad \lambda_{\min} \leq \lambda \leq \lambda_{max} \tag{3-1}$$

where, $\lambda_{\max}$ and $\lambda_{\min}$ are the maximum and minimum diameter of pores in porous media, respectively; λ is the diameter of a pore, and d_f is the area fractal dimension of pores.

Figure 3-1 shows a schematic of porous medium comprised of a bundle of tortuous capillaries in porous materials, whose sizes and tortuosities follow the classical fractal scaling laws. The applied pressure difference (ΔP) across the straight-line distance (l_0) of the porous material, whose cross-section area is A_{cs}, and l_t is the actual distance for liquid or gas going through the fractal porous materials.

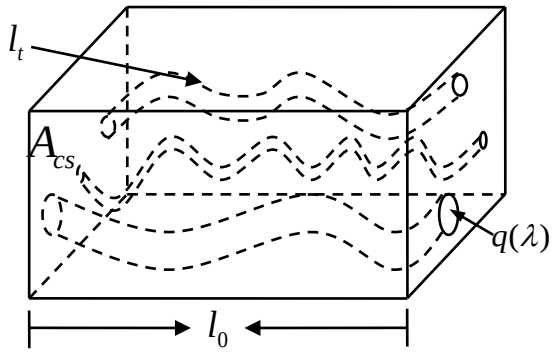

Figure 3-1 A schematic of the fractal porous materials comprised of a bundle of tortuous capillaries

Differentiating Eq. (3-1) with respect to λ yields

$$-dN = d_f \lambda_{\max}^{d_f} \lambda^{-(d_f+1)} d\lambda \tag{3-2}$$

Eq. (3-2) gives the quantity of pores between the pore size λ and $\lambda + d\lambda$. The negative mark in Eq. (3-2) means that the quantity of pores increases with the decrease of pore size, and $-dN > 0$. The total quantity of the pores from the

minimum diameter $\lambda_{\min}$ to the maximum diameter $\lambda_{\max}$ can be derived from Eq. (3-1) as (Yu and Cheng, 2002)

$$N_t(L \geq \lambda_{\min}) = (\lambda_{\max} / \lambda_{\min})^{d_f} \tag{3-3}$$

Dividing Eq. (3-2) by Eq. (3-3) results in

$$-dN / N_t = d_f \lambda_{\min}^{d_f} \lambda^{-(d_f+1)} d\lambda = f(\lambda) d\lambda \tag{3-4}$$

where, $f(\lambda) = d_f \lambda_{\min}^{d_f} \lambda^{-(d_f+1)}$ is the mathematical probability density function. Patterned after the well known probability theory, the mathematical probability density function $f(\lambda)$ should meet the following normalization relation or total cumulative probability (Yu and Cheng, 2002):

$$\int_{\lambda_{\min}}^{\lambda_{\max}} f(\lambda) d\lambda = 1 - \left(\frac{\lambda_{\min}}{\lambda_{\max}} \right)^{d_f} \cong 1 \tag{3-5}$$

The integration result of Eq. (3-5) shows that Eq. (3-5) holds if and only if

$$\left(\frac{\lambda_{\min}}{\lambda_{\max}} \right)^{d_f} \cong 0 \tag{3-6}$$

is satisfied. Eq. (3-6) is looked as a criterion whether a porous material can be described by the classical fractal geometry approach. Generally (Yu and Cheng, 2002), most porous media have $\lambda_{\min} / \lambda_{\max} = m \leq 10^{-2}$, thus Eq. (3-6) approximately holds. Thus, the fractal geometry approach can be used to describe the characteristic of the porous material.

The fractal dimension d_f in Eqs. (3-1)-(3-6) is given by (Yu and Li, 2001)

$$d_f = d - \frac{\ln \phi}{\ln \frac{\lambda_{\min}}{\lambda_{\max}}} \tag{3-7}$$

where, d is the well known Euclidean dimension, and equals 2 or 3 in 2-D or 3-D rooms, respectively; ϕ is the porosity of porous material in Figure 3-1.

In the present work, it is supposed that the real porous material consist of a bundle of tortuous capillaries with different diameters. As shown in Figure 3-1, the flow rate $q(\lambda)$ through a single tortuous capillary can be given by Hagen-Poiseulle formula (Denn, 1986)

$$q(\lambda) = \frac{\pi}{128} \frac{\Delta P}{l_t(\lambda)} \frac{\lambda^4}{\mu} \tag{3-8}$$

where μ is the viscosity of the fluid, ΔP is the pressure difference and λ is the hydraulic diameter of a single capillary tube. Because the tortuosity of capillaries has been proven to follow the well known fractal scaling laws (Yu and Cheng, 2002; Wu et al., 2011; Zheng et al., 2012), the total distance of a tortuous capillary can be expressed as (Yu and Cheng, 2002)

$$l_t(\lambda) = \lambda^{1-D_T} l_0^{D_T} \tag{3-9}$$

where, D_T is the tortuosity fractal dimension ($1 < D_T < 2$ in two dimensions) which is given by (Yu, 2005)

$$D_T = 1 + \frac{\ln \tau_{av}}{\ln(l_0 / \lambda_{av})} \tag{3-10}$$

where τ_{av} is the mean tortuosity of tortuous capillaries and λ_{av} is the average diameter of capillaries. And the purpose of introducing the tortuosity of tortuous

capillaries is to include the effect of the complexity of the geometrical shape on fluid permeability. For fluid flow paths in a porous material, an approximate relationship between the average tortuosity and the porosity is expressed as (Yu and Li, 2004)

$$\tau_{av} = \frac{1}{2}[1+\frac{1}{2}\sqrt{1-\phi}+\sqrt{1-\phi}\frac{\sqrt{(\frac{1}{\sqrt{1-\phi}}-1)^2+\frac{1}{4}}}{1-\sqrt{1-\phi}}] \tag{3-11}$$

The average diameter of capillaries can be found with the aid of Eq. (3-4)

$$\lambda_{av} = \int_{\lambda_{\min}}^{\lambda_{\max}} \lambda f(\lambda) d\lambda = \frac{d_f}{d_f - 1}\lambda_{\min}[1-(\frac{\lambda_{\min}}{\lambda_{\max}})^{d_f-1}] \tag{3-12}$$

Due to $\lambda_{\min}/\lambda_{\max} = m$, Eq. (3-12) can be further modified as

$$\lambda_{av} = \frac{md_f}{d_f - 1}\lambda_{\max}(1-m^{d_f-1}) \tag{3-13}$$

Eq. (3-13) depicts a fractal expression of the average diameter of capillaries in the porous materials.

In Figure 3-1, the pores in the intersecting surface can be looked as the circles with different diameters λ; consequently, the intersecting surface area can be obtained with the aid of Eq. (3-2):

$$A_{cs} = \frac{\int_{\lambda_{\min}}^{\lambda_{\max}} \pi(\lambda/2)^2(-dN)}{\phi} = \frac{\pi d_f(1-m^{2-d_f})}{4(2-d_f)\phi}\lambda_{\max}^2 \tag{3-14}$$

By inserting Eq. (3-7) into Eq. (3-14), Eq. (3-14) can be further modified as

$$A_{cs} = \frac{\pi d_f(1-\phi)}{4(2-d_f)\phi}\lambda_{\max}^2 \tag{3-15}$$

The cross-section area can be also expressed as (Yu et al., 2001)

$$A_{cs} = l_0^2 \tag{3-16}$$

Comparing Eqs. (3-15) and (3-16), the straight-line distance (l_0) can be written as

$$l_0 = \frac{\lambda_{\max}}{2}\sqrt{\frac{\pi d_f (1-\phi)}{(2-d_f)\phi}} \tag{3-17}$$

By inserting Eq. (3-13) into Eq. (3-17), a relation between the straight-line distance and the average diameter of capillaries can be further modified as

$$\frac{l_0}{\lambda_{av}} = \frac{d_f - 1}{2md_f(1-m^{d_f-1})}\sqrt{\frac{\pi d_f (1-\phi)}{(2-d_f)\phi}} \tag{3-18}$$

Inserting Eqs. (3-11) and (3-18) into Eq. (3-10), the tortuosity fractal dimension for tortuous capillaries in the porous materials can be further modified as

$$D_T = 1 + \frac{\ln\{\frac{1}{2}[1+\frac{1}{2}\sqrt{1-\phi}+\sqrt{1-\phi}\frac{\sqrt{(\frac{1}{\sqrt{1-\phi}}-1)^2+\frac{1}{4}}}{1-\sqrt{1-\phi}}]\}}{\ln[\frac{d_f-1}{2md_f(1-m^{d_f-1})}\sqrt{\frac{\pi d_f(1-\phi)}{(2-d_f)\phi}}]} \tag{3-19}$$

where d_f is obtained from Eq. (3-7). Eq. (3-19) indicates that the tortuosity fractal dimension for tortuous capillary in the porous materials is a function of the porosity (ϕ) and the area fractal dimensions of pore (d_f).

Generally, the pressure difference may include the mechanical pressure or the injection pressure (P_m), the gravitational (P_g) and the capillary pressures (P_c) due to surface tension. So the total pressure difference in the porous materials can be

expressed as (Ahn et al., 1991)

$$\Delta P = P_m + P_g + P_c \tag{3-20}$$

In practical applications, the gravitational pressure, which is relatively low compared with the applied mechanical pressure and the capillary pressure, can be neglected. Thus, here we assume $\Delta P = P_m + P_c$.

The capillary pressure can be expressed as (Ahn et al., 1991)

$$P_c = \frac{FT_{st}\cos\theta}{\lambda}\frac{1-\phi}{\phi} \tag{3-21}$$

In Eq. (3-21), T_{st} is surface tension of fluids, θ is the contact angle between the liquid and the solid, and F is the shape factor depending on the geometry structure of a material and on the fluid flow direction (F=4 when the capillary is cylindrical, see Ahn. et al. (1991)). Eq. (3-21) can be used to predict the capillary pressure for different pore sizes (Ahn et al., 1991). Several studies (Liu et al., 2007; Yun et al., 2008; Bal et al., 2011) reported the transport properties of porous media based on Eq. (3-21), and good agreement between the model (Eq. (3-21)) prediction results and the available experimental data were derived by using Eq. (3-21). So, Eq. (3-21) is also used in our work.

It is known that the contact angle is related to wettability. And the wettability can be defined as the tendency of a fluid to spread on or adhere to one solid exterior in the presence of other immiscible fluids. So the wettability affects the relative permeability because it is a physical factor in the control of position, the fluid flow,

and the distribution of fluid in the porous material. The results (Owens and Archer, 1971) showed that when the relative permeability of water is increased, the relative permeability of oil is decreased when the system develops into more oil-wet. Besides, for a two-fluid system, the model (Bradford et al., 1997) predicted that a decrease in the contact angle or organic-wet part of a marerial would be accompanied by a decrease in the relative permeability (k_{rw}) for the wetting phase (such as water), and a decrease in the relative permeability (k_{rg}) for non-wetting phase (such as organic). This result (Bradford et al., 1997) occured because of the variation in the roles (wetting versus non-wetting) of water and organic as θ increased. The mentioned trends are agreed with the published experimental results (Owens and Archer, 1971).

In the unsaturated fractal porous material, for the wetting phase, Eq. (3-8) can be modified as

$$q_w(\lambda_w) = \frac{\pi}{128} \frac{\Delta P_w}{l_t(\lambda_w)} \frac{\lambda_w^4}{\mu_w} = \frac{\pi}{128} \frac{(P_m + P_{c,w})}{l_t(\lambda_w)} \frac{\lambda_w^4}{\mu_w} \tag{3-22}$$

where, λ_w is the equality diameter for the wetting phase, and the capillary pressure for wetting phase in the unsaturated porous media is derived by modifying Eq. (3-21) as

$$P_{c,w} = \frac{FT_{st} \cos\theta}{\lambda_w} \frac{1-\phi_w}{\phi_w} \tag{3-23}$$

where ϕ_w is volume fractions for the water phase. In the porous material, because of the distribution of diverse pore sizes, the physical concept of the mean capillary pressure is more helpful (Liu et al., 2007; Bal et al., 2011). The average capillary

pressure for the wetting phase can be obtained with the help of Eq. (3-4):

$$\overline{P_{c,w}} = \int_{\lambda_{\min,w}}^{\lambda_{\max,w}} P_{c,w} f(\lambda_w) d\lambda_w = \frac{d_{f,w}}{d_{f,w}+1} \frac{FT_{st}\cos\theta}{\lambda_{\min,w}} \frac{1-\phi_w}{\phi_w} [1-(\frac{\lambda_{\min,w}}{\lambda_{\max,w}})^{d_{f,w}+1}] \qquad (3\text{-}24)$$

where $d_{f,w}$ is the well known fractal dimension for the wetting phase. Since $\lambda_{\min}/\lambda_{\max} \le 10^{-2}$, $0 < d_{f,w} < 2$, so $(\lambda_{\min,w}/\lambda_{\max,w})^{d_{f,w}+1} << 1$, Eq. (3-24) can be further reduced to

$$\overline{P_{c,w}} = \frac{d_{f,w}}{1+d_{f,w}} \frac{FT_{st}\cos\theta}{\lambda_{\min,w}} \frac{1-S\phi}{S\phi} \qquad (3\text{-}25)$$

where S is the saturation of the wetting phase and is connected with the porosity by $\phi_w = S\phi$ (Bear, 1972), $d_{f,w}$ is derived by extending the above mentioned fractal dimension for the saturated fluid as (Yu et al., 2003)

$$d_{f,w} = d - \frac{\ln\phi_w}{\ln\frac{\lambda_{\min,w}}{\lambda_{\max,w}}} = d - \frac{\ln(S\phi)}{\ln\frac{\lambda_{\min}}{\lambda_{\max}}} \qquad (3\text{-}26)$$

where, $\lambda_{\max,w}$ and $\lambda_{\min,w}$ are the maximum and minimum equivalent diameters for the wetting phase in unsaturated porous media, which are related by (Yu et al., 2003)

$$\lambda_{\min,w} = \lambda_{\min}\sqrt{S}, \quad \lambda_{\max,w} = \lambda_{\max}\sqrt{S} \qquad (3\text{-}27)$$

Similarly, for the non-wetting phase, we have (Yu et al., 2003)

$$d_{f,g} = d - \frac{\ln\phi_g}{\ln\frac{\lambda_{\min,g}}{\lambda_{\max,g}}} = d - \frac{\ln[(1-S)\phi]}{\ln\frac{\lambda_{\min}}{\lambda_{\max}}} \qquad (3\text{-}28)$$

where, $d_{f,g}$ is the special fractal dimension for non-wetting phase in unsaturated porous maaterial, $\lambda_{\max,g}$ and $\lambda_{\min,g}$ are the maximum and minimum equivalent

diameters for non-wetting phase in the unsaturated porous material, which can be related by (Yu et al., 2003)

$$\lambda_{\min,g} = \lambda_{\min}\sqrt{1-S}\,,\ \lambda_{\max,g} = \lambda_{\max}\sqrt{1-S} \tag{3-29}$$

The total flow rate Q_w for wetting phase in a single unit cell is derived by summing up the flow rates through all capillaries, i.e.

$$Q_w = \sum_{i=1}^{J} q_w(\lambda_i) = \sum_{i=1}^{J} \frac{\pi}{128}\frac{(P_m + P_{c,w})}{l_t(\lambda_w)}\frac{\lambda_{w,i}^4}{\mu_w} \tag{3-30}$$

For creeping fluid flow via the porous materials, Darcy's law (Bear, 1972) also applies, thus the total flow rate for wetting phase may also be expressed by

$$Q_w = \frac{K_w A_{cs}\Delta P}{\mu_w l_0} = \frac{K_w A_{cs}(P_m + \overline{P_{c,w}})}{\mu_w l_0} \tag{3-31}$$

where K_w is the permeability for wetting phase in the unsaturated porous material.

Comparing Eq. (3-30) with Eq. (3-31), we can derive the permeability of the wetting phase in the unsaturated porous material as

$$K_w = \frac{\pi}{128}\frac{l_0^{1-D_T}}{A_{cs}(P_m + \overline{P_{c,w}})}(P_m\sum_{i=1}^{J}\lambda_{w,i}^{3+D_T} + FT_{st}\cos\theta\frac{1-S\phi}{S\phi}\sum_{i=1}^{J}\lambda_{w,i}^{2+D_T}) \tag{3-32}$$

where $\overline{P_{c,w}}$ is the average capillary pressure for wetting phase which is given by Eq. (3-25).

If we apply the above analysis to saturated porous media, we can obtain the permeability in saturated porous media as

$$K=\frac{\pi}{128}\frac{l_0^{1-D_T}}{A_{cs}(P_m+\overline{P_c})}(P_m\sum_{i=1}^{J}\lambda_i^{3+D_T}+FT_{st}\cos\theta\frac{1-\phi}{\phi}\sum_{i=1}^{J}\lambda_i^{2+D_T}) \tag{3-33}$$

where the average capillary pressure in saturated porous media can be obtained with the aid of Eq. (3-4):

$$\overline{P_c}=\int_{\lambda_{\min}}^{\lambda_{\max}}P_c f(\lambda)d\lambda=\frac{d_f}{1+d_f}\frac{FT_{st}\cos\theta}{\lambda_{\min}}\frac{1-\phi}{\phi} \tag{3-34}$$

Based on the physical definition of the relative permeability, $k_{rw}=K_w/K$, dividing Eq. (3-33) by Eq. (3-32), we can derive the relative permeability of the wetting phase in the unsaturated porous material

$$k_{rw}=\frac{(P_m+\frac{d_f}{1+d_f}\frac{FT_{st}\cos\theta}{\lambda_{\min}}\frac{1-\phi}{\phi})(P_m\sum_{i=1}^{J}\lambda_{w,i}^{3+D_T}+FT_{st}\cos\theta\frac{1-S\phi}{S\phi}\sum_{i=1}^{J}\lambda_{w,i}^{2+D_T})}{(P_m+\frac{d_{f,w}}{1+d_{f,w}}\frac{FT_{st}\cos\theta}{\lambda_{\min,w}}\frac{1-S\phi}{S\phi})(P_m\sum_{i=1}^{J}\lambda_i^{3+D_T}+FT_{st}\cos\theta\frac{1-\phi}{\phi}\sum_{i=1}^{J}\lambda_i^{2+D_T})} \tag{3-35}$$

Applying the above analysis to the gas flow in the non-wetting phase of unsaturated porous media, the total gas flow rate and the permeability of non-wetting phase can be derived. Note that, unlike that in the special wetting phase, the special capillary pressure P_c can be zero in the non-wetting phase. So the total flow rate Q_g of non-wetting phase in a unit cell is

$$Q_g=\sum_{i=1}^{J}q_g(\lambda_{g,i})=\sum_{i=1}^{J}\frac{\pi}{128}\frac{\Delta P_m}{l_t(\lambda_g)}\frac{\lambda_{g,i}^4}{\mu_g} \tag{3-36}$$

where λ_g is the special equivalent diameter of the non-wetting phase in the unsaturated porous material. Thus, the permeability of the non-wetting phase can be expressed as

$$K_g = \frac{\pi}{128}\frac{l_0^{1-D_T}}{A_{cs}}\sum_{i=1}^{J}\lambda_{g,i}^{3+D_T} \tag{3-37}$$

Based on the physical definition of the relative permeability $k_{rg} = K_g / K$, dividing Eq. (3-33) by Eq. (3-37), we can derive the relative permeability of the non-wetting phase in the unsaturated porous material

$$k_{rg} = \frac{(P_m + \frac{d_f}{1+d_f}\frac{FT_{st}\cos\theta}{\lambda_{\min}}\frac{1-\phi}{\phi})\sum_{i=1}^{J}\lambda_{g,i}^{3+D_T}}{P_m\sum_{i=1}^{J}\lambda_i^{3+D_T} + FT_{st}\cos\theta\frac{1-\phi}{\phi}\sum_{i=1}^{J}\lambda_i^{2+D_T}} \tag{3-38}$$

Eqs. (3-35) and (3-38) indicate that the relative permeability of the unsaturated porous material can be a function of parameters P_m, F, T_{st}, θ, ϕ and the microstructural parameters (d_f, D_T, and $\lambda_{\min}$) of a medium.

3.3 Monte Carlo Simulation

The present Monte Carlo approach can be used to simulate the fractal distribution of the sizes and tortuosity of capillaries for calculation of relative permeability.

The cumulative mathematical probability (R) in the scope of $\lambda_{\min} \sim \lambda$ is found by

$$R(\lambda) = \int_{\lambda_{\min}}^{\lambda} f(\lambda)d\lambda = \int_{\lambda_{\min}}^{\lambda} d_f\lambda_{\min}^{d_f}\lambda^{-(1+d_f)}d\lambda = 1-(\lambda_{\min}/\lambda)^{d_f} \tag{3-39}$$

Eq. (3-39) shows that $R = 0$ when $\lambda \to \lambda_{\min}$ and $R \approx 1$ when $\lambda \to \lambda_{\max}$.

From Eq. (3-39), we can obtain

$$1-R=(\lambda_{\min}/\lambda)^{d_f} \tag{3-40}$$

From Eq. (3-40), a pore size λ can be expressed as

$$\lambda=\lambda_{\min}/(1-R)^{1/d_f}=\lambda_{\max}\frac{m}{(1-R)^{1/d_f}} \tag{3-41}$$

where $\lambda_{\min}\le\lambda\le\lambda_{\max}$. Eq. (3-41) is the mathematical probability model for the distributions of pore size in the present numerical simulations. And for the i th capillary selected arbitrarily, Eq. (3-41) can be expressed as

$$\lambda_i=\lambda_{\min}/(1-R_i)^{1/d_f}=m[\lambda_{\max}/(1-R_i)^{1/d_f}] \tag{3-42}$$

where, R_i is a cumulative mathematical probability in the scope of $\lambda_{\min}\sim\lambda_i$. By randomly assigning a value of R_i within [0, 1], we can simulate the capillary size distribution, provided that we know the maximum and minimum capillary sizes.

For the special bi-dispersed porous material, the maximum capillary size and $\lambda_{\min}/\lambda_{\max}=m$ can be respectively estimated by (Yu and Cheng, 2002)

$$\lambda_{\max}=\frac{\overline{R}_c}{2}\left[\sqrt{2\left(\frac{1-\phi_m}{1-\phi}-1\right)}+\sqrt{\frac{2\pi}{\sqrt{3}}\frac{1-\phi_m}{1-\phi}}-2\right] \tag{3-43}$$

$$m=\frac{\sqrt{2}}{d^+}\sqrt{\frac{1-\phi}{1-\phi_m}} \tag{3-44}$$

where, $\overline{R}_c=0.03\,cm$ is the cluster average radius, $d^+=24$ is the ratio of the above mentioned cluster average size to the minimum grain size (Yu and Cheng, 2002), and ϕ_m is the special micro porosity in the above mentioned cluster and expressed as (Chen et al., 2000)

$$\phi_m = 0.342\phi \tag{3-45}$$

The convergence criterion is as follows:

$$A_J = A_p / \phi > A_{cs} \tag{3-46}$$

where, A_p is the total area of pore in the single unit cell, i.e.

$$A_p = \sum_{i=1}^{J} \pi\lambda_i^2 / 4 \tag{3-47}$$

Stop the above numerical simulations and keep an account of the total simulated number (*J*) and the last/convergent relative permeability in one run for a special given porosity. And in Eq. (3-46), A_J is the special area computed after the *J*th calculation in one run. If the special converged relative permeability is derived in one run, establish the relative permeability as k_{rn} (*n*= 1, 2, 3, ..., $N^{'}$). So the mean relative permeability for a special given porosity can be written as

$$\langle k_r \rangle = \frac{1}{N^{'}} \sum_{n=1}^{N^{'}} k_{rn} \tag{3-48}$$

where $N^{'}$ is the total number of the mentioned runs for the special given porosity. Thus, the variation can be defined by

$$\sigma = \sqrt{\langle k_r^2 \rangle - \langle k_r \rangle^2} \tag{3-49}$$

where, $\langle k_r^2 \rangle = \frac{1}{N^{'}} \sum_{n=1}^{N^{'}} k_{rn}^2$.

The above algorithm for calculation of the relative permeability in fractal unsaturated porous material can be summarized as follows:

1. Given the fixed porosity ϕ, determine the micro porosity ϕ_m in the above mentioned cluster from Eq. (3-45).

2. Determine *m* and $\lambda_{\max}$ from Eqs. (3-44) and (3-43), respectively.

3. d_f and D_T are obtained from Eqs. (3-7) and (3-19), respectively, calculate the mentioned pressure ΔP, the surface tension T, the contact angle θ (In this simulation, we used the parameters reported in Amico and Lekakou (2001), i.e. T=0.044N.m, $\theta = 57^\circ$, $\Delta P = 20000.0 Pa$).

4. Generate an arbitrary number R_i of 0-1 by present Monte-Carlo approach.

5. Compute λ_i by using Eqs. (3-42)-(3-44).

6. If $\lambda_i > \lambda_{\max}$, return to the program 4, otherwise go on the next program.

7. Determine A_p from Eq. (3-47).

8. Compute the relative permeability （k_{rw} and k_{rg}）from Eqs. (3-35) and (3-38), respectively.

Steps 5-8 can be repeated for computation of relative permeability until a converged value is derived at a given fixed porosity. Step 6 implies that the arbitrarily generated pore size λ_i in the numerical simulations is not permitted to outstrip the maximum pore size $\lambda_{\max}$ so as to comply with the practical physical condition.

3.4 Results and discussion

Figure 3-2 shows the capillary sizes arbitrarily selected by the mathematical probability model described by Eq. (3-42) in the present simulations for the special bi-dispersed porous material at the porosity of 0.25. It is found from Figure 3-2 that the minimum size of pore is approximately $7.2\mu m$. Calculation from Eqs. (3-27), (3-43) and Eq. (3-44) gives $\lambda_{\min,w} = 7.3\mu m$ at the porosity of 0.25. The error is only 1.4%, which means that Monte Carlo simulations are accurate. From Figure 3-2 it can be observed that the number of the larger capillaries is much less than that of smaller ones, and this is agreed with the classical fractal geometry.

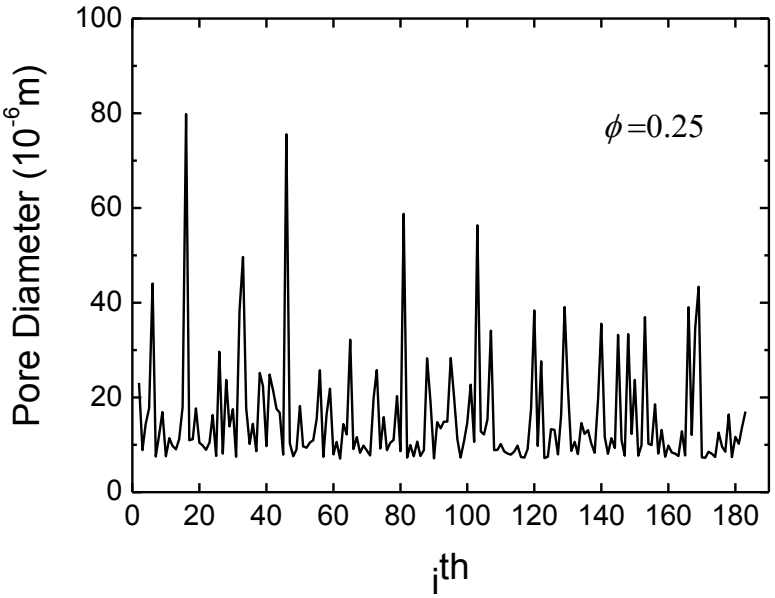

Figure 3-2 The pore sizes of the unsaturated porous material simulated by Monte Carlo technique

Figure 3-3 displays a comparison of the average capillary pressure estimated by this model (by Eq. (3-25)) and that from available experiments with non-crimp fabrics (Verrey et al., 2006). It can be observed that there is good agreement between the model predictions and the available experimental data (Verrey et al., 2006). Figure 3-3 also shows that the average capillary pressure decreases with the increase of porosity, and this is agreed with the practical physical condition. Figure 3-4 displays a comparison on the capillary pressure versus saturation at three different porosities. Figure 3-4 shows that the capillary pressure decreases with increasing saturation, and the capillary pressure increases sharply with decreasing saturation at small saturation.

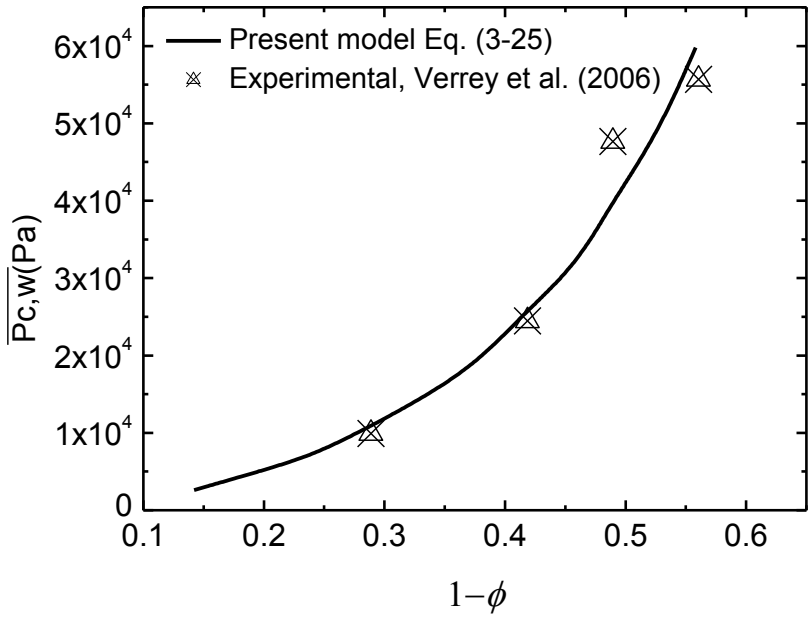

Figure 3-3 Influence of porosity on the average capillary pressure

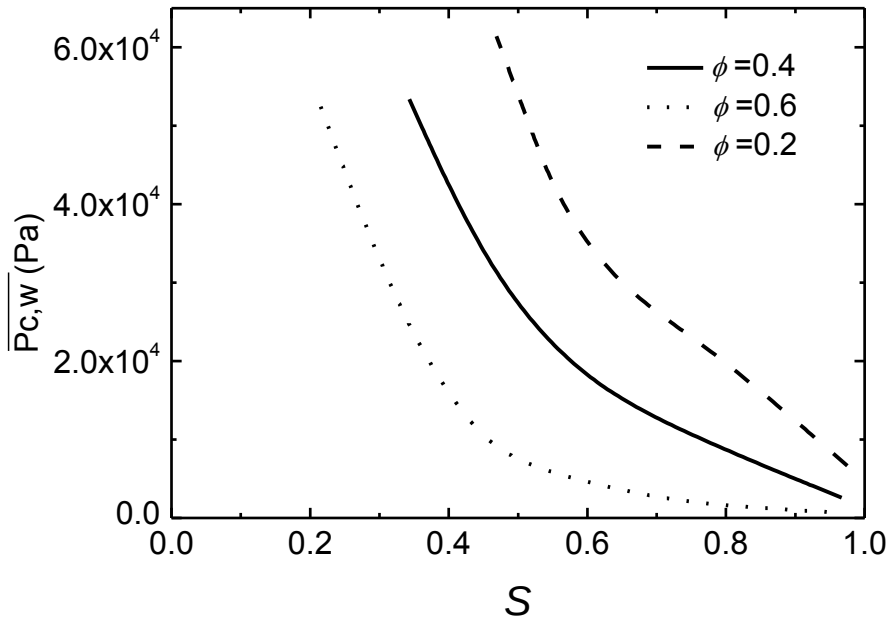

Figure 3-4 The average capillary pressure of wetting phase in unsaturated porous media versus saturation for three different porosities

Figure 3-5 compares the capillary pressure from the present model predictions by Eq. (3-25) and those from experiments (Dana and Skoczylas, 2002). It is seen that there is a fair agreement between the model predictions and the available experimental result (Dana and Skoczylas, 2002). The capillary pressure can reach $5.34\times10^4\,pa$ when saturation decreases to 0.34 at $\phi=0.4$. So the influence of capillary pressure of the unsaturated porous material on relative permeability cannot be ignored at low saturation.

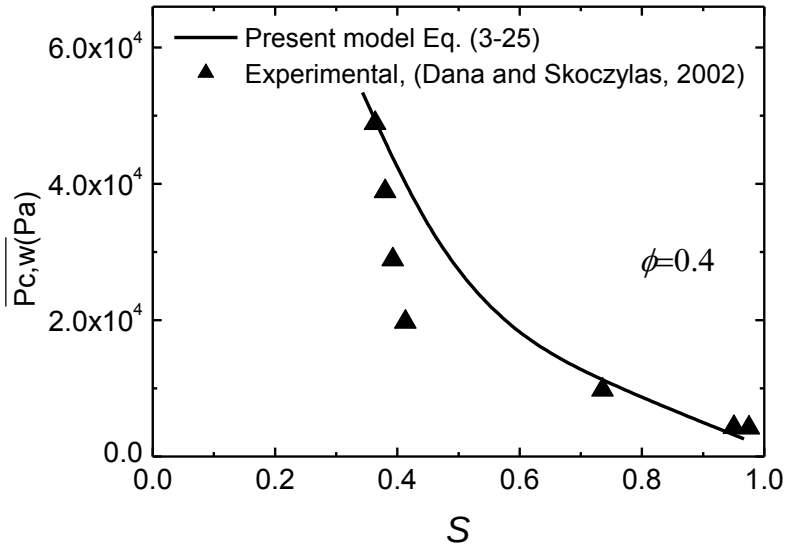

Figure 3-5 A comparison between the mean capillary pressure for wetting phase in the unsaturated porous material by present model and the available experimental result (Dana and Skoczylas, 2002)

Figure 3-6 shows that the fractal dimension of wetting phase and non-wetting phase depend on the porosity of unsaturated porous material according to Eqs. (3-26) and (3-28). The figure denotes that the larger the porosity, the larger the fractal dimension. The phenomenon can be explained by the fact that larger porosity means higher pore area, leading to a higher phase area/volume and larger fractal dimension. It is further seen that the fractal dimension of non-wetting phase increases with decreasing saturation. The phenomenon may be explained that an increase in saturation results in the area of non-wetting phase decreasing and the decrease of the fractal dimension of non-wetting phase.

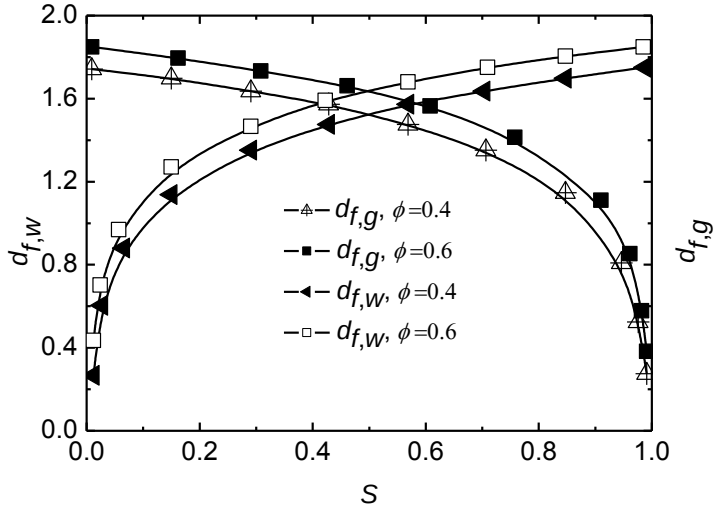

Figure 3-6 Effects of porosity on the fractal dimension of wetting phase and non-wetting phase

Figure 3-7(A) compares the predictions from the simulations (by Eq. (3-35)) for monodispersed porous media and the published experimental result (Levec et al., 1986; Kaviany, 1995) (the experimental data are from Figure 5 in Ref. (Levec et al., 1986)), and good agreement between the model estimations from the simulations and the available experimental data is found. Li and Hone (2001) discussed the predicted data and the comparison in the special nitrogen-water systems. Figure 3-7(B) shows a comparison of the relative permeability calculated by Monte Carlo technique (by Eq. (3-38)) and the published experimental data (Li and Hone, 2001), and good agreement between them is again observed. Figure 3-7 shows that relative permeability for the wetting phase (k_{rw}) decreases as saturation of the wetting phase decreases. On the contrary, from Figure 3-7 it is found that relative permeability for the non-wetting phase (k_{rg}) decreases as saturation of the wetting phase increases. This is

understandable as higher saturation of the wetting phase (*S*) means more fluid and less gas.

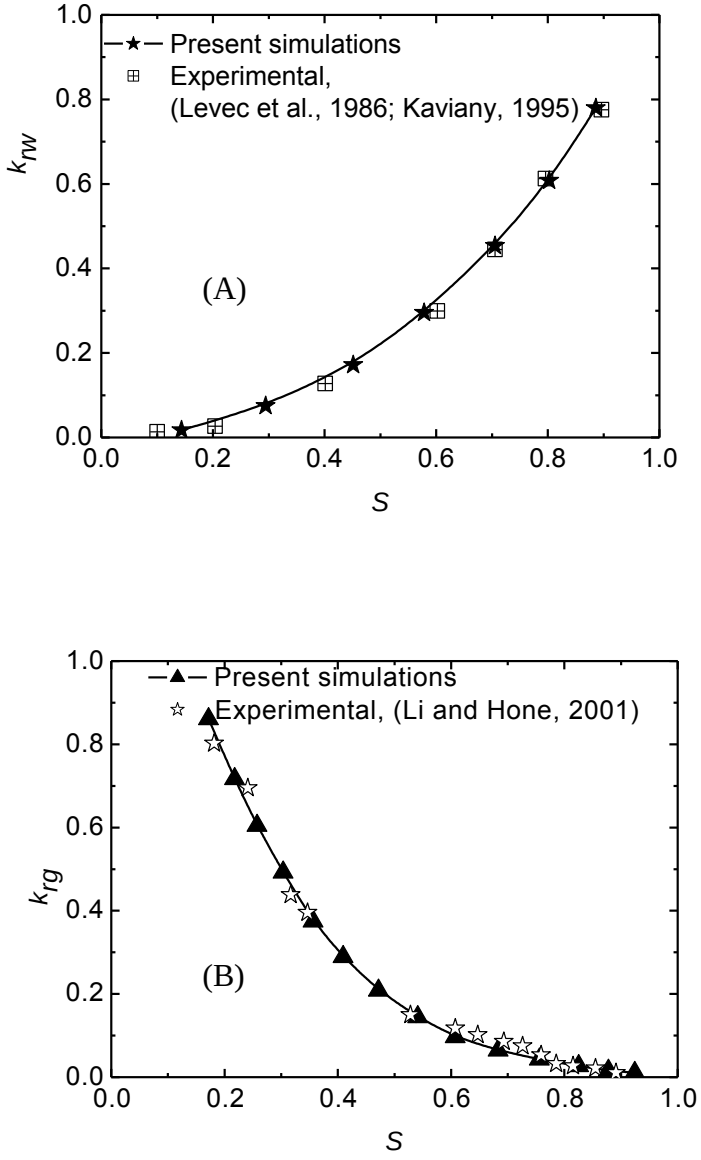

Figure 3-7 Comparison between this Mont Carlo technique and the published experimental result (Levec et al., 1986; Kaviany, 1995; Li and Hone, 2001) for the wetting phase (k_{rw}) and the non-wetting phase (k_{rg}), respectively

3.5 Conclusions

The relative permeability of unsaturated porous material has been modeled and predicted by using the Monte Carlo Simulation technique in this chapter. The proposed model can be expressed as a function of the porosity of the unsaturated porous material, the area fractal dimension for pores, the fractal dimension of tortuous capillaries, saturation, capillary pressure and microstructural geometry parameters of a medium. It is found that the capillary pressure decreases with increasing saturation, and the capillary pressure increases sharply with decreasing saturation at small saturation. In addition, it is found that the fractal dimension of wetting phase and non-wetting phase depend on the porosity of the unsaturated porous material. The present model contains no additional or empirical constant, which is normally required in conventional models. The model calculations are compared with the available experimental result, and good agreement between the model calculations and the published experimental result is found. So the validity of our model is thus verified. Therefore, the proposed probability model can reveal the physical mechanisms of relative permeability in porous media.

Chapter 4 Prediction of permeabilities of fibrous gas diffusion layer in proton exchange membrane fuel cells by means of fractal geometry

4.1 Introduction

The proton exchange membrane fuel cells (PEMFCs) are promising energy supply equipments for stationary and mobile practical applications because of high power density, low emissions, high efficiency, low noise, low operating temperature, and great environmental compatibility (Kannan et al., 2008; Cindrella et al., 2009; Chan et al., 2012; Zhu, 2013; Shou et al., 2013). The PEMFCs are composed of gas diffusion layer (GDL) including gas diffusion backing (GDB) and microporous layer (MPL), membrane electrode assembly (MEA), and bipolar plates with gas channels. The fibrous GDL is a core component of a PEMFC, enabling transport of gases, liquids and electricity within the cell. One of the major limitations to the performance of PEMFCs is flooding of water, which hinders the transport of reactant gas to the reaction sites, deteriorating the power output. It is therefore crucial to understand the transport of water and gas through the fibrous GDL in PEMFCs. Hence, the study of permeability, water and gas relative permeabilities of fibrous GDL has attracted the attention of many researchers. For example, Cindrella and Kannan (2009) provided a comprehensive and systematic review of the published work on the GDL including, the essential properties of the GDL, the characterization techniques for GDL, the current status and future directions of GDL in PEMFCs, etc. Zhu (2013) derived a modified fractal geometry model to estimate the through-plane permeability of water

in GDL. In this model (Zhu, 2013), a theoretical model of the porous structure of fibrous GDL was presented as a composite object of parallel and perpendicular fluid channels to the flow direction. Benziger et al. (2005) investigated the water flow in GDL of PEMFCs experimentally and showed that few percent of the void part of fibrous GDL was essential for the water transport and the smaller micro-pores could be remained free for the physical diffusion of reactant gas. Zamel et al. (2011) presented a morphology geometry model to investigate the effects of water on physical diffusion process in GDL of PEMFCs. Rama et al. (2010) considered three different types of treatments, viz. electrochemical, fluid dynamics and porous flow treatments, for the transport mechanistic models of fluids in GDL of PEMFCs. Numerical simulator, like MUFTE_UG (Acosta et al., 2006), was also applied to study the water and gas transport based on extended Darcy's law and experimentally determined porosity and tortuosity. The complex behavior of the two-phase fluid flow in fibrous GDL of PEMFCs was also studied using lattice Boltzmann method (LBM) (Koido et al., 2008). Besides, Hao and Cheng (2010) investigated the relative permeabilities of GDL in PEMFCs using the free energy multiphase LBM. Because LBM requires regular square grids, it is only approximate when applied to the curved surface of fibers. Dawes et al. (2009) proposed a three-dimensional numerical model to investigate the influences of water flooding on the cell performance parameters. In this mentioned model (Dawes et al., 2009), parametric analyses were undertaken, which consisted of investigations into the influences of diffusivity and permeability, to determine the way to simulate the transport restrictions caused by liquid water

flooding. However, so as to cut down the complicacy of the simulation, the most important liquid phase of water cannot be modeled directly in their work (Dawes et al., 2009). Additionally, Fan and He (2012) obtained a mathematical model of the air permeability in a hierarchic porous material. The proposed model (Fan and He, 2012) was successfully used to elucidate the new physical phenomenon of air permeability in the cocoon. Recently, based on the special assumption that GDL consists of many periodical unit cells, Shou and Fan (2013) also established semi-mathematical formulas to determine the effective diffusivities of GDL in PEMFCs. Although the prediction of Shou and Fan's (2013) model is consistent with the available experimental data and numerical results, the assumption was idealized because most fibrous structures are not composed of periodical unit cells.

Although many researchers have studied the transport properties of fibrous GDL through experimental investigation and numerical simulations, analytical studies is needed to further elucidate the relationship between the micro-structure of fibrous GDL and its water and gas relative permeabilities. In the present investigation, a fractal model is applied to study the permeabilities of fibrous GDL, as it has been well established that porous fibrous materials are fractal bodies (Yu and Cheng, 2002; Shi et al., 2008; Shou et al., 2010; Wu et al., 2011).

4.2 Fractal characteristics of porous fibrous GDL

The transfer routes of fluids in porous fibrous materials have fractal characteristics and can be described as arbitrary fractal tubes (Yu and Cheng, 2002). The fibrous GDL of PEMFCs is typically a dual-layer carbon-based porous substrate. The experimental studies on permeation have displayed that the tortuous capillaries in porous fibrous GDL are fractal objects (Bal et al., 2011; Wu et al., 2011). Figure 4-1 displays an example of a porous random fibrous structure in GDL. Due to the complexity of the fibrous structure, it is difficult to directly determine the permeability and relative permeabilities of fibrous GDL by solving the fluid dynamics equations. We assume that the fibrous structure of GDL is constructed by a bundle of fractal tortuous capillaries with different pore sizes, as shown in Figure 4-2, and the water and gas permeation within the GDL is equivalent to that within the capillaries channels with various sizes. Make the diameter of a common capillary tube in GDL be λ, and its tortuous distance along the transport direction be $l_t(\lambda)$, the actual distance $l_t(\lambda)$ for liquid or gas traveling in GDL is related to the capillary size via the following fractal relation (Yu and Cheng, 2002):

$$l_t(\lambda) = \lambda^{1-D_T} l_0^{D_T} \tag{4-1}$$

where l_0 is the distance of the straight capillary, is equivalent to the thickness of fibrous GDL, and D_T is the tortuosity fractal dimension, with $1 \le D_T \le 2$, standing for the degree of convolutedness of the capillary pathways for water or gas flow via the porous fibrous GDL. High value of D_T within this scope is equivalent to a

highly tortuous capillary, while $D_T = 1$ represents the straight capillary pathway, $D_T = 2$, is equivalent to a highly tortuous line that fills a flat surface.

Besides the capillary convolutedness, the quantity of capillaries with diameter λ is another significant geometry parameter for the fractal analysis of porous fibrous GDL. For the fractal porous fibrous materials, the quantity of capillaries whose sizes are within the infinitesimal scope from λ to $\lambda + d\lambda$ can be expressed as (Yu and Cheng, 2002)

$$-dN = d_f \lambda_{\max}^{d_f} \lambda^{-(d_f+1)} d\lambda \tag{4-2}$$

where, N is the total quantity of capillaries with the diameter larger than λ, $\lambda_{\max}$ and $\lambda_{\min}$ are the maximum and minimum diameter of capillary in porous fibrous materials, respectively; and d_f is the area fractal dimension of pores, with $1 < d_f < 2$, relating to the quantity of capillaries in fibrous GDL of PEMFCs; and the higher the value of d_f is, the more the quantity of capillaries. The negative sign in Eq. (4-2) implies that capillary quantity decreases with increasing λ, and $-dN > 0$.

The area fractal dimension of pores can be expressed as (Yu and Li, 2001)

$$d_f = 2 - \frac{\ln \phi}{\ln m} \tag{4-3}$$

where ϕ is the porosity of the porous GDL. In general, the porosity of porous fibrous GDL of PEMFCs is greater than 0.70. For porous media with $\lambda_{\min} / \lambda_{\max} = m \le 10^{-2}$, Eqs. (4-2) and (4-3) hold approximately. In reported literatures (Katz and Thompson, 1985; Feng et al., 2004; Cai et al., 2010; Cai et al., 2012), both $m = 10^{-2}$ and $m = 10^{-3}$ are applied for fractal porous material. For example, Katz

and Thompson (1985) employed SEM and physical optics result to display that the pore rooms of some sandstones and found that the fractal statistics with $m=10^{-2}$ provided very good estimation of porosity. Cai et al. (2010; 2012) proposed effective fractal methods to investigate the invasion depth of extraneous fluids and spontaneous Co-current imbibition in porous reservoir rocks using $m=10^{-2}$. And the models predictions (Cai et al., 2010; Cai et al., 2012) were in good agreement with the published results. Additionally, Feng et al. (2004) found that $m=10^{-3}$ was the fitting to the experimental data for estimating the fractal dimension of fractal Sierpinski carpet.

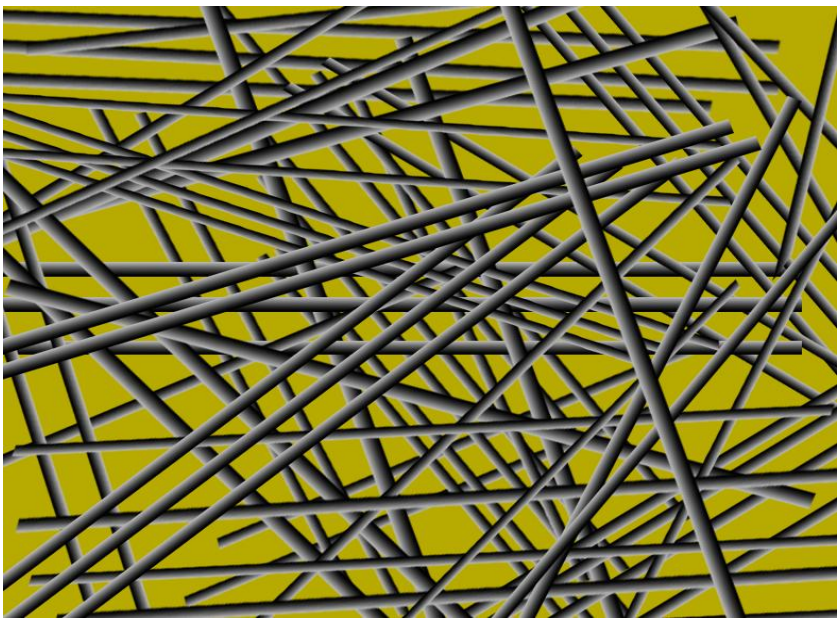

Figure 4-1 An example of a porous medium with random fibrous structure

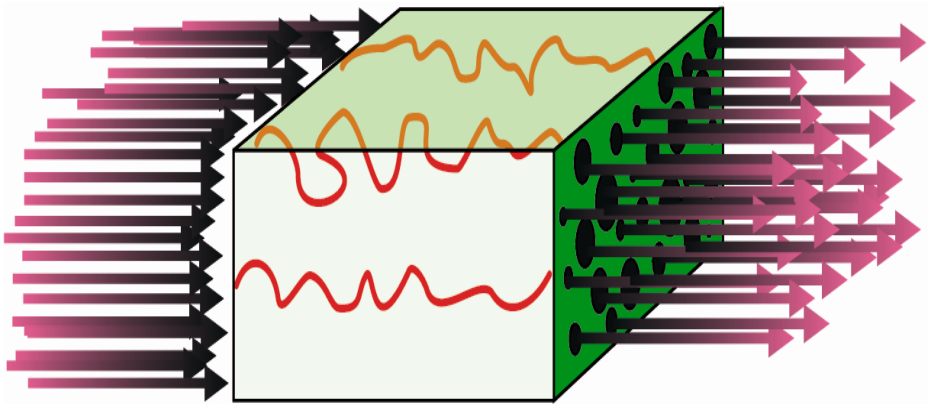

Figure 4-2 Fractal models for water and gas transport through porous fibrous GDL of PEMFCs

4.3 Fractal analysis of permeability and relative permeabilities of porous GDL

The relative permeabilities of water phase and gas phase also are of great importance to performance of PEMFCs. In the presence of special two phases, the permeability of one phase is decreased because the quantity of available fluid flow pathways is decreased by the presence of the other phase. The relative permeability is the ratio of the effective permeability of one phase to the intrinsic permeability of the fibrous medium, viz. (Demond and Roberts, 1993)

$$k_{rn}(S) = \frac{K_n(S)}{K} \tag{4-4}$$

where $k_{rn}(S)$ is the relative permeability of one phase, and $K_n(S)$ is the effective permeability of one phase as a function of liquid saturation (S).

Take into account a bundle of tortuous capillary tubes making up of a unit cell in Figure 4-2. The total flow rate $Q(\lambda)$ in the special unit cell is derived by

summing up the flow rates via all the single capillaries. As shown in Figure 4-2, the flow rate $q(\lambda)$ via a individual tortuous capillary can be expressed by the Hagen-Poiseulle formula (Eq. (3-8)) (Denn, 1986).

Then with the aid of Eq. (4-2), the total flow rate $Q(\lambda)$ is derived by integrating the single flow rate, $q(\lambda)$, over the total scope of pore sizes from $\lambda_{\min}$ to $\lambda_{\max}$ in the above mentioned unit cell in virtue of the fractal bundle capillaries model illustrated in Figure 4-2, as follows:

$$Q(\lambda)=\int_{\lambda_{\min}}^{\lambda_{\max}} q(\lambda)(-dN)=\int_{\lambda_{\min}}^{\lambda_{\max}}[\frac{\pi}{128}\frac{\Delta p}{(\lambda^{1-D_T}l_0^{D_T})}\frac{\lambda^4}{\mu}][d_f\lambda_{\max}^{d_f}\lambda^{-(d_f+1)}d\lambda]$$

$$=\frac{\pi\Delta p l_0^{-D_T}}{128\mu}\frac{d_f}{3+D_T-d_f}[1-m^{3+D_T-d_f}]\lambda_{\max}^{3+D_T} \tag{4-5}$$

For creeping flow through a porous medium, applying Darcy's law, we can derive the intrinsic permeability of fibrous porous GDL as follows:

$$K=\frac{\mu l_0 Q(\lambda)}{\Delta p A_{cs}}=\frac{\pi l_0^{1-D_T}}{128A_{cs}}\frac{d_f}{3+D_T-d_f}[1-m^{3+D_T-d_f}]\lambda_{\max}^{3+D_T} \tag{4-6}$$

where A_{cs} is the cross-section area. For fiber reinforced composites, A_{cs} can be approximately expressed as (Yu et al., 2001)

$$l_0=\sqrt{A_{cs}} \tag{4-7}$$

Substituting Eq. (4-7) into Eq. (4-6), Eq. (4-6) can be further modified as

$$K=\frac{\pi}{128A_{cs}^{(1+D_T)/2}}\frac{d_f}{3+D_T-d_f}[1-m^{3+D_T-d_f}]\lambda_{\max}^{3+D_T} \tag{4-8}$$

The total pore area in intersecting surface can be derived with the aid of Eq. (4-2):

$$A_p = \int_{\lambda_{\min}}^{\lambda_{\max}} \pi(\frac{\lambda}{2})^2(-dN) = \frac{\pi d_f(1-m^{2-d_f})}{4(2-d_f)}\lambda_{\max}^2 \tag{4-9}$$

Due to

$$d_f = 2 - \frac{\ln\phi}{\ln m} \Rightarrow \phi = m^{2-d_f} \tag{4-10}$$

By inserting Eq. (4-10) into Eq. (4-9), Eq. (4-9) can be further reduced to

$$A_p = \frac{\pi d_f(1-\phi)}{4(2-d_f)}\lambda_{\max}^2 \tag{4-11}$$

Whereas the cross-section area is

$$A_{cs} = \frac{A_p}{\phi} = \frac{\pi d_f(1-\phi)}{4(2-d_f)\phi}\lambda_{\max}^2 \tag{4-12}$$

Inserting Eq. (4-12) into Eq. (4-8), the intrinsic permeability of porous fibrous GDL can be further modified as

$$K = \frac{\pi}{128}\frac{d_f}{3+D_T-d_f}[\frac{4(2-d_f)\phi}{\pi d_f(1-\phi)}]^{(1+D_T)/2}[1-m^{3+D_T-d_f}]\lambda_{\max}^2 \tag{4-13}$$

Due to $1<D_T<2$, $m\le 10^{-2}$, $1<d_f<2$, $m^{3+D_T-d_f} << 1$, Eq. (4-13) can be further reduced to

$$K = \frac{\pi}{128}\frac{d_f}{3+D_T-d_f}[\frac{4(2-d_f)\phi}{\pi d_f(1-\phi)}]^{(1+D_T)/2}\lambda_{\max}^2 \tag{4-14}$$

Eq. (4-14) shows that the intrinsic permeability of GDL is connected with the tortuosity fractal dimension, the porosity, the pore area fractal dimension, and the geometry structural parameters of porous GDL ($\lambda_{\max}$). Besides, Eq. (4-14) indicates the intrinsic permeability of GDL is very impressible to the maximum ($\lambda_{\max}$), and the

intrinsic permeability is basically decided by the maximum pore. It is found that the present intrinsic permeability of GDL does not include any empirical constant in this fractal model. However, the Kozeny–Carman equation shown in Eq. (2-3) has two empirical constants. Besides, the Kozeny–Carman equation does not characterize the influences of structural parameters of the fibrous materials on the intrinsic permeability of the porous materials.

Since the hydraulic sizes of capillaries are non-uniform in porous materials, the average hydraulic radius of capillary can be obtained as (Yun et al., 2008)

$$r_h = (\sum_{i=1}^{N} N_i r_i^4)^{1/4} \tag{4-15}$$

where *Ni* (*i* = 1, 2, . . . , *N*) is the quantity of capillaries with radius r_i in porous materials. In general, *Ni* is unknown and it is difficult to obtain directly from Eq. (4-15). Because the number of capillaries is numerous in porous media, the average hydraulic radius of capillaries can be obtained with the aid of Eq. (4-2):

$$r_h = [\int_{r_{\min}}^{r_{\max}} r^4 (-dN)]^{1/4} = (1 - m^{4-d_f})^{1/4} (\frac{d_f}{4-d_f})^{1/4} r_{\max} \tag{4-16}$$

Since $0 < d_f < 2$, $4 - d_f > 2$, $m \le 10^{-2}$, $m^{4-d_f} << 1$, Eq. (4-16) can be further reduced to

$$r_h \cong (\frac{d_f}{4-d_f})^{1/4} r_{\max} \tag{4-17}$$

where $r_{\max} = \lambda_{\max} / 2$ is the maximum hydraulic radius of capillary. Eq. (4-17) shows a fractal expression of the average hydraulic radius in porous materials.

For random homogeneous fiber structures (see Figure 4-1), assuming that porous isotropic fiber bundle is a collection of non-uniform capillary tubes (see Figure 4-2, the average radius of capillaries can be estimated as a function of the porosity and the average diameter of fibre (Tomadakis and Robertson, 2005; Li et al., 2010):

$$r_h = \frac{\phi}{2(1-\phi)} D_f \tag{4-18}$$

Combining Eq. (4-17) and Eq. (4-18), the maximum hydraulic diameter of capillary is as a function of average fiber diameter, the porosity and pore area fractal dimensions:

$$\lambda_{\max} = \frac{\phi}{(1-\phi)} \left(\frac{4-d_f}{d_f}\right)^{1/4} D_f \tag{4-19}$$

Eq. (4-19) is a fractal expression of maximum hydraulic diameter of capillary in porous materials.

By inserting Eq. (4-19) into Eq. (4-14), we can derive a mathematical analytical model for the dimensionless permeability of fibrous GDL:

$$\frac{K}{D_f^2} = \frac{\pi d_f}{128(3+D_T-d_f)} \left(\frac{4-d_f}{d_f}\right)^{1/2} \left[\frac{4(2-d_f)\phi}{\pi d_f (1-\phi)}\right]^{(1+D_T)/2} \left[\frac{\phi}{(1-\phi)}\right]^2 \tag{4-20}$$

Eq. (4-20) depicts that the dimensionless permeability of fibrous GDL can be a function of the pore fractal dimension, the porosity and tortuosity fractal dimension.

The transport rate of water and gas through fibrous GDL depend on the two phases transport properties (viz. relative permeabilities to water and gas flow) and their relation to the level of water saturation. The water saturation (S) is usually defined as (Bear, 1972)

$$S = \frac{V_w}{V_p} \tag{4-21}$$

where V_p is pore volume, and V_w is the volume occupied by water.

And

$$\frac{V_w}{V_p} + \frac{V_g}{V_p} = 1 \tag{4-22}$$

where V_g is the volume taken up by gas. Based on Eqs. (4-21) and (4-22), we have

$$1 - S = \frac{V_g}{V_p} = \frac{\pi\lambda_g^2 / 4}{\pi\lambda^2 / 4} = \frac{\lambda_g^2}{\lambda^2} \tag{4-23}$$

Hence, according to Eq. (4-23), the effective diameter (λ_g) of gas taking up the intersecting surface of a capillary route can be expressed as a function of water saturation (*S*) and the diameter (λ) of a capillary pathway:

$$\lambda_g = \lambda\sqrt{1 - S} \tag{4-24}$$

The volume, V_w, taken up by the water can be written as

$$V_w = V_p - V_g = \frac{\pi\lambda^2}{4} - \frac{\pi\lambda_g^2}{4} = \frac{\pi\lambda_w^2}{4} \tag{4-25}$$

Based on the definition of water saturation, we have

$$S = \frac{V_w}{V_p} = \frac{\lambda_w^2}{\lambda^2} \tag{4-26}$$

Similarly, according to Eq. (4-26), the effective diameter (λ_w) of water taking up the intersecting surface of a capillary route can be expressed as a function of water saturation (*S*) and the diameter (λ) of a capillary pathway:

$$\lambda_w = \lambda\sqrt{S} \tag{4-27}$$

According to Eq. (4-27), the effective maximum ($\lambda_{\max,w}$) and the smallest ($\lambda_{\min,w}$) diameters for water phase can be obtained as

$$\lambda_{\max,w} = \lambda_{\max}\sqrt{S}\,,\quad \lambda_{\min,w} = \lambda_{\min}\sqrt{S} \tag{4-28}$$

Employing the analogy between the single-phase and two-phase, and modifying Eq. (4-3), the fractal dimension for water phase may be written as

$$d_{f,w} = 2 - \frac{\ln \phi_w}{\ln \dfrac{\lambda_{\min,w}}{\lambda_{\max,w}}} \tag{4-29}$$

where ϕ_w is the volume fractions for water phase in a unit cell which can be expressed as (Bear, 1972)

$$\phi_w = S\phi \tag{4-30}$$

Inserting Eqs. (4-28) and (4-30) into Eq. (4-29), Eq. (4-29) can be rewritten as

$$d_{f,w} = 2 - \frac{\ln(S\phi)}{\ln \dfrac{\lambda_{\min}\sqrt{S}}{\lambda_{\max}\sqrt{S}}} = 2 - \frac{\ln(S\phi)}{\ln m} \tag{4-31}$$

For a common capillary pipe partly filled with water and gas in porous media, we assume that water and gas flow via tortuous routes have approximately the same tortuosity as the single-phase fluid flow, that is, $D_T = D_{T,w} = D_{T,g}$.

Now we apply the above analysis to the two-phase fluid flows and modify the single-phase permeability model (Eq. (4-14)). Besides, $\lambda_{\max}$ is replaced by $\lambda_{\max,w}$, d_f is replaced by $d_{f,w}$, and ϕ is replaced by ϕ_w in Eq. (4-14). Thus we can

obtain the phase permeability of GDL for water as follows

$$K_w = \frac{\pi}{128}\frac{d_{f,w}}{3+D_T-d_{f,w}}\left[\frac{4(2-d_{f,w})\phi_w}{\pi d_{f,w}(1-\phi_w)}\right]^{(1+D_T)/2}\lambda_{\max,w}^2 \tag{4-32}$$

Inserting Eqs. (4-28) and (4-30) into Eq. (4-32), Eq. (4-32) can be further modified as

$$K_w(S) = \frac{\pi}{128}\frac{d_{f,w}}{3+D_T-d_{f,w}}\left[\frac{4(2-d_{f,w})S\phi}{\pi d_{f,w}(1-S\phi)}\right]^{(1+D_T)/2}(\lambda_{\max}\sqrt{S})^2 \tag{4-33}$$

According to the definition of relative permeability, $k_{rn}(S) = K_n(S)/K$, dividing Eq. (4-14) by Eq. (4-33), we can derive the water relative permeability of fibrous GDL as

$$k_{rw}(S) = \frac{K_w(S)}{K} = \frac{\frac{d_{f,w}}{3+D_T-d_{f,w}}\left[\frac{4(2-d_{f,w})S\phi}{\pi d_{f,w}(1-S\phi)}\right]^{(1+D_T)/2}}{\frac{d_f}{3+D_T-d_f}\left[\frac{4(2-d_f)\phi}{\pi d_f(1-\phi)}\right]^{(1+D_T)/2}}S \tag{4-34}$$

For the common saturated porous media, each capillary pipe is filled with a single fluid and we have *S*=1. Thus Eq. (4-28) indicates that $\lambda_{\max,w} = \lambda_{\max}$ and $\lambda_{\min,w} = \lambda_{\min}$ as *S*=1, Eq. (4-31) will be reduced to Eq. (4-3), leading to $k_{rw}(S) = \frac{K_w(S)}{K} = 1 \Rightarrow K_w(S) = K$, meaning that the medium becomes a single phase/saturated porous one. Generally, $0 < S < 1$, the capillary tubes are partly filled with water and gas for the two phases in porous GDL.

According to Eq. (4-24), the effective maximum ($\lambda_{\max,g}$) and the smallest ($\lambda_{\min,g}$) diameters for gas phase can be obtained as

$$\lambda_{\max,g} = \lambda_{\max}\sqrt{1-S}, \quad \lambda_{\min,g} = \lambda_{\min}\sqrt{1-S} \tag{4-35}$$

Similarly, modifying Eq. (4-3), the fractal dimension for gas phase can be expressed

as

$$d_{f,g} = 2 - \frac{\ln \phi_g}{\ln \frac{\lambda_{\min,g}}{\lambda_{\max,g}}} \tag{4-36}$$

where ϕ_g is the volume fractions for gas phase in a unit cell which is expressed as (Bear, 1972)

$$\phi_g = (1-S)\phi \tag{4-37}$$

Inserting Eqs. (4-35) and (4-37) into Eq. (4-36), Eq. (4-36) can be rewritten as

$$d_{f,g} = 2 - \frac{\ln[(1-S)\phi]}{\ln \frac{\lambda_{\min}\sqrt{1-S}}{\lambda_{\max}\sqrt{1-S}}} = 2 - \frac{\ln[(1-S)\phi]}{\ln m} \tag{4-38}$$

Similarly, $\lambda_{\max}$ is replaced by $\lambda_{\max,g}$, d_f is replaced by $d_{f,g}$, and ϕ is replaced by ϕ_g in Eq. (4-14). Modifying Eq. (4-14), the phase permeability of GDL for gas can be determined as

$$K_g = \frac{\pi}{128} \frac{d_{f,g}}{3 + D_T - d_{f,g}} \left[\frac{4(2-d_{f,g})\phi_g}{\pi d_{f,g}(1-\phi_g)}\right]^{(1+D_T)/2} \lambda_{\max,g}^2 \tag{4-39}$$

Inserting Eqs. (4-35) and (4-37) into Eq. (4-39), Eq. (4-39) can be further modified as

$$K_g(S) = \frac{\pi}{128} \frac{d_{f,g}}{3 + D_T - d_{f,g}} \left\{\frac{4(2-d_{f,g})[(1-S)\phi]}{\pi d_{f,g}[1-(1-S)\phi]}\right\}^{(1+D_T)/2} (\lambda_{\max}\sqrt{1-S})^2 \tag{4-40}$$

Based on the definition of relative permeability, $k_{rg}(S) = K_g(S)/K$, the gas relative permeability of porous fibrous GDL can be determined as

$$k_{rg}(S)=\frac{K_g(S)}{K}=\frac{\dfrac{d_{f,g}}{3+D_T-d_{f,g}}\left\{\dfrac{4(2-d_{f,g})[(1-S)\phi]}{\pi d_{f,g}[1-(1-S)\phi]}\right\}^{(1+D_T)/2}}{\dfrac{d_f}{3+D_T-d_f}[\dfrac{4(2-d_f)\phi}{\pi d_f(1-\phi)}]^{(1+D_T)/2}}(1-S) \tag{4-41}$$

Eq. (4-35) indicates that $\lambda_{\max,g}=\lambda_{\max}$ and $\lambda_{\min,g}=\lambda_{\min}$ as S=0, Eq. (4-38) will be reduced to Eq. (4-3), leading to $k_{rg}(S)=\dfrac{K_g(S)}{K}=1\Rightarrow K_g(S)=K$, implying that the porous medium becomes a single phase/saturated porous one.

Eqs. (4-34) and (4-41) indicate that the water (k_{rw}) and gas (k_{rg}) relative permeabilities of porous fibrous GDL are explicitly related to the water saturation (S), porosity (ϕ), area fractal dimension (d_f, $d_{f,w}$ and $d_{f,g}$), tortuosity fractal dimension (D_T), and there is no empirical constant in this analytical models of relative permeabilities. In most literature (Acosta et al., 2006; Koido et al., 2008; Dawes et al., 2009; Hao and Cheng, 2010; Zamel et al., 2011; Xiao et al., 2012), the most common expressions of the water and gas relative permeabilities are represented by a function of the water saturation, which are consistent with our Eqs. (4-34) and (4-41).

The tortuosity fractal dimension can be estimated by Monte Carlo technique or the box-counting approach. Yu and Cheng (2002) determined the tortuosity fractal dimension for the five random flow pathways, they got $D_T=1.10$. Based on Monte Carlo technique, Wheatcraft and Tyler (1988) conducted the numerical simulations of random walk in the heterogeneous porous media and derived the tortuosity fractal dimension of $D_T=1.081$. Besides, Wu et al. (2011) used $D_T=1.1447$ to compute the oxygen effective diffusivity of TGP-H-060 carbon paper in porous GDL of

PEMFCs for both the dry and wet conditions and showed that this model prediction was in good agreement with the available experimental result. So, in this work we choose the average value $D_T = 1.10$ as the tortuosity fractal dimension of porous fibrous GDL when we compare our model predictions with the experimental data.

4.4 Results and discussion

PEMFCs most commonly operate at room temperature and ambient pressure. The prediction of the present model is highly consistent with the analytical, experimental and numerical results of GDL of PEMFCs operated under the temperatures lower than 65 ℃. For PEMFCs operated at a higher temperature (>80 ℃), which is considered to be an effective way to improve the performance of fuel cell (Bonville et al., 2005; Cheng et al., 2007; Stuckey et al., 2010; Cindrella and Kannan, 2010; Hung et al., 2013), the present model may need to be modified for GDL of PEMFCs operated at a higher temperature due to the possible effects of phase change on both heat and mass transport.

4.4.1 Predicted dimensionless permeability of porous fibrous GDL

4.4.1.1 Effects of porosity on dimensionless permeability

From Figure 4-3, it can be observed that the dimensionless permeability of

fibrous GDL increases markedly with porosity. This may be interpreted by the physical fact that an increase in porosity means more void space for fluid flow, leading to the increase of permeability. Figure 4-3 compares Eq. (4-20) with the available experimental data and models collected from different sources (Davies, 1952; Kirsch and Fuchs, 1967; Molnar et al., 1989; Zobel et al., 2007; Van Doormaal and Pharoah, 2009; Tamayol and Bahrami, 2011) for fibrous materials with high porosities at $m=10^{-2}$. The experiments in the literature (Davies, 1952; Kirsch and Fuchs, 1967; Molnar et al., 1989; Zobel et al., 2007; Tamayol and Bahrami, 2011) were performed on different porous fibrous materials such as carbon fibers and cotton wool for applications in filtration and fuel cells. It can be observed from Figure 4-3 that the dimensionless permeability predicted using our model agrees well with experimental data (Davies, 1952; Kirsch and Fuchs, 1967; Molnar et al., 1989; Zobel et al., 2007; Tamayol and Bahrami, 2011) and numerical simulation results (Van Doormaal and Pharoah, 2009; Tamayol and Bahrami, 2011) when porosity is greater than 0.70. The validity of the present fractal analytical model for the dimensionless permeability of fibrous GDL is thus verified. It should be noted that fibrous GDL possesses a very large porosity, which can change from 0.70 to 0.95, meaning that GDL is predominantly void space. For example, the porosity of Toray-090 carbon paper is 0.78 (Gostick et al., 2006), SGL10BB (w/MPL) paper is 0.87 (Gostick et al., 2006) and SGL10BA paper is 0.91 (Gostick et al., 2006). Therefore, our present model is appropriate to fibrous GDL.

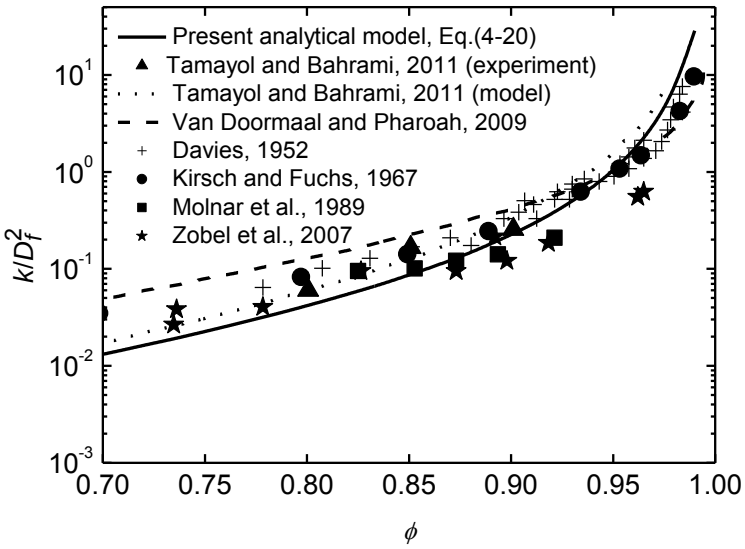

Figure 4-3 A comparison on the dimensionless permeability of porous fibrous GDL between the fractal analytical model and the available experimental result and models

4.4.1.2 Effects of tortuosity fractal dimension on dimensionless permeability

Figure 4-4 plots the dimensionless permeability of porous fibrous GDL (K / D_f^2) by the present fractal model (by Eq. (4-20)) versus tortuosity fractal dimension (D_T) for three different porosities (ϕ). From Figure 4-4, it can be found that the dimensionless permeability of porous fibrous GDL decreases markedly with increasing tortuosity fractal dimension. The physical phenomenon can be interpreted by the fact that an increase in tortuosity fractal dimension causes the increase of fluid flow resistance, leading to the decrease of fluid flow rate. Previous models such as those described in Eqs. (2-3), (2-4), (2-10), (2-13)-(2-20) did not consider the effect of tortuosity flow pathways on permeability of porous fibrous GDL. Therefore, the

present analytical model can better characterize the transport mechanisms of fluid flow in GDL of PEMFCs.

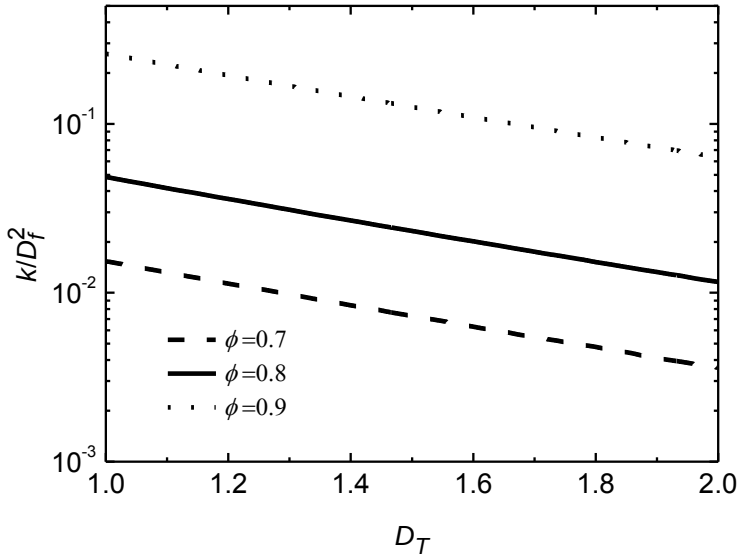

Figure 4-4 Influence of tortuosity fractal dimension on the dimensionless permeability of fibrous GDL by present fractal model

4.4.2 Effects of porosity on pore area fractal dimension (d_f), and water phase ($d_{f,w}$) and gas phase ($d_{f,g}$) fractal dimensions

Figure 4-5 plots the pore area fractal dimension (d_f) and water phase fractal dimension ($d_{f,w}$) at two different levels of water saturations against varying porosity at $m=10^{-3}$. It is seen that the pore area fractal dimension (d_f) and water phase fractal dimension ($d_{f,w}$) increase with the increase of porosity (ϕ), and as ϕ approaches to 1, d_f is close to 2. Another significant phenomenon, which may be observed from Figure 4-5,

is that the curve shape of $d_{f,w}$ is close to the curve shape of d_f. Figure 4-6 shows the effects of water saturation on the water phase ($d_{f,w}$) and gas phase ($d_{f,g}$) fractal dimensions in fibrous GDL. It is again observed from Figure 4-6 that the water phase and gas phase fractal dimensions increase with porosity. It is further seen that the gas phase fractal dimension decreases with increasing water saturation, resulting in an increase in the water phase fractal dimension. This can be explained by the common fact that an increase in water saturation causes the decrease of the gas phase area and gas phase fractal dimension, leading to the increase of the water phase area and water phase fractal dimension. Therefore, the present results are reasonable.

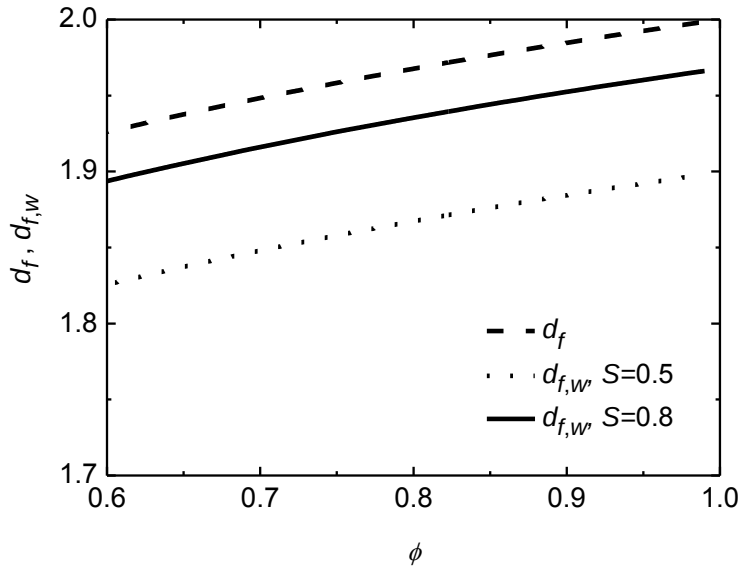

Figure 4-5 A comparison of pore area fractal dimension (d_f) and water phase fractal dimension ($d_{f,w}$) versus porosity at different water saturations (S) in porous fibrous GDL

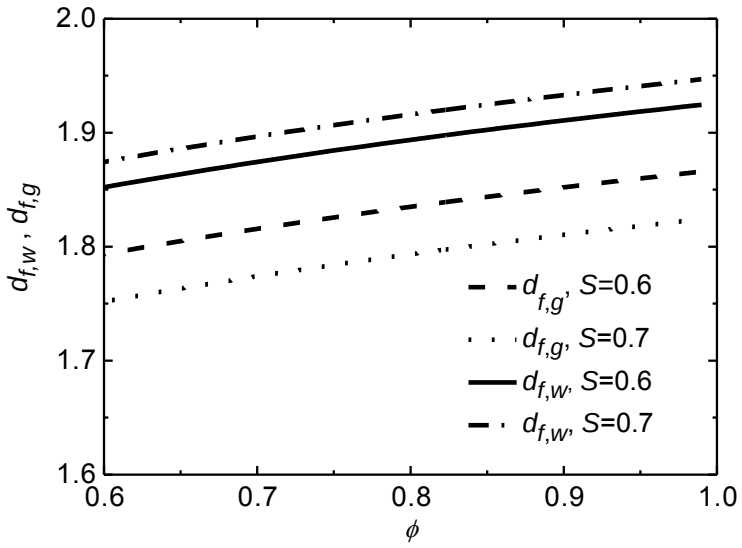

Figure 4-6 Effects of water saturation (*S*) on the water phase ($d_{f,w}$) and gas phase ($d_{f,g}$) fractal dimensions in porous fibrous GDL

4.4.3 Effects of water saturation on water phase and gas phase fractal dimensions

Figure 4-7 compares the phase fractal dimensions ($d_{f,w}$ and $d_{f,g}$) versus levels of water saturation at different porosities of porous fibrous GDL. It is again seen from Figure 4-7 that the water phase and gas phase fractal dimensions depend on porosity. In the limiting case, it should be noted that as water saturation approaches to 1, the porous fibrous GDL are fully filled with water, the fractal dimension becomes just the same as that for the saturated porous material. One interpretation for this is that, higher water saturation means larger proportion of water phase, leading to higher water phase fractal dimension, and the same is true for gas phase fractal dimension.

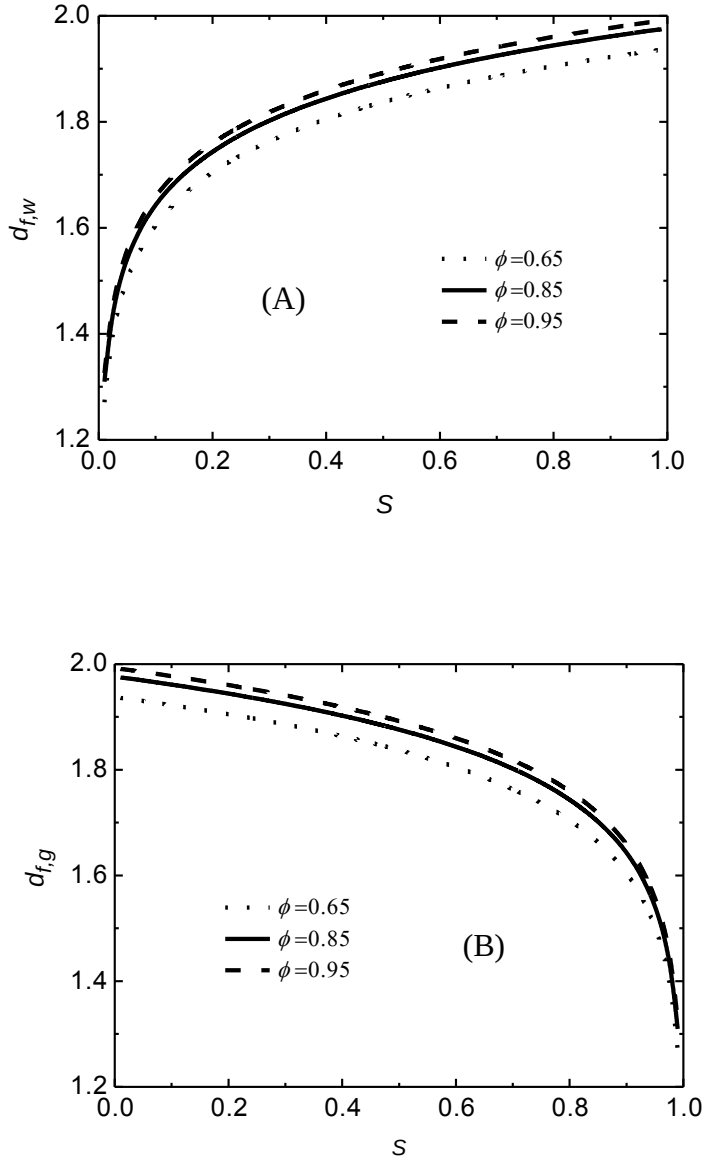

Figure 4-7 A comparison of the water phase and gas phase fractal dimensions versus water saturation for three different porosities in porous fibrous GDL

4.4.4 Predicted the water and gas relative permeabilities of porous fibrous GDL

4.4.4.1 Effects of porosity on relative permeabilities

Figure 4-8 gives the water (k_{rw}) and gas (k_{rg}) relative permeabilities of porous fibrous GDL calculated using the present model (by Eqs. (4-34) and (4-41)) at varying porosity and at different level of water saturations. It can be seen that the porosity hardly has any effect on the water and gas relative permeabilities.

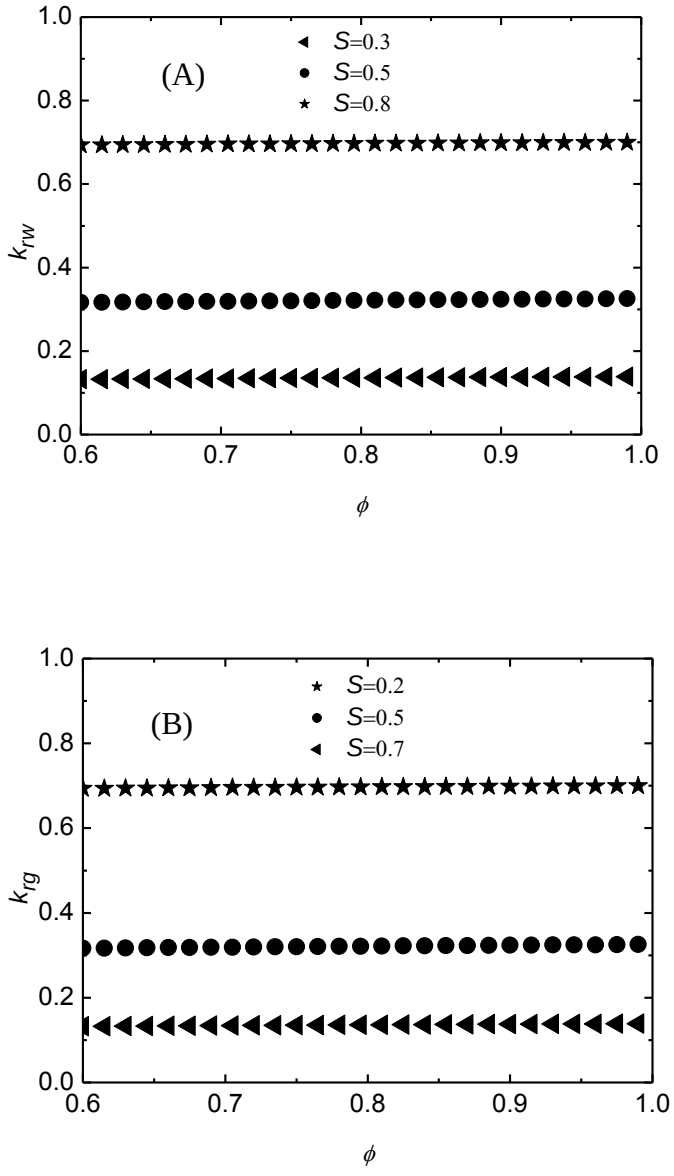

Figure 4-8 The water (k_{rw}) and gas (k_{rg}) relative permeabilities of porous fibrous GDL versus porosity at different water saturations

4.4.4.2 Effects of water saturation on relative permeabilities

Figure 4-9 presents the water and gas relative permeabilities of porous fibrous GDL (by Eqs. (4-34) and (4-41)) versus level of water saturation at different porosities. Figure 4-9 shows that the water relative permeability increases as the water saturation increases, and it is close to 1.0, as water saturation approaches to 1.0. On the contrary, from Figure 4-9 it can be found that the gas relative permeability decreases as the water saturation increases, and it approaches to zero, as water saturation approachs to 1.0. This is understandable as higher water saturation means more water and less gas, and as lower level of water saturation means more gas and less water. From Figure 4-9, it can also be observed that $k_{rw}+k_{rg}<1$, this is consistent with several experimental results (Acosta et al., 2006; Koido et al., 2008; Hao and Cheng, 2010; Luo et al., 2010; Zamel et al., 2011), and the shapes of the relative permeabilities curves are consistent with what is reported in published literature (Acosta et al., 2006; Koido et al., 2008; Hao and Cheng, 2010; Luo et al., 2010; Zamel et al., 2011). Figures 4-8 and 4-9 indicate that, although the water phase and gas phase fractal dimensions depend on porosity (see Figure 4-7), the water (k_{rw}) and gas (k_{rg}) relative permeabilities calculated from Eqs. (4-34) and (4-41) have no relationship with porosity and are a function of water saturation only. The analogous results were also reported from experiments (Kaviany, 1995).

Generally, $\phi=0.80$ is a representative value for Toray carbon paper of GDL in PEMFCs, as $\phi=0.78$ was reported for Toray-090 carbon paper (Gostick et al., 2006), and $\phi=0.80$ was reported for Toray-120 carbon paper (Zamel et al., 2011).

So, in this work we choose $\phi = 0.80$ as the porosity of porous fibrous GDL when we compare our model calculations with the published experimental result and past model calculations. Figure 4-10 shows a comparison of the predictions using the proposed fractal analytical model and the available experimental result reported in the published literature (Specchia et al., 1977; Levec et al., 1986; Dana and Skoczylas, 2002; Nguyen et al., 2006; Owejan et al., 2006) and predictions of past numerical (Koido et al., 2008; Hao and Cheng, 2010) and analytical (Acosta et al., 2006; Kumbur et al., 2007; Gostick et al., 2007; Li, 2011) models. A good agreement is found. Thus the validity of our fractal model for water and gas relative permeabilities of porous fibrous GDL in PEMFCs is verified.

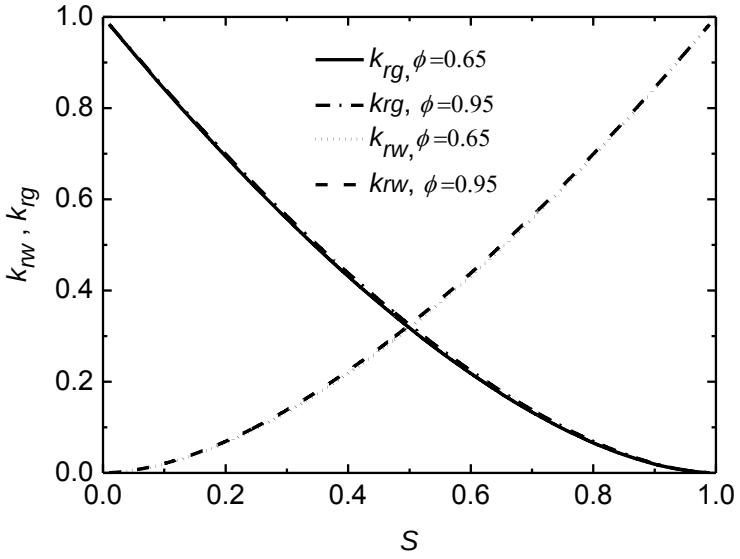

Figure 4-9 The water (k_{rw}) and gas (k_{rg}) relative permeabilities of porous fibrous GDL versus water saturation at different porosities

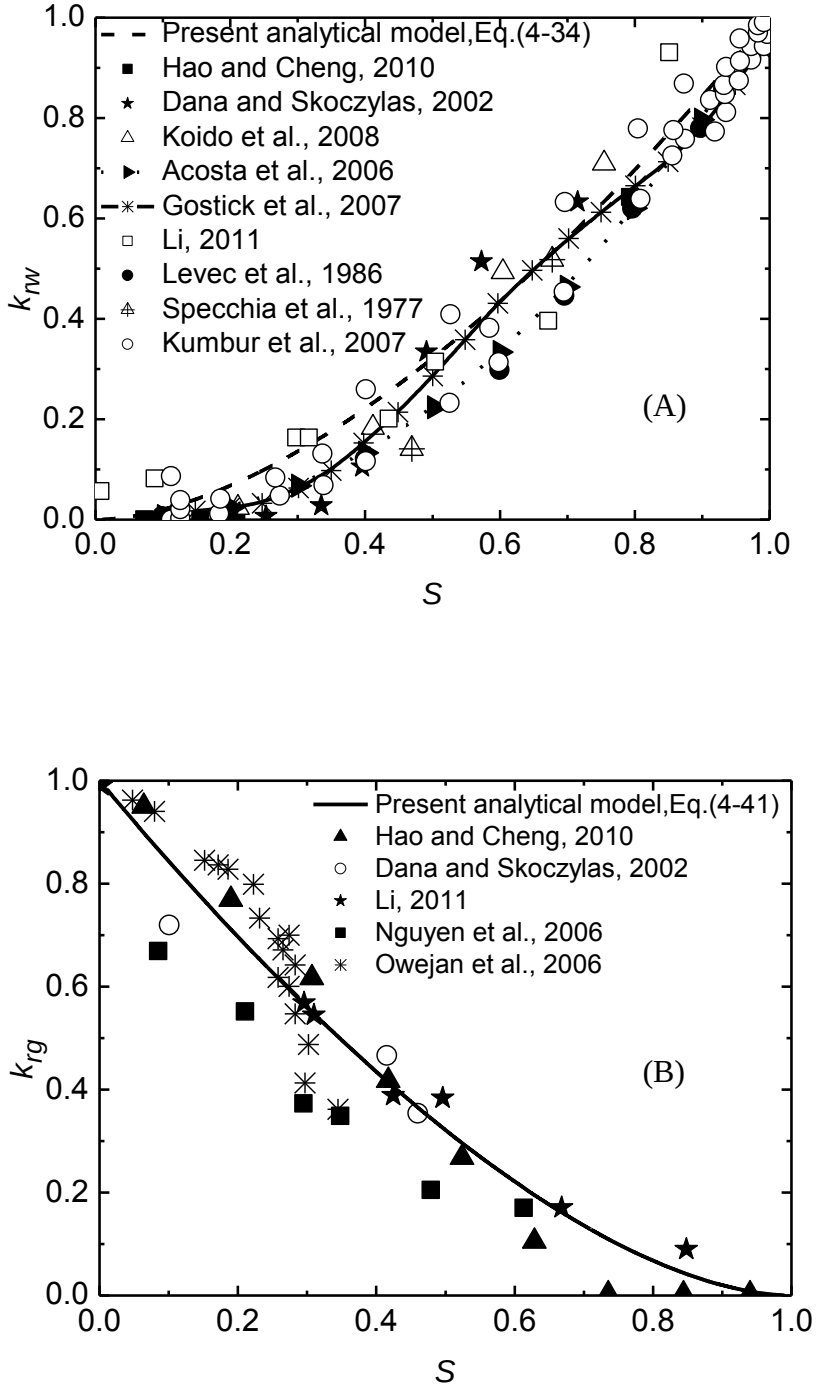

Figure 4-10 Comparison of the present fractal analytical models for water and gas relative permeabilities of fibrous GDL in PEMFCs with existing experimental data, numerical and analytical results

4.4.4.3 Effects of tortuosity fractal dimension on relative permeabilities

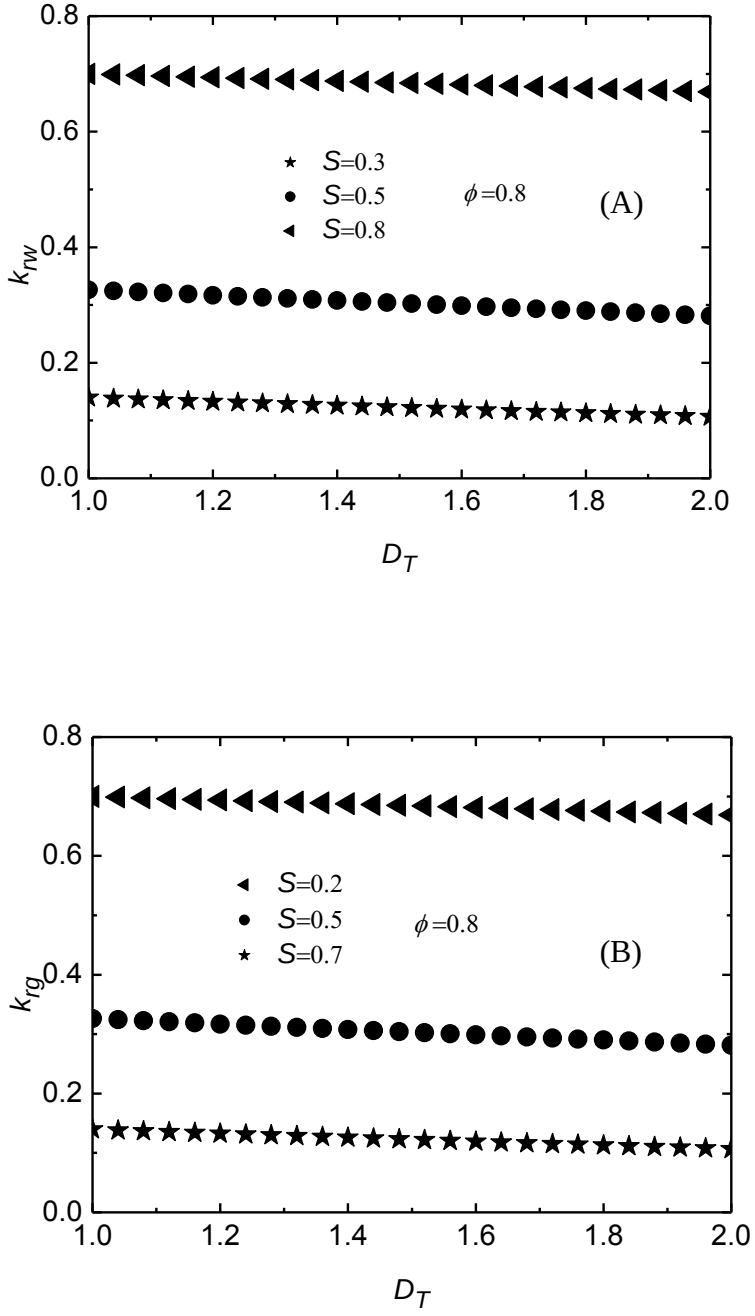

Figure 4-11 The water (k_{rw}) and gas (k_{rg}) relative permeabilities of porous fibrous GDL versus tortuosity fractal dimension at different water saturations

Figure 4-11 plots the water and gas relative permeabilities of porous fibrous GDL versus tortuosity fractal dimension at different water saturations. It is seen that there is a small decrease in the water and gas relative permeability when tortuosity fractal dimension increases.

4.5 Conclusions

In the present chapter, a fractal analytical model is proposed to calculate the dimensionless permeability, water and gas relative permeabilities of fibrous GDL in PEMFCs. The proposed model explicitly relates the permeabilities to the micro-structural parameters (tortuosity and pore area fractal dimensions, porosity) of fibrous GDL in PEMFCs. It is found that the dimensionless permeability, water phase and gas phase fractal dimensions strongly depend on porosity, but the water and gas relative permeabilities have no relationship with the porosity and are a function of water saturation only. Besides, it is shown that the dimensionless permeability increases markedly with the decrease of tortuosity fractal dimension. But there is only a small increase in the water and gas relative permeabilities when tortuosity fractal dimension decreases. From the parametric influence analysis, we draw a conclusion that the water phase fractal dimension and water relative permeability are positively correlated with the water saturation. But the gas phase fractal dimension and the gas relative permeability are negatively correlated with the water saturation. The model calculations are compared with the available experimental result and past models

calculations, and good agreement can be found. One advantage of the fractal analytical model is that it contains no empirical constant, which is normally required in past models. The present model improved the understanding of the physical mechanisms of water and gas transport through fibrous GDL of PEMFCs.

It should be pointed out that we applied Monte Carlo approach to determine the relative permeability of unsaturated fractal porous material, considering the effect of capillary pressure in Chapter 3. It was found that the used algorithm was very simple for predicting the relative permeability by using Monte Carlo method. However, the prediction of relative permeability requires 100,000 runs (see Figure 3-2) in a microcomputer in Chapter 3. Besides, Monte Carlo simulation is complementary to analytical methods, but does not give exact results. For example, it can be observed from Figure 3-2 that the minimum pore size is about $7.2\mu m$. However, estimation from Eqs. (3-27), (3-43) and Eq. (3-44) gives $\lambda_{\min,w} = 7.3\mu m$. The error is 1.4%, which means $7.2\mu m$ from Monte Carlo simulations is an approximation. Additionally, the fractal analytical model requires much less computational cost for optimization solutions as permeability of the fibrous materials can be expressed analytically in Chapter 4.

Chapter 5 Optimization of the fractal like architecture of porous fibrous materials

5.1 Introduction

In this chapter, specific optimization models for heat and mass transfer via fibrous materials are presented. The influences of geometrical parameters of the fibrous porous media on the transport properties are analysed. The developed models can be applied to optimized porous architecture of fibrous materials for different applications. The established theoretical models are applied to analyze the fibrous optimization structure for wind/water resistant fabric and clothing insulation. For wind proof and/or water resistant fabric, low permeability and high diffusivity are required. And for clothing insulation, low effective thermal conductivity and high diffusivity are required.

5.2 Optimization of the fractal like architecture of porous fibrous materials related to permeability and diffusivity

From Eq. (4-20), the dimensionless permeability of porous fibrous materials can be expressed as

$$Y_1 = \frac{K}{D_f^2} = \frac{\pi d_f}{128(3+D_T-d_f)}\left(\frac{4-d_f}{d_f}\right)^{1/2}\left[\frac{4(2-d_f)\phi}{\pi d_f(1-\phi)}\right]^{(1+D_T)/2}\left[\frac{\phi}{(1-\phi)}\right]^2 \quad (5\text{-}1)$$

The dimensionless effective diffusivity of porous fibrous materials was given by (Shou and Fan, 2014)

$$Y_2 = \frac{D_e}{D_b} = \frac{\phi l_0^{D_T-1}\left(2-d_f\right)\int_{\frac{\lambda_{\min}}{2}}^{\frac{\lambda_{\max}}{2}} \frac{(0.5\lambda)^{D_T+1-d_f}}{\lambda+3\lambda_{mf}} d\lambda}{\left(1-m^{2-d_f}\right)\left(\frac{\lambda_{\max}}{2}\right)^{2-d_f}} \tag{5-2}$$

where λ_{mf} is the mean free path of diffusion molecule.

By inserting Eq. (4-10) ($\phi = m^{2-d_f}$) into Eq. (5-2), Eq. (5-2) can be further reduced to

$$Y_2 = \frac{D_e}{D_b} = \frac{\phi l_0^{D_T-1}\left(2-d_f\right)\int_{\frac{\lambda_{\min}}{2}}^{\frac{\lambda_{\max}}{2}} \frac{(0.5\lambda)^{D_T+1-d_f}}{\lambda+3\lambda_{mf}} d\lambda}{(1-\phi)\left(\frac{\lambda_{\max}}{2}\right)^{2-d_f}} \tag{5-3}$$

Dividing Eq. (5-3) by Eq. (5-1), we can obtain the formula of analyzing the optimization of the fractal like architecture of porous fibrous materials related to permeability and diffusivity:

$$Y_3 = \frac{\text{The dimensionless permeability}}{\text{The dimensionless effective diffusivity}} = \frac{Y_1}{Y_2} = \frac{K/D_f^2}{D_e/D_b}$$

$$= \frac{\frac{\pi d_f}{128(3+D_T-d_f)}\left(\frac{4-d_f}{d_f}\right)^{1/2}\left[\frac{4(2-d_f)\phi}{\pi d_f(1-\phi)}\right]^{(1+D_T)/2}\left[\frac{\phi}{(1-\phi)}\right]^2}{\frac{\phi l_0^{D_T-1}\left(2-d_f\right)\int_{\frac{\lambda_{\min}}{2}}^{\frac{\lambda_{\max}}{2}} \frac{(0.5\lambda)^{D_T+1-d_f}}{\lambda+3\lambda_{mf}} d\lambda}{(1-\phi)\left(\frac{\lambda_{\max}}{2}\right)^{2-d_f}}} \tag{5-4}$$

The tortuosity fractal dimension (D_T) which can be expressed as (Yu, 2005)

$$D_T = 1 + \frac{\ln \tau}{\ln(l_0/\lambda_{av})} \tag{5-5}$$

For circular flow path, a relationship between the mean tortuosity and porosity can be obtained as (Comiti and Renaud, 1989)

$$\tau = 1 + 0.41\ln(\frac{1}{\phi}) \tag{5-6}$$

According to Eq. (4-17), a correlation between the straight-line distance (l_0) and the average pore diameter (λ_{av}) in fibrous porous media may be written as

$$\frac{l_0}{\lambda_{av}} = \frac{l_0}{\lambda_{\max}}(\frac{4-d_f}{d_f})^{1/4} \tag{5-7}$$

Comparing Eqs. (4-7) and (4-12), a correlation between the straight-line distance (l_0) and the maximum diameter of pore can be written as

$$\frac{l_0}{\lambda_{\max}} = \sqrt{\frac{\pi d_f(1-\phi)}{4(2-d_f)\phi}} \tag{5-8}$$

By inserting Eq. (5-8) into Eq. (5-7), Eq. (5-7) can be expressed as

$$\frac{l_0}{\lambda_{av}} = [\frac{\pi^2(4-d_f)d_f(1-\phi)^2}{16(2-d_f)^2\phi^2}]^{1/4} \tag{5-9}$$

Inserting Eqs. (5-6) and (5-9) into Eq. (5-5), the tortuosity fractal dimension for tortuous capillary of fibrous porous media can be further modified as

$$D_T = 1 + \frac{\ln[1+0.41\ln(1/\phi)]}{\ln\left\{[\frac{\pi^2(4-d_f)d_f(1-\phi)^2}{16(2-d_f)^2\phi^2}]^{1/4}\right\}} \tag{5-10}$$

Eq. (5-10) indicates that the tortuosity fractal dimension of tortuous capillary in fibrous porous media is a function of porosity (ϕ) and the area fractal dimensions of pore (d_f).

Figure 5-1 plots the tortuosity fractal dimension by the proposed model (by Eq. (5-10) versus porosity for three different ratios ($m = \lambda_{\min}/\lambda_{\max}$). It can be observed

from Figure 5-1 that the tortuosity fractal dimension decreases with increasing porosity. This is because the increase of the porosity means the pore area is increasing, resulting in the decrease of the tortuosity fractal dimension. From Figure 5-1 it can also be found that the tortuosity fractal dimension increases as the ratio of $m = \lambda_{\min} / \lambda_{\max}$. This can be explained that the difference between smaller pores and larger pores decrease, leading to the higher D_T. The limiting case of $D_T = 2$, is equivalent to a highly tortuous line that fills a plane.

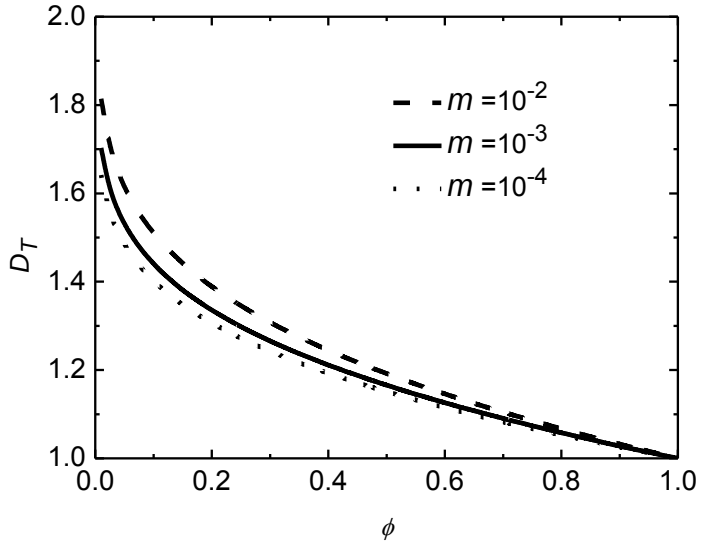

Figure 5-1 The tortuosity fractal dimension versus porosity at different ratios of *m*

In Figure 5-2, the optimization of the fractal like architecture of porous fibrous materials related to permeability and diffusivity is analyzed by applying the established theoretical model (by Eq. (5-4)). From Figure 5-2, it is found that the ratio of dimensionless permeability over dimensionless effective diffusivity ($Y_3 = (K / D_f^2) / (D_e / D_b)$) of the fractal like architecture of porous fibrous materials

increases with porosity. The result indicates that lower porosity is beneficial to wind/water resistant fabric, as it reduces the ratio of dimensionless permeability over dimensionless effective diffusivity ($Y_3 = (K / D_f^2) / (D_e / D_b)$), resulting in lower permeability and higher diffusivity. It is further seen that there is an increase in the ratio of dimensionless permeability over dimensionless effective diffusivity ($Y_3 = (K / D_f^2) / (D_e / D_b)$) when the ratio of *m* increases.

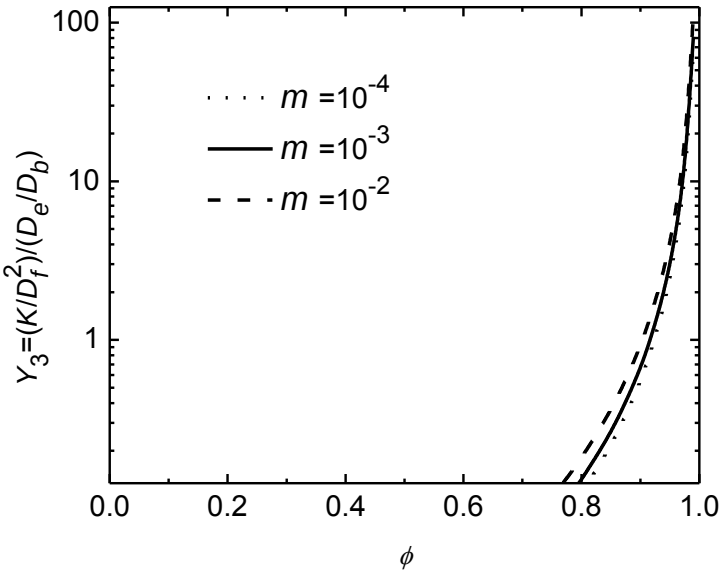

Figure 5-2 Influence of porosity on the ratio of dimensionless permeability over dimensionless effective diffusivity ($Y_3 = (K / D_f^2) / (D_e / D_b)$) of the fractal like architecture of porous fibrous materials

In Figure 5-3, we analyze the optimization of the fractal like architecture of porous fibrous materials related to permeability and diffusivity at varying tortuosity fractal dimension and at different level of porosities. It can be found that the ratio of dimensionless permeability over dimensionless effective diffusivity

($Y_3 = (K / D_f^2) / (D_e / D_b)$) decreases with the decrease of tortuosity fractal dimension, which implies lower tortuosity fractal dimension is beneficial to wind/water resistant fabric, as it reduces the ratio of dimensionless permeability over dimensionless effective diffusivity ($Y_3 = (K / D_f^2) / (D_e / D_b)$). To create low tortuosity fractal dimension, the tortuosity of fibrous materials should be reduced, which implies fibers in the fibrous materials should be more aligned. In others words, fabrics with more aligned fibers are preferred for protective clothing. Besides, it is seen that there is a small increase in the ratio of dimensionless permeability over dimensionless effective diffusivity ($Y_3 = (K / D_f^2) / (D_e / D_b)$) with porosity lower than 0.80 when tortuosity fractal dimension increases.

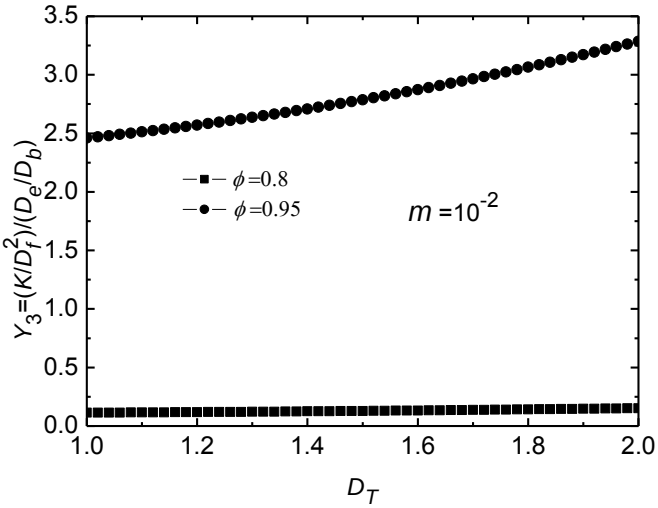

Figure 5-3 Influence of tortuosity fractal dimension on the ratio of dimensionless permeability over dimensionless effective diffusivity ($Y_3 = (K / D_f^2) / (D_e / D_b)$) of the fractal like architecture of porous fibrous materials

5.3 Optimization of the fractal like architecture of porous fibrous materials related to thermal conductivity and diffusivity

Considering a porous fibrous material covered with relatively dense fabrics, heat transfer takes place by heat conduction and radiative heat transfer, but heat transfer by convection may be ignored.

With regard to heat conduction, the effective thermal conductivity ($k_{c,eff}$) of porous fibrous materials is given by (Kou et al., 2009; Zhu et al., 2010)

$$k_{c,eff} = (\frac{\lambda_{\max}}{l_0})^{D_T-1} \frac{(2-d_f)\phi(1-m^{D_T-d_f+1})}{(D_T-d_f+1)(1-\phi)} k_g + (1-\phi)k_s \tag{5-11}$$

where $k_{c,eff}$ is the effective thermal conductivity of porous fibrous materials to heat conduction, k_g and k_s are the thermal conductivities of solid (viz. fiber) and gas (in most cases, it is still air) phases phases, respectively.

By inserting Eq. (5-8) into Eq. (5-11), Eq. (5-11) can be further modified as

$$k_{c,eff} = (\frac{4}{\pi d_f})^{\frac{1}{2}(D_T-1)} [\frac{(2-d_f)\phi}{(1-\phi)}]^{\frac{1}{2}(D_T+1)} \frac{(1-m^{D_T-d_f+1})}{(D_T-d_f+1)} k_g + (1-\phi)k_s \tag{5-12}$$

With regard to heat transfer by radiation in fibrous porous media, the effective conductivity (k_{rh}) can be estimated by (Strong et al., 1960; Wan et al., 2009; Song and Yu, 2012)

$$k_{rh} = C_3 \sigma T^3 \frac{r_f}{e(1-\phi)} \tag{5-13}$$

where σ is Boltzmann constant ($\sigma = 5.672\times10^{-8}\, Wm^{-2}K^{-4}$), T is the temperature, e is the surface emissivity of the fibre, r_f is the mean radius of the fibres, and C_3=5.4 (Wan et al., 2009) is a constant determined by fiber orientation.

The total effective thermal conductivity to heat conduction and radiation is then:

$$k_{tot,eff} = k_{c,eff} + k_{rh}$$

$$= (\frac{4}{\pi d_f})^{\frac{1}{2}(D_T-1)} [\frac{(2-d_f)\phi}{(1-\phi)}]^{\frac{1}{2}(D_T+1)} \frac{(1-m^{D_T-d_f+1})}{(D_T-d_f+1)} k_g + (1-\phi)k_s + C_3\sigma T^3 \frac{r_f}{e(1-\phi)} \qquad (5\text{-}14)$$

The dimensionless total effective thermal conductivity of the fibrous porous media to heat conduction and radiation can be expressed as

$$Y_4 = \frac{k_{tot,eff}}{k_g} = (\frac{4}{\pi d_f})^{\frac{1}{2}(D_T-1)} [\frac{(2-d_f)\phi}{(1-\phi)}]^{\frac{1}{2}(D_T+1)} \frac{(1-m^{D_T-d_f+1})}{(D_T-d_f+1)} + (1-\phi)\frac{k_s}{k_g} + \frac{C_3\sigma r_f T^3}{e(1-\phi)k_g} \qquad (5\text{-}15)$$

Dividing Eq. (5-3) by Eq. (5-15), we can obtain the formula of analyzing the optimization of the fractal like architecture of porous fibrous materials related to thermal conductivity and diffusivity:

$$Y_5 = \frac{\text{The dimensionless total effective thermal conductivity}}{\text{The dimensionless effective diffusivity}} = \frac{Y_4}{Y_2} = \frac{k_{tot,eff}/k_g}{D_e/D_b}$$

$$= \frac{(\frac{4}{\pi d_f})^{\frac{1}{2}(D_T-1)} [\frac{(2-d_f)\phi}{(1-\phi)}]^{\frac{1}{2}(D_T+1)} \frac{(1-m^{D_T-d_f+1})}{(D_T-d_f+1)} + (1-\phi)\frac{k_s}{k_g} + \frac{C_3\sigma r_f T^3}{e(1-\phi)k_g}}{\frac{\phi l_0^{D_T-1}(2-d_f)\int_{\frac{\lambda_{\min}}{2}}^{\frac{\lambda_{\max}}{2}} \frac{(0.5\lambda)^{D_T+1-d_f}}{\lambda+3\lambda_{mf}} d\lambda}{(1-\phi)(\frac{\lambda_{\max}}{2})^{2-d_f}}} \qquad (5\text{-}16)$$

Figure 5-4 plots the dimensionless total effective thermal conductivity of the fibrous porous media to heat conduction and radiative heat transfer by the present model (by Eq. (5-15)) versus porosity. From Figure 5-4, it is found that the

dimensionless total effective thermal conductivity of porous fibrous materials ($k_{tot,eff}/k_g$) decreases with increasing porosity when porosity is lower than 0.92. However, it is found that the dimensionless total effective thermal conductivity ($k_{tot,eff}/k_g$) increases with increasing porosity when porosity is greater than 0.92. The physical phenomenon can be interpreted by the fact that heat conduction is the primary heat transfer pattern and conductive thermal conductivity ($k_{c,eff}$) is much larger than that radiative conductivity (k_{rh}) when porosity is lower than 0.92. As porosity decreases, heat transfer by radiation is limited well and radiative conductivity decreases quickly when porosity is lower than 0.92, and finally it could keep at a quite low standard. It is well known that radiative heat transfer increases with porosity in porous fibrous materials. However, heat conduction decreases with increasing porosity in porous fibrous materials (Song and Yu, 2012; Xie et al., 2013). On the other hand, heat transfer by radiation is the primary heat transfer pattern and radiative conductivity is much larger than that conductive thermal conductivity when porosity is greater than 0.92. The analogous trend curve for total effective thermal conductivity of porous media to heat conduction and radiative heat transfer was reported (Song and Yu, 2012).

In Figure 5-5, the optimization of the fractal like architecture of porous fibrous materials related to thermal conductivity and diffusivity is analyzed by applying the established theoretical model (by Eq. (5-16)). From Figure 5-5, it is found that the ratio of dimensionless total effective thermal conductivity over dimensionless effective diffusivity ($Y_5 = (k_{eff}/k_g)/(D_e/D_b)$) of the fractal like architecture of

porous fibrous materials decreases with increasing of porosity when porosity is lower than 0.92. However, it can be found that the ratio of dimensionless total effective thermal conductivity over dimensionless effective diffusivity ($Y_5 = (k_{eff} / k_g) / (D_e / D_b)$) increases with porosity when porosity is greater than 0.92. These results indicate that low effective thermal conductivity and high diffusivity are required for clothing insulation.

In Figure 5-6, we analyze the optimization of the fractal like architecture of porous fibrous materials related to thermal conductivity and diffusivity at varying tortuosity fractal dimension and at different level of porosities. It is again observed from Figure 5-6 that the ratio of dimensionless total effective thermal conductivity over dimensionless effective diffusivity ($Y_5 = (k_{eff} / k_g) / (D_e / D_b)$) decreases with increasing porosity if porosity is lower than 0.92. It is observed that the ratio of dimensionless total effective thermal conductivity over dimensionless effective diffusivity ($Y_5 = (k_{eff} / k_g) / (D_e / D_b)$) increases with the increase of tortuosity fractal dimension, which implies lower tortuosity fractal dimension is beneficial to clothing insulation, as it reduces the ratio of dimensionless total effective thermal conductivity over dimensionless effective diffusivity ($Y_5 = (k_{eff} / k_g) / (D_e / D_b)$). To make tortuosity fractal dimension smaller, the tortuosity of porous fibrous materials should be reduced, which implies fibers in porous fibrous materials should be more aligned. In others words, fabrics with more aligned fibers are preferred for clothing insulation.

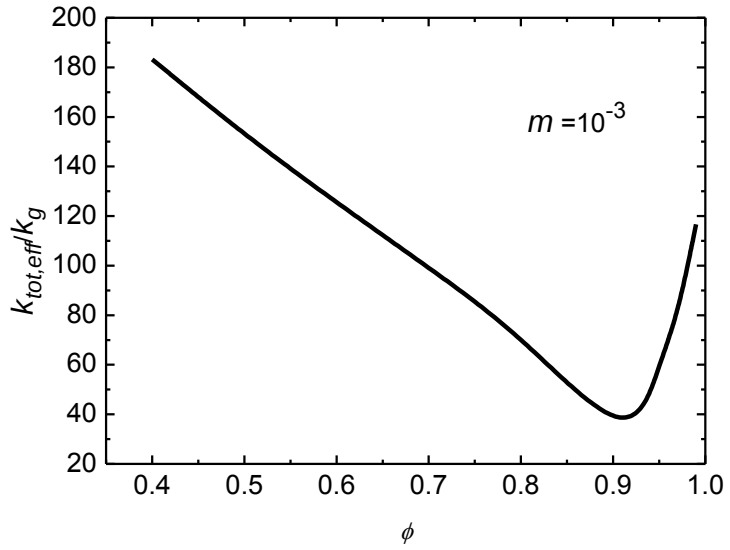

Figure 5-4 The dimensionless total effective thermal conductivity of the fibrous porous media to heat conduction and radiation versus porosity

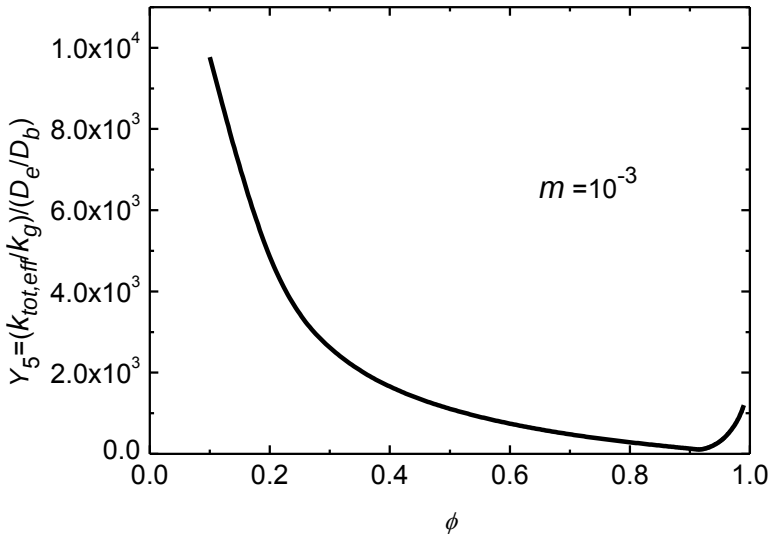

Figure 5-5 Influence of porosity on the ratio of dimensionless total effective thermal conductivity over dimensionless effective diffusivity ($Y_5 = (k_{eff} / k_g) / (D_e / D_b)$) of the fractal like architecture of porous fibrous materials

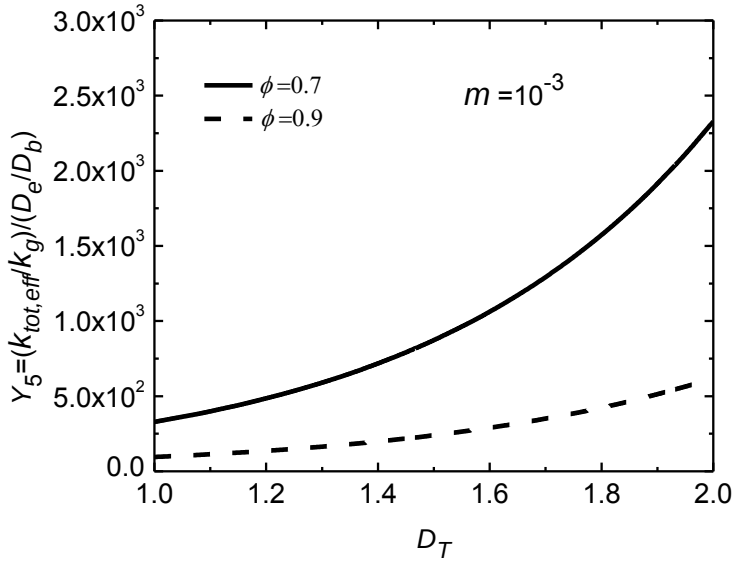

Figure 5-6 Influence of tortuosity fractal dimension on the ratio of dimensionless total effective thermal conductivity over dimensionless effective diffusivity ($Y_5 = (k_{eff} / k_g) / (D_e / D_b)$) of the fractal like architecture of porous fibrous materials

5.4 Conclusions

In this chapter, we analyze the optimization of the fractal like architecture of porous fibrous materials related to permeability, diffusivity, and thermal conductivity by applying the established theoretical models. In the analysis, the geometrical structure of porous fibrous materials is characterized in the light of the fractal dimension of pore area, the porosity, and the tortuosity fractal dimension. Besides, we predict the optimized structure of porous fibrous materials for different applications by using fractal theory. It can be observed that the ratio of dimensionless permeability over dimensionless effective diffusivity ($Y_3 = (K / D_f^2) / (D_e / D_b)$) of the fractal like

architecture of porous fibrous materials increases with increasing porosity and tortuosity fractal dimension, respectively, which indicates that lower porosity and tortuosity fractal dimension are beneficial to wind/water resistant fabric, as the ratio of dimensionless permeability over dimensionless effective diffusivity ($Y_3 = (K / D_f^2) / (D_e / D_b)$) is reduced, resulting in lower permeability and higher diffusivity. Besides, it can be found that the ratio of dimensionless total effective thermal conductivity over dimensionless effective diffusivity ($Y_5 = (k_{eff} / k_g) / (D_e / D_b)$) of the fractal like architecture of porous fibrous materials decreases with increasing porosity when porosity is lower than 0.92. However, it is observed that the ratio of dimensionless total effective thermal conductivity over dimensionless effective diffusivity ($Y_5 = (k_{eff} / k_g) / (D_e / D_b)$) increases with the increase of porosity when porosity is greater than 0.92. Furthermore, it is found that the ratio of dimensionless total effective thermal conductivity over dimensionless effective diffusivity ($Y_5 = (k_{eff} / k_g) / (D_e / D_b)$) increases with the increase of tortuosity fractal dimension, which means lower tortuosity fractal dimension is beneficial to clothing insulation, as the ratio of dimensionless total effective thermal conductivity over dimensionless effective diffusivity ($Y_5 = (k_{eff} / k_g) / (D_e / D_b)$) is reduced. The optimization results indicate that fabrics with more aligned fibers are preferred for protective clothing such as water resistant fabric and clothing insulation, as the low tortuosity fractal dimension means fibers in the fibrous materials should be more aligned. The optimization models improved the understanding of the physical mechanisms of fluids transport through porous fibrous materials.

Chapter 6 Summary and future work

6.1 Introduction

This chapter summarizes the research work, the results and insights yielded from this investigation, and also presents the suggestions for future work. In this thesis, we investigated the relative permeability with the effect of capillary pressure in unsaturated porous material by using fractal-Monte Carlo simulations. Besides, we proposed a fractal analytical model to study the permeabilities of fibrous gas diffusion layer in proton exchange membrane fuel cells. Additionally, we analyzed the optimization of the fractal like architecture of porous fibrous materials for wind/water resistant fabric and clothing insulation.

6.2 Summary of major findings

The conclusive contributions of this thesis are summarized as follows:

(1) Monte Carlo approach is used to estimate the relative permeability of the unsaturated porous material, considering the influence of capillary pressure and tortuosity of capillaries. The predicted relative permeability is expressed as a function of porosity, area fractal dimension of pores, fractal dimension of tortuous capillaries, degree of saturation and capillary pressure. It is found that the fractal dimension of wetting phase and non-wetting phase depend on the porosity of the unsaturated porous material. Besides, it is shown that the capillary pressure decreases with increasing saturation, and the capillary pressure increases sharply with decreasing saturation at

small saturation. The calculated relative permeability obtained by the proposed Monte Carlo simulation is shown to have a good agreement with the available experimental results reported in the literature. The present model improved the understanding of the physical mechanisms of liquid transport through porous fibrous materials. However, it should be pointed out that Monte Carlo simulation is complementary to analytical methods, but does not give exact results.

(2) The analytical models of dimensionless permeability, and water and gas relative permeabilities of fibrous GDL in PEMFCs are derived by using fractal theory. In our models, the structure of fibrous GDL is characterized in the light of porosity, tortuosity fractal dimension (D_T), pore area fractal dimensions (d_f), water phase ($d_{f,w}$) and gas phase ($d_{f,g}$) fractal dimensions. The predicted dimensionless permeability, water and gas relative permeabilities based on the proposed models are in good agreement with the available experimental result and predictions of numerical simulations reported in the published literature. The model reveals that, although water phase and gas phase fractal dimensions strongly depend on porosity, the water and gas relative permeabilities have no relationship with the porosity and are a function of water saturation only. It is also observed that the dimensionless permeability decreases significantly with increasing tortuosity fractal dimension. But there is only a small decrease in the water and gas relative permeabilities when tortuosity fractal dimension increases.

(3) The optimization of the fractal like architecture of porous fibrous materials related to permeability, diffusivity, and thermal conductivity is analyzed by applying the

established theoretical models based on fractal theory. The influences of different material parameters on the optimization of the fractal like architecture of porous fibrous materials are discussed. It is shown that the ratio of dimensionless permeability over dimensionless effective diffusivity ($Y_3 = (K / D_f^2) / (D_e / D_b)$) of the fractal like architecture of porous fibrous materials increases with increasing porosity and tortuosity fractal dimension, respectively, which means that lower porosity and tortuosity fractal dimension are beneficial to wind/water resistant fabric, as it reduces the ratio of dimensionless permeability over dimensionless effective diffusivity ($Y_3 = (K / D_f^2) / (D_e / D_b)$), resulting in lower permeability and higher diffusivity. It can be observed that the ratio of dimensionless total effective thermal conductivity over dimensionless effective diffusivity ($Y_5 = (k_{eff} / k_g) / (D_e / D_b)$) of the fractal like architecture of porous fibrous materials decreases with increasing porosity when the porosity is lower than 0.92. On the other hand, it is found that the ratio of dimensionless total effective thermal conductivity over dimensionless effective diffusivity ($Y_5 = (k_{eff} / k_g) / (D_e / D_b)$) increases with increasing porosity when porosity is greater than 0.92. Additionally, it can be observed that the ratio of dimensionless total effective thermal conductivity over dimensionless effective diffusivity ($Y_5 = (k_{eff} / k_g) / (D_e / D_b)$) increases with the increase of tortuosity fractal dimension, which implies lower tortuosity fractal dimension is beneficial to clothing insulation, as it reduces the ratio of dimensionless total effective thermal conductivity over dimensionless effective diffusivity ($Y_5 = (k_{eff} / k_g) / (D_e / D_b)$).

(4) It should be pointed out that the classical Darcy's law is a special case of the linear

version of the generalized Darcy's law (from three fundamental principles: principle of frame-indifference, principle of observed transformation, and second law of thermodynamics) when the velocity strain vanishes. Its applicability condition is thus the vanishing of the velocity strain instead of the small Reynolds number. This has also been confirmed experimentally. Besides, Heat transport in porous media is known of dual-phase-lagging type. The Fourier's law of heat conduction is valid only for some limiting cases.

6.3 The recommendations for future work

Based on the progress achieved on this work, the following further investigations are suggested:

(1) To modify and improve the established theoretical models for the optimization of the fractal like architecture of porous fibrous materials wherever necessary. For example, fibrous materials are widely used for building insulation. In this application, they are required to have high thermal resistance with minimum thickness and weight. When fibrous materials are used for clothing, they are required to provide protection from the external environment (e.g. wind, rain, temperature extremes, radiation, and toxicity) and comfort, which means maintaining the body temperature, keeping the skin dry, and being light weight and flexible.

(2) For different applications, there will be different optimization targets. For example, for gas diffusion layer in fuel cells, it is desirable to maximize capillary water flow

under sufficient gas diffusivity. For clothing insulation, the ideal fibrous material should maximum insulation (i.e. minimum effective thermal conductivity) and maximum diffusivity. For wind proof and/or water resistant fabric, it is desirable to have minimum hydraulic permeability, but maximum diffusivity. For filters, it is desirable to have maximum permeability (for minimizing pressure drop) and, at the same time, maximum filtration efficiency.

(3) To fabricate fibrous materials with optimized transport properties for clothing material, gas diffusion layer of proton exchange membrane fuel cells, filters, etc, as predicted by the developed models.

(4) To develop prototype fibrous materials by engineering the fractal-like architecture of the materials for use as thermal insulation in cold protective clothing and for use as surgical gown.

References

Acosta, M., Merten, C., Eigenberger, G., Class, H., Helmig, R., Thoben, B. & Steinhagen, H. M. (2006) Modeling non-isothermal two-phase multicomponent flow in the cathode of PEM fuel cells. *Journal of Power Sources*, 159, 1123-1141.

Ahn, K. J., Seferis, J. C. & Berg, J. C. (1991) Simultaneous measurements of permeability and capillary pressure of thermosetting matrices in woven fabric reinforcements. *Polymer Composites*, 12, 146-152.

Akbari, A., Akbari, M. & Hill, R. J. (2013) Effective thermal conductivity of two-dimensional anisotropic two-phase media. *International Journal of Heat and Mass Transfer*, 63, 41-50.

Amico, S. & Lekakou, C. (2001) An experimental study of the permeability and capillary pressure in resin-transfer moulding. *Composites Science and Technology*, 61, 1945-1959.

Angirasa, D. (2002) Forced convective heat transfer in metallic fibrous materials. *ASME Journal of Heat Transfer*, 124, 739-745.

Arambakam, R., Tafreshi, H. V. & Pourdeyhimi, B. (2012) Analytical Monte Carlo Ray Tracing simulation of radiative heat transfer through bimodal fibrous insulations with translucent fibers. *International Journal of Heat and Mass Transfer*, 55, 7234-7246.

Asllanaj, F., Jeandel, G., Roche, J. R. & Lacroix, D. (2004) Transient combined radiation and conduction heat transfer in fibrous media with temperature and flux

boundary conditions. *International Journal of Thermal Sciences*, 43, 939-950.

Ayatollahi, S., Lashanizadegan, A. & Kazemi, H. (2005) Temperature effects on the oil relative permeability during tertiary gas oil gravity drainage (GOGD). *Energy & Fuels*, 19, 977-983.

Bal, K., Fan, J. T., Sarkar, M. K. & Ye, L. (2011) Differential spontaneous capillary flow through heterogeneous porous media. *International Journal of Heat and Mass Transfer*, 54, 3096-3099.

Bartelt-Hunt, S. L. & Smith, J. A. (2002) Measurement of effective air diffusion coefficients for trichloroethene in undisturbed soil cores. *Journal of Contaminant Hydrology*, 56, 193-208.

Bear, J. (1972) Dynamics of fluids in porous media. *American Elsevier Publishing Company*, New York: Elsevier.

Beavers, G. S. & Sparrow, E. M. (1969) Non-Darcy flow through fibrous porous media. *ASME Journal of Applied Mechanics*, 36, 711-714.

Bechtold, G. & Ye, L. (2003) Influence of fiber distribution on the transverse flow permeability in fiber bundles. *Composites Science and Technology*, 63, 2069-2079.

Behzad, T. & Sain, M. (2007) Measurement and prediction of thermal conductivity for hemp fiber reinforced composites. *Polymer Engineering & Science*, 47, 977-983.

Benziger, J., Nehlsen, J., Blackwell, D., Brennan, T. & Itescu, J. (2005) Water flow in the gas diffusion layer of PEM fuel cells. *Journal of Membrane Science*, 261,

98-106.

Bonville, L. J., Kunz, H. R., Song, Y., Mientek, A., Williams, M., Ching, A. & Fenton, J. M. (2005) Development and demonstration of a higher temperature PEM fuel cell stack. *Journal of Power Sources*, 144, 107-112.

Boulet, P., Jeandel, G. & Morlot, G. (1993) Model of radiative transfer in fibrous media-matrix method. *International Journal of Heat and Mass Transfer*, 36, 4287-4297.

Bradford, S. A., Abriola, L. M. & Leij, F. J. (1997) Wettability effects on two-and three-fluid relative permeabilities. *Journal of Contaminant Hydrology*, 28, 171-191.

Cai, J. C., Hu, X. Y., Standnes, D. C. & You, L. J. (2012) An analytical model for spontaneous imbibition in fractal porous media including gravity. *Colloids and Surfaces A: Physicochemical and Engineering Aspects*, 414, 228-233.

Cai, J. C., Yu, B. M., Zou, M. Q. & Luo, L. (2010) Fractal characterization of spontaneous co-current imbibition in porous media. *Energy & Fuels*, 24, 1860-1867.

Carman, P. C (1956) Flow of gases through porous media. *London: Butterworth*.

Chan, C., Zamel, N., Li, X. G. & Shen, J. (2012) Experimental measurement of effective diffusion coefficient of gas diffusion layer/microporous layer in PEM fuel cells. *Electrochimica Acta*, 65, 13-21.

Chen, X. M. & Papathanasiou, T. D. (2006) On the variability of the Kozeny constant for saturated flow across unidirectional disordered fiber arrays. *Composites: Part*

A, 37, 836-846.

Chen, Z. Q., Cheng, P. & Hus, C. T. (2000) A theoretical and experimental study on stagnant thermal conductivity of bi-dispersed porous media. *International Communications in Heat and Mass Transfer*, 27, 601-610.

Cheng, C. Y. (2011) Double diffusion from a horizontal cylinder of elliptic cross section with uniform wall heat and mass fluxes in a porous medium. *International Communications in Heat and Mass Transfer*, 38, 1201-1205.

Cheng, X., Zhang, J. L., Tang, Y. H., Song, C. J., Shen, J., Song, D. T. & Zhang, J. J. (2007) Hydrogen crossover in high-temperature PEM fuel cells. *Journal of Power Sources*, 167, 25-31.

Choi, M. A., Lee, M. H., Chang, J. & Leed, S. J. (1998) Permeability modeling of fibrous media in composite processing. *Journal of Non-Newtonian Fluid Mechanics*, 79, 585-598.

Cindrella, L. & Kannan, A. M. (2010) Development and evaluation of gas diffusion layer using paraffin wax carbon for proton exchange membrane fuel cells. *Fuel Cells*, 10563.

Cindrella, L., Kannan, A. M., Lin, J. F., Saminathan, K., Ho, Y., Lin, C. W. & Wertz, J. (2009) Gas diffusion layer for proton exchange membrane fuel cells-A review. *Journal of Power Sources*, 194, 146-160.

Clague, D. S., Kandhai, B. D., Zhang, R. & Sloot, P. M. A. (2000) Hydraulic permeability of (un)bounded fibrous media using the lattice Boltzmann method. *Physical Review E*, 61, 616-625.

Comiti, J. & Renaud, M. (1989) A new model for determining mean structure parameters of fixed beds from pressure drop measurements: application to beds packed with parallelepipedal particles. *Chemical Engineering Science*, 44, 1539-1545.

Crawford, R., Jones, G. F., You, L. D. & Wu, Q. H. (2011) Compression-dependent permeability measurement for random soft porous media and its implications to lift generation. *Chemical Engineering Science*, 66, 294-302.

Dana, E. & Skoczylas, F. (2002) Experimental study of two-phase flow in three sandstones. II. Capillary pressure curve measurement and relative permeability pore space capillary models, *International Journal of Multiphase Flow*, 28, 1965-1981.

Darcy, H. (1856) Les fontaines publiques de la ville de Dijon. *Dalmont, Paris*.

Daryabeigi, K. (1999) Effective thermal conductivity of high temperature insulations for reusable launch vehicles. *NASA*, TM-1999-208972.

Davies, C. N. (1952) The separation of airborne dust and particle. *Proceedings of the Institution of Mechanical, Institute of Mechanical Engineers*, London, B1, 185-213.

Dawes, J. E., Hanspal, N. S., Family, O. A. & Turan, A. (2009) Three-dimensional CFD modelling of PEM fuel cells: An investigation into the effects of water flooding. *Chemical Engineering Science*, 64, 2781-2794.

Demond, A. H. & Roberts, P. V. (1993) Estimation of two-phase relative permeability relationships for organic liquid contaminants. *Water Resources Research*, 29,

1081-1090.

Denn, M. M. (1986) Process Fluid Mechanics, *Prentice Hall*, Englewood Cliffs, N.J.

Drummond, J .E. & Tahir, M. I. (1984) Laminar viscous flow through regular arrays of parallel solid cylinders. *International Journal of Multiphase Flow*, 10, 515-540.

Du, N., Fan, J. T., Wu, H. J., Chen, S. & Liu, Y. (2007) An improved model of heat transfer through penguin feathers and down. *Journal of Theoretical Biology*, 248, 727-735.

Dullien, F. A. L. (1979) Porous media: fluid transport and pore structure. *Academic Press*, New York.

Fan, J. & He, J. H. (2012) Fractal derivative model for air permeability in hierarchic porous media. *Abstract and Applied Analysis*, 2012, 354701.

Falla, W. R., Mulski, M. & Cussler, E. L. (1996) Estimating diffusion through flake-filled membranes. *Journal of Membrane Science*, 119, 129-138.

Fan, J. T., Cheng, X. Y. & Chen Y. S. (2003) An experimental investigation of moisture absorption and condensation in fibrous insulations under low temperature. *Experimental Thermal and Fluid Science*, 27, 723-729.

Fan, J. T., Luo, Z. X. & Li, Y. (2000) Heat and moisture transfer with sorption and condensation in porous clothing assemblies and numerical simulation. *International Journal of Heat and Mass Transfer*, 43, 2989-3000.

Feng, Y. J., Yu, B. M., Zou, M. Q. & Zhang, D. M. (2004) A generalized model for the effective thermal conductivity of porous media based on self-similarity. *Journal of Physics D: Applied Physics*, 37, 3030-3040.

Feser, J. P., Prasad, A. K. & Advani, S. G. (2006) On the relative influence of convection in serpentine flow fields of PEM fuel cells. *Journal of Power Sources*, 162, 1226-1231.

Flückiger, R., Freunberger, S. A., Kramer, D., Wokaun, A., Scherer, G. G. & Büchi, F. N. (2008) Anisotropic, effective diffusivity of porous gas diffusion layer materials for PEFC. *Electrochimica Acta*, 54, 551-559.

Fu, S. Y. & Mai, Y. W. (2003) Thermal conductivity of misaligned short-fiber-reinforced polymer composites. *Journal of Applied Polymer Science*, 88, 1497-1505.

Gebart, B. R. (1992) Permeability of Unidirectional Reinforcements for RTM. *Journal of Composite Materials*, 26, 1100-1133.

Gostick, J. T., Fowler, M. W., Ioannidis, M. A., Pritzker, M. D., Volfkovich, Y. M. & Sakars, A. (2006) Capillary pressure and hydrophilic porosity in gas diffusion layers for polymer electrolyte fuel cells. *Journal of Power Sources*, 156, 375-387.

Gostick, J. T., Ioannidis, M. A., Fowler, M. W. & Pritzker, M. D. (2007) Pore network modeling of fibrous gas diffusion layers for polymer electrolyte membrane fuel cells. *Journal of Power Sources*, 173, 277-290.

Hao, L. & Cheng, P. (2010) Pore-scale simulations on relative permeabilities of porous media by lattic Boltzmann method. *International Journal of Heat and Mass Transfer*, 53, 1908-1913.

Henderson, N., Brettas, J. C. & Sacco, W. F. (2010) A three-parameter

Kozeny-Carman generalized equation for fractal porous media. *Chemical Engineering Science*, 65, 4432-4442.

Hou, J., Luo, F. Q., Wang, C. F., Zhang, Y. H., Zhou, K. & Pan, G. M. (2011) Quantitative prediction model for the water-oil relative permeability curve and its application in reservoir numerical simulation. Part 1: modeling. *Energy & Fuels*, 25, 4405-4413.

Hou, J., Luo, F. Q., Wang, D. G., Li, Z. Q. & Bing, S. X. (2012) Estimation of the water-oil relative permeability curve from radial displacement experiments. Part 2: reasonable experimental parameters. *Energy & Fuels*, 26, 4300-4309.

Hu, J. L. (2008) Properties, applications and modelling of three-dimensional textile structures. *Woodhead Publishing Series in Textiles*, No. 74.

Hung, C. J., Liu, C. H., Ko, T. H., Chen, W. H., Cheng, S. H., Chen, W. S., Yu, A. & Kannan, A. M. (2013) Effect of diffusion layers fabricated with different fiber diameters on the performance of low temperature proton exchange membrane fuel cells. *Journal of Power Sources*, 221, 134-140.

Hunt, M. L. & Tien, C. L. (1988) Effects of thermal dispersion on forced convection in fibrous media. *International Journal of Heat and Mass Transfer*, 31, 301-309.

Jackson, G. W. & James, D. F. (1986) The permeability of fibrous porous media. *The Canadian Journal of Chemical Engineering***,** 64, 364-374.

Jeng, T. M. & Tzeng, S. C. (2007) Experimental study of forced convection in metallic porous block subject to a confined slot jet. *International Journal of Thermal Sciences*, 46, 1242-1250.

Kannan, A. M., Cindrella, L. & Munukutla, L. (2008) Functionally graded nano-porous gas diffusion layer for proton exchange membrane fuel cells under low relative humidity conditions. *Electrochimica Acta*, 53, 2416-2422.

Katz, A. J. & Thompson, A. H. (1985) Fractal sandstone pores: Implications for conductivity and pore Formation. *Physical Review Letters*, 54, 1325-1328.

Kaviany, M. (1995) Principles of heat transfer in porous media, second ed. *Springer-Verlag*, inc., New York.

Kim, S. W., Lee, S. H., Kang, J. S. & Kang, K. H. (2006) Thermal conductivity of thermoplastics reinforced with natural fibers. *International Journal of Thermophysics*, 27, 1873-1881.

Kirsch, A. A. & Fuchs, N. A. (1967) Studies on fibrous aerosol filters, II. Pressure drops in systems of parallel cylinders. *The Annals of Occupational Hygiene*, 10, 23-30.

Koido, T., Furusawa, T. & Moriyama, K. (2008) An approach to modeling two-phase transport in the gas diffusion layer of a proton exchange membrane fuel cell. *Journal of Power Sources*, 175, 127-136.

Koponen, A., Kandhai, D., Hellén, E., Alava, M., Hoekstra, A., Kataja, M., Niskanen, K., Sloot, P. & Timonen, J. (1998) Permeability of Three-Dimensional Random Fiber Webs. *Physical Review Letters*, 80, 716-719.

Koponen, A., Kataja, M. & Timonen, J. (1996) Tortuous flow in porous media. *Physical Review E*, 54, 406-410.

Koponen, A., Kataja, M. & Timonen, J. (1997) Permeability and effective porosity of

porous media. *Physical Review E*, 56, 3319-3325.

Kou, J. L., Wu, F. M., Lu, H. J., Xu, Y. S. & Song, F. Q. (2009) The effective thermal conductivity of porous media based on statistical self-similarity. *Physics Letters A*, 374, 62-65.

Kozeny, J. (1927) Ueber kapillare Leitung des Wassers im Boden. *Stizungsber Akad Wiss Wien*, 136,271-306.

Kumbur, E. C., Sharp, K. V. & Mench, M. M. (2007) On the effectiveness of Leverett approach for describing the water transport in fuel cell diffusion media. *Journal of Power Sources*, 168, 356-368.

Langlais, C., Guilbert, G., Banner, D. & Klarsfeld, C. (1995) Influence of the chemical composition of glass on heat transfer through glass fiber insulations in relation to their morphology and temperature of use. *Journal of Building Physics*, 18, 350-376.

Larkin, B. K. & Churchill, S. W. (1959) Heat transfer by radiation through porous insulations. *AIChE Journal*, 5, 467-474.

Lee, J. (2010) Experimental study on the dissociation behavior and productivity of gas hydrate by brine injection scheme in porous rock. *Energy & Fuels*, 24, 456-463.

Lee, J., Shin, C. & Lee, Y. (2010) Experimental investigation to improve the storage potentials of gas hydrate under the unstirring condition. *Energy & Fuels*, 24, 1129-1134.

Lee, S. C. (1989) Effect of fiber orientation on thermal radiation in fibrous media. *International Journal of Heat and Mass Transfer*, 32, 311-319.

Lei, Z., Zhu, S. K. & Pan, N. (2010) Transient methods of thermal properties measurement on fibrous materials. *ASME Journal of Heat Transfer*, 132, 032601.

Levec, J., Sáez, A. E. & Carbonell, R. G. (1986) The hydrodynamics of tricking flow in packed beds. Part II: Experimental observations. *AIChE Journal*, 32, 369-380.

Li, H. Y., Zand, A. R., Sikorski, Y., Markicevic, B., Meyers, J., Rincon, C., Bowden, E., Bethel, T., Sanders, M. S., Navaz, H. K. & Smith, M. R. (2011) Simple and effective method to measure the diffusion coefficient of organic vapors in porous media. *Analytical Methods*, 3, 2809-2814.

Li, J. H. & Yu, B. M. (2011) Tortuosity of flow paths through a Sierpinski Carpet, *Chinese physics letters*, 28, 034701.

Li, K. W. (2011) Interrelationship between resistivity index, capillary pressure and relative permeability. *Transport in Porous Media*, 88, 385-398.

Li, K. W. & Hone, R. N. (2001) An experimental and analytical study of steam/water capillary pressure. *SPE Reservoir Evaluation & Engineering*, 4, 477-482.

Li, M., Wang, S. K., Gu, Y. Z., Zhang, Z. G., Li, Y. X. & Potter, K. (2010) Dynamic capillary impact on longitudinal micro-flow in vacuum assisted impregnation and the unsaturated permeability of inner fiber tows. *Composites Science and Technology*, 70, 1628-1636.

Li, X., Tabil, L. G., Oguocha, I. N. & Panigrahi, S. (2008) Thermal diffusivity, thermal conductivity, and specific heat of flax fiber-HDPE biocomposites at processing temperatures. *Composites Science and Technology*, 68, 1753-1758.

Li, Y. & Luo, Z. X. (1999) An improved mathematical simulation of the coupled diffusion of moistures and heat in wool fabric. *Textile Research Journal*, 69, 760-768.

Li, Y. & Luo, Z. X. (2000) Physical mechanisms of moisture diffusion into hygroscopic fabrics during humidity transients. *Journal of the Textile Institute*, 91, 302-316.

Liu, K., Takagi, H., Osugi, R. & Yang, Z. M. (2012) Effect of lumen size on the effective transverse thermal conductivity of unidirectional natural fiber composites. *Composites Science and Technology*, 72, 633-639.

Liu, Y. J., Yu, B. M., Xu, P. & Wu, J. S. (2007) Study of the effect of capillary pressure on permeability. *Fractals*, 15, 55-62.

Lu, Y., Donaldson, K. Y., Hasselman, D. P. H. & Thomas, J. R. (1995) Thermal conductivity of uniaxial coated cylindrically orthotropic fiber-reinforced composite with thermal barriers. *Journal of Composite Materials*, 29, 1719-1724.

Luo, G., Ji, Y., Wang, C. Y. & Sinha. P. K. (2010) Modeling liquid water transport in gas diffusion layers by topologically equivalent pore network. *Electrochimica Acta*, 55, 5332-5341.

Malek, K. & Coppens, M. O. (2003) Knudsen self- and Fickian diffusion in rough nanoporous media. *Journal of Chemical Physics*, 119, 2801-2811.

Mandelbrot, B. B. (1982) The fractal geometry of nature. *New York: W. H. Freeman*.

Mangal, R., Saxena, N. S., Sreekala, M. S., Thomas, S. & Singh, K. (2003) Thermal

properties of pineapple leaf fiber reinforced composites. *Materials Science and Engineering: A*, 339, 281-285.

Matyka, M., Khalili, A. & Koza1, Z. (2008) Tortuosity-porosity relation in porous media flow. *Physical Review E*, 78, 026306.

Mehrafarin, M. & Faghihi, M. (2001) Random-walk diffusion and drying of porous materials. *Physica A*, 301, 163-168.

Molnar, J. A., Trevino, L. & Lee, L. J. (1989) Liquid flow in molds with prelocated fiber mats. *Polymer Composites*,10, 414-423.

Mu, D. Q., Liu, Z. S., Huang, C. & Djilali, N. (2008) Determination of the effective diffusion coefficient in porous media including Knudsen effects. *Microfluid Nanofluid*, 4, 257-260.

Nabovati, A., Llewellin, E. W. & Sousa, A. C. M. (2010) Through-thickness permeability prediction of three-dimensional multifilament woven fabrics. *Composites Part A: Applied Science and Manufacturing*, 41, 453-463.

Nam, J. H. & Kaviany, M. (2003) Effective diffusivity and water-saturation distribution in single- and two-layer PEMFC diffusion medium. *International Journal of Heat and Mass Transfer*, 46, 4595-4611.

Nilsson, L. & Stenström, S. (1995) Gas diffusion through sheets of fibrous porous media. *Chemical Engineering Science*, 50, 361-371.

Nisipeanu, E. & Jones, P. D. (2003) Monte Carlo simulation of radiative heat transfer in coarse fibrous media. *ASME Journal of Heat Transfer*, 125, 748-752.

Ngo, N. D. & Tamma, K. K. (2001) Microscale permeability predictions of porous

fibrous media. *International Journal of Heat and Mass Transfer*, 44, 3135-3145.

Nguyen, T. V., Lin, G., Ohn, H., Wang, X., Hussey, D. S., Jacobson, D. L. & Arif, M. (2006) Measurements of two-phase flow properties of the porous media used in PEM fuel cells. *ECS Transactions*, 3, 415-423.

Olives, R. & Mauran, S. (2001) A highly conductive porous Medium for solid-gas reactions: effect of the dispersed phase on the thermal tortuosity. *Transport in Porous Media*, 43, 377-394.

Owens, W. W. & Archer, D. L. J. (1971) the effect of rock wettability on oil-water relative permeability relationships. *Journal of Petroleum Technology*, 23, 873-878.

Owejan, J. P., Trabold, T. A., Jacobson, D. L., Baker, D. R., Hussey, D. S. & Arif, M. (2006) In situ investigation of water transport in an operating PEM fuel cell using neutron radiography: part 2-transient water accumulation in an interdigitated cathode flow field. *International Journal of Heat and Mass Transfer*, 49, 4721-4731.

Pharoah, J. G., Karan, K. & Sun, W. (2006) On effective transport coefficients in PEM fuel cell electrodes: Anisotropy of the porous transport layers. *Journal of Power Sources*, 161, 214-224.

Pitchumani, R. & Yao, S. C. (1991) Correlation of thermal conductivities of unidirectional fibrous composites using local fractal techniques. *ASME Journal of Heat Transfer*, 113, 788-796.

Rama, P., Liu, Y., Chen, R., Ostadi, H., Jiang, K., Gao, Y., Zhang, X. X., Fisher, R. &

Jeschke, M. (2010) Multiscale modeling of single-phase multicomponent transport in the cathode gas diffusion layer of a polymer electrolyte fuel cell. *Energy & Fuels*, 24, 3130-3143.

Ramousse, J., Didierjean, S., Lottin, O. & Maillet, D. (2008) Estimation of the effective thermal conductivity of carbon felts used as PEMFC gas diffusion layers. *International Journal of Thermal Sciences*, 47, 1-6.

Roux, J. A. (2003) Radiative properties of high and low density fiberglass insulation in the 4-38.5 μm wavelength region. *Journal of Thermal* Envelope and *Building Science*, 27, 135-149.

Saadatfar, M. & Sahimi, M. (2002) Diffusion in disordered media with long-range correlations:anomalous, fickian, and superdiffusive transport and log-periodic oscillations. *Physical Review E*, 65, 036116.

Sadeghi, E., Djilali, N. & Bahrami, M. (2011) A novel approach to determine the in-plane thermal conductivity of gas diffusion layers in proton exchange membrane fuel cells. *Journal of Power Sources*, 196, 3565-3571.

Schieferstein, E. & Heinrich, P. (1997) Diffusion coefficients calculated for microporous solids from structural parameters evaluated by fractal geometry. *Langmuir*, 13, 1723-1728.

Shen, C. & Springer, G. (1981) Environmental Effect on Composite Materials. *Springer*.

Shen, L. H. & Chen, Z. X. (2007) Critical reviewof the impact of tortuosity on diffusion. *Chemical Engineering Science*, 62, 3748-3755.

Shi, Y., Xiao, J. S., Quan, S. H., Pan, M. & Yuan, R. Z. (2008) Fractal model for prediction of effective thermal conductivity of gas diffusion layer in proton exchange membrane fuel cell. *Journal of Power Sources*, 185, 241-247.

Shih, C. H. & Lee, L. J. (1998) Effect of fiber architecture on permeability in liquid composite molding. *Polymer Composites*, 19, 626-639.

Shou, D. H., Fan, J. T. & Ding, F. (2010) A difference-fractal model for the permeability of fibrous porous media. *Physics Letters A*, 374, 1201-1204.

Shou, D. H., Fan, J. T. & Ding, F. (2011) Hydraulic permeability of fibrous porous media. *International Journal of Heat and Mass Transfer*, 54, 4009-4018.

Shou, D. H., Fan, J. T. & Ding, F. (2013) Effective diffusivity of gas diffusion layer in proton exchange membrane fuel cells. *Journal of Power Sources*, 225, 179-186.

Shou, D. H., Fan, J. T., Mei, M. F. & Ding, F. (2014) An analytical model for gas diffusion though nanoscale and microscale fibrous media. *Microfluids and Nanofluids*, 16, 381-389.

Sobera, M. P. & Kleijn, C. R. (2006) Hydraulic permeability of ordered and disordered single-layer arrays of cylinders. *Physical Review E*, 74, 036301.

Song, W. F. & Yu, W. D. (2012) Heat transfer through fibrous assemblies by fractal method. *Journal of Thermal Analysis and Calorimetry*, 110, 897-905.

Song, Y. S., Heider, D. & Youn, J. R. (2009) Statistical characteristics of out-of-plane permeability for plain-woven structure. *Polymer Composites*, 30, 1465-1472.

Specchia, V. & Baldi, G. (1977) Pressure drop and liquid holdup for two phase concurrent flow in packed beds. *Chemical Engineering Science*, 32, 515-523.

Strong, H. M., Bundy, F. P. & Bovenkerk, H. P. (1960) Flat panel vacuum thermal insulation. *Journal of Applied Physics*, 31:39-50.

Stylianopoulos, T., Yeckel, A., Derby, J. J., Luo, X. J., Shephard, M. S., Sander, E. A. & Barocas, V. H. (2008) Permeability calculations in three-dimensional isotropic and oriented fiber networks. *Physics of Fluids*, 20, 123601.

Stuckey, P. A., Lin, J. F., Kannan, A. M. & Ghasemi-Nejhad, M. N. (2010) Gas diffusion layers for proton exchange membrane fuel cells using in situ modified carbon papers with multi-walled carbon nanotubes nanoforest. *Fuel Cells*, 10, 369-374.

Tamayol, A. & Bahrami, M. (2009) Analytical determination of viscous permeability of fibrous porous media. *International Journal of Heat and Mass Transfer*, 52, 2407-2414.

Tamayol, A. & Bahrami, M. (2010) Parallel flow through ordered fibers: An analytical approach. *Journal of Fluids Engineering*, 132, 114502-114507.

Tamayol, A. & Bahrami, M. (2011) Transverse permeability of fibrous porous media. *Physical Review E*, 83, 046314.

Teertstra, P., Karimi, G. & Li, X. (2011) Measurement of in-plane effective thermal conductivity in PEM fuel cell diffusion media. *Electrochimica Acta*, 56, 1670-1675.

Tomadakis, M. M. & Robertson, T. J. (2005) Viscous permeability of random fiber structures: comparison of electrical and diffusional estimates with experimental and analytical results. *Journal of Composite Materials*, 39, 163-188.

Tomadakis, M. M. & Sotirchos, S. V. (1993a) Ordinary, transition, and knudsen regime diffusion in random capillary structures. *Chemical Engineering Science*, 48, 3323-3333.

Tomadakis, M. M. & Sotirchos, S. V. (1993b) Ordinary and transition regime diffusion in random fiber structures. *AIChE Journal*, 39, 397-412.

Tong, T. W. & Tien, C. L. (1980) Analytical models for thermal radiation in fibrous insulations. *Journal of Building Physics*, 4, 27-44.

Utaka, Y., Tasaki, Y., Wang, S. X., Ishiji, T. & Uchikoshi, S. (2009) Method of measuring oxygen diffusivity in microporous media. *International Journal of Heat and Mass Transfer*, 52, 3685-3692.

Van Doormaal, M. A. & Pharoah, J. G. (2009) Determination of permeability in fibrous porous media using the lattice Boltzmann method with application to PEM fuel cells. *International Journal for Numerical Methods in Fluids*, 59, 75-89.

Vassal, J. P., Orgéas, L. & Favier, D. (2008) Modelling microstructure effects on the conduction in fibrous materials with fibre-fibre interface barriers. *Modelling and Simulation in Materials Science and Engineering*, 16, 035007.

Veiseh, S. & Hakkaki-Fard, A. (2009) Numerical modeling of combined radiation and conduction heat transfer in mineral wool insulations. *Heat Transfer Engineering*, 30, 477-486.

Verrey, J., Michaud, V. & Manson, J. A. E. (2006) Dynamic capillary effects in liquid composite moulding with non-crimp fabrics. *Composites Part A: Applied Science and Manufacturing*, 37, 92-102.

Wan, X. F., Fan, J. T. & Wu, H. J. (2009) Measurement of thermal radiative properties of penguin down and other fibrous materials using FTIR. *Polymer Testing*, 28, 673-679.

Wang, F. L. & Tarabara, V. V. (2009) Permeability of fiber-filled porous media: Kozeny-Carman-Ethier modeling approach. *Environmental Engineering Science*, 26, 1149-1155.

Wang, J. F. & Hwang, W. R. (2008) Permeability prediction of fibrous porous media in a bi-periodic domain. *Journal of composite materials*, 42, 909-929.

Wang, M. R., He, J. H., Yu, J. Y. & Pan, N. (2007) Lattice Boltzmann modeling of the effective thermal conductivity for fibrous materials. *International Journal of Thermal Sciences*, 46, 848-855.

Westhuizen, J. V. & Pless, J. P. D. (1994) Qualification of unidirectional fiber bed permeability. *Journal of Composite Materials*, 28, 619-637.

Wheatcraft, S. W. & Tyler, S. W. (1988) An explanation of scale-dependent dispersivity in heterogeneous aquifers using concepts of fractal geometry. *Water Resources Research*, 24, 566-578.

Wu, R., Zhu, X., Liao, Q., Wang, H., Ding, Y. D., Li, J. & Ye, D. D. (2010) Determination of oxygen effective diffusivity in porous gas diffusion layer using a three-dimensional pore network model. *Electrochimica Acta*, 55, 7394-7403.

Wu, R., Liao, Q., Zhu, X. & Wang, H. (2011) A fractal model for determining oxygen effective diffusivity of gas diffusion layer under the dry and wet conditions. *International Journal of Heat and Mass Transfer*, 54, 4341-4348.

Xia, D. H., Guo, S. S. & R, L. (2010) Fractal structure reconstruction for alumina-silicate refractory fiber and simulation of the thermal conductivity. *Journal of Thermal Science*, 19, 80-86.

Xiao, B. Q., Fan, J. T. & Ding, F. (2012) Prediction of relative permeability of unsaturated porous media based on fractal theory and monte carlo simulation. *Energy & Fuels*, 26, 6971-6978.

Xiao, B. Q., Fan, J. T. & Ding, F. (2014) A fractal analytical model for the permeabilities of fibrous gas diffusion layer in proton exchange membrane fuel cells. *Electrochimica Acta*, 134, 222-231.

Xie, T., He, Y. L. & Hu, Z. J. (2013) Theoretical study on thermal conductivities of silica aerogel composite insulating material. *International Journal of Heat and Mass Transfer*, 58, 540-552.

Xu, D. H., Cheng, J. X. & Zhou, X. H. (2011) A model of heat and moisture transfer through parallel pore textiles. *Journal of Fiber Bioengineering and Informatics*, 3, 250-255.

Yang, C. & Nakayama, A. (2010) A synthesis of tortuosity and dispersion in effective thermal conductivity of porous media. *International Journal of Heat and Mass Transfer*, 53, 3222-3230.

Yazdchi, K., Srivastava, S. & Luding, S. (2011) Microstructural effects on the

permeability of periodic fibrous porous media. *International Journal of Multiphase Flow*, 37, 956-966.

Yu, B. M. (2005) Fractal character for tortuous streamtubes in porous media. *Chinese physics letters*, 22, 158-160.

Yu, B. M. & Cheng, P. (2002) A fractal permeability model for bi-dispersed porous media. *International Journal of Heat and Mass Transfer*, 45, 2983-2993.

Yu, B. M. & Lee, L. J. (2000) A Simplified in-plane permeability model for textile fabrics. *Polymer Composites*, 21, 660-685.

Yu, B. M. & Li, J. H. (2001) Some fractal characters of porous media. *Fractals*, 9, 365-372.

Yu, B. M., Lee, L. J. & Cao, H. Q. (2001) Fractal characters of pore microstructures of textile fabrics. *Fractals*, 9, 155-163.

Yu, B. M., Lee, L. J. & Cao, H. Q. (2002) A fractal in-plane permeability model for fabrics. *Polymer Composites*, 23, 201-221.

Yu, B. M. & Li, J. H. (2004) A geometry model for tortuosity of flow path in porous media. *Chinese physics letters*, 21, 1569-1571.

Yu, B. M., Li, J. H., Li, Z. H. & Zou, M. Q. (2003) Permeabilities of unsaturated porous media. *International Journal of Multiphase Flow*, 29, 1625-1642.

Yun, M. J., Yu, B. M. & Cai, J. C. (2008) A fractal model for the starting pressure gradient for Bingham fluids in porous media. *International Journal of Heat and Mass Transfer*, 51, 1402-1408.

Yun, M. J., Yu, B. M., Xu, P. & Wu, J. S. (2006) Geometrical models for tortuosity of

streamlines in three dimensional porous media. *The Canadian Journal of Chemical Engineering*, 84, 301-309.

Yun, M. J., Yu, B. M., Zhang, B. & Huang, M. T. (2005) A geometry model for tortuosity of streamtubes in porous media with spherical particles. *Chinese physics letters*, 22, 1464-1467.

Zalc, J. M., Reyes, S. C. & Iglesia, E. (2004) The effects of diffusion mechanism and void structure on transport rates and tortuosity factors in complex porous structures. *Chemical Engineering Science*, 59, 2947-2960.

Zamel, N., Astrath, N. G. C., Li, X. G., Shen, J., Zhou, J. Q., Astrath, F. B. G., Wang, H. J. & Liu, Z. S. (2010) Experimental measurements of effective diffusion coefficient of oxygen-nitrogen mixture in PEM fuel cell diffusion media. *Chemical Engineering Science*, 65, 931-937.

Zamel, N., Becker, J. & Wiegmann, A. (2012) Estimating the thermal conductivity and diffusion coefficient of the microporous layer of polymer electrolyte membrane fuel cells. *Journal of Power Sources*, 207, 70-80.

Zamel, N., Li, X. G., Becker, J. & Wiegmann, A. (2011) Effect of liquid water on transport properties of the gas diffusion layer of polymer electrolyte membrane fuel cell. *International Journal of Hydrogen Energy*, 36, 5466-5478.

Zeng, S. Q., Hunt, A. J., Greif, R. & Cao, W. (1995) Approximate formulation for coupled conduction and radiation through a medium with arbitrary optical thickness. *ASME Journal of Heat Transfer*, 117, 797-799.

Zheng, Q., Yu, B. M., Wang, S. F. & Luo, L. (2012) A diffusivity model for gas

diffusion through fractal porous media. *Chemical Engineering Science*, 68, 650-655.

Zhu, F. L. (2013) Fractal geometry model for through-plane liquid water permeability of fibrous porous carbon cloth gas diffusion layers. *Journal of Power Sources*, 243, 887-890.

Zhu, F. L., Cui, S. Z. & Gu, B. H. (2010) Fractal analysis for effective thermal conductivity of random fibrous porous materials. *Physics Letters A*, 374, 4411-4414.

Zhu, Q. Y., Xie, M. H., Yang, J. & Li, Y. (2011) A fractal model for the coupled heat and mass transfer in porous fibrous media. *International Journal of Heat and Mass Transfer*, 54, 1400-1409.

Zobel, S., Maze, B., Tafreshi, H. V., Wang, Q. & Pourdeyhimi, B. (2007) Simulating permeability of 3-D calendered fibrous structures. *Chemical Engineering Science*, 62, 6285-6296.

Zou, M. Z., Yu, B. M. & Zhang, D. M. (2002) An analytical solution for transverse thermal conductivities of unidirectional fibre composites with thermal barrier. *Journal of Physics D: Applied Physics*, 35, 1867-1874.